ON-LINE MONITORING AND CONTROL OF SURFACE ROUGHESS IN TURNING OPERATION

By

Avisekh Banerjee

DEPARTMENT OF MECHANICAL ENGINEERING

Indian Institute of Technology Kanpur

APRIL, 2003

ON-LINE MONITORING AND CONTROL OF SURFACE ROUGHNESS IN TURNING OPERATION

A Thesis Submitted
in Partial Fulfillment of the Requirements
for the Degree of

MASTER OF TECHNOLOGY

by
Avisekh Banerjee
Y110505

Department of Mechanical Engineering
Indian Institute of Technology Kanpur
April 2003

CERTIFICATE

It is certified that the work contained in this thesis entitled "*On-line Monitoring and Control of Surface Roughness in turning operation*," by Mr. Avisekh Banerjee (Roll No. Y110505) has been carried out under my supervision and that this work has not been submitted elsewhere for a degree.

16.4.03

S K Choudhury

Professor

Department of Mechanical Engineering

Indian Institute of Technology Kanpur

April 2003

Abstract

Measurement of surface roughness had always been a post machining operation in quality control practices of machined parts. By the time the operator is aware of the higher than desired surface roughness value, metal had been removed. Thus either re-work or rejection of the part has to be done. For unmanned machining this poses a big hurdle, which can be solved by developing a robust monitoring and control strategy while the machining is taking place, referred as "*On-line Monitoring and Control of Surface Roughness*".

In this work, "O*n-line monitoring of surface roughness"* was achieved with the help of a bifurcated optical transducer and a laser gun, based on the principle of scattering of the laser beam from the surface of the turned part. Mathematical models were developed to investigate the effect of cutting parameters on surface roughness. Vibration was taken as an input parameter and correlated to surface roughness.

The "*On-line control of surface roughness*" will improve the productivity of machining operations to a great extent if it can be implemented on the shop floor. Vibration is identified as the source of machine tool chatter which leads to unwanted relative displacement between tool and workpiece in the radial direction. An active vibration control strategy with the help of an accelerometer, PID controller and a piezo electric actuator had been proposed. The cutting process and the machine tool structure dynamics were modeled with help of experimental data, and the whole process was simulated to study the onset of chatter. It was shown that the proposed control strategy was effective to reduce the displacement between tool and work piece which would lead to improved surface finish.

Acknowledgment

First of all, I am grateful to S K Choudhury for guiding me in my first venture in engineering research. Our technical and non-technical discussions kept the spirits high, thus making the stay at I.I.T. Kanpur enjoyable and motivating. Moreover his guidance has helped me to develop the various facets of my personality and own self. He reinforced my belief that anything is do-able and any goal is achievable through focus and sincere efforts.

I am indebted to Professor A K Mallik and N N Vyas, for his invaluable advices and suggestions that not only helped in my thesis work but also in shaping my career. The resources and the materials in his office have helped a lot in this work. I thank all the faculty members of the institute who helped me learn the basics and guided me to face the various challenges of engineering problems. I thank Mr Phool Chand, Rakesh, Atul, Virendra, Ravinder and Rajinder for helping me in my experimental work and fabricating electronic circuits.

Words are insufficient to describe my indebtness to my family and close ones whose encouragement and guidance have helped me strive forward throughout the Masters program. Special thanks to my father for his contribution in providing me with custom made materials very essential in fabricating of my experimental setup.

Special thanks to Sanjoy, Sandip and Debraj for helping me with difficulties throughout my thesis. I am grateful to Ankur and Prashantha for helping me carry out experiments.

The list of people whom I befriended is too long and the memorable experiences that I shared are too many. Still great injustice will be done if some of the names are not mentioned. My Manufacturing-mates and seniors Deepak, Sanjoy, D K Singh, Trimurthy, Ravi, Vijay and Santosh, and my hall-mates Nati, Sona, Hulo, Sakila, President, Ashokeg, Malayda, all made my stay enjoyable.

I acknowledge gratefully the contribution of Kanpur city restaurants, e.g. *China Town Restaurant, Tandoori Nights, Baba, Anaicha, Host, Chung Fa, Mehfil, Kandhar* in my thesis for their stimulating cuisines.

Avisekh

Table of Contents

Chapter IV: Result and Discussion of Experimentations

Chapter V: Vibration due to regenerative chatter and its control

Chapter VI: Conclusion

List of Tables

List of Figures

List of Symbols

Symbol	*Description*
R_a	Centre Line Average Roughness (μm)
v	Cutting Speed (m/min)
f	Feed (mm/rev)
α	Rake Angle (°)
s_k	Skewness
k	Kurtosis
y	Response Variable of Regression Models
β_i	Regression Co-efficients
x_i	Independent or controllable variables in Regressor Models
ε	Random error in Regression Model
L	Least Square Function
$\hat{y}$	Fitted Response Variable
SS_R	Sum of Squares Residual
SS_E	Sum of Squares Error
SS_{yy}	Sum of Squares Total
MS_E	Mean Square Residual
MS_R	Mean Square Error
$a(t)$	Activation Function of *ANN*
$Y(t)$	Output Value of *ANN*
$W(t)$	Weight of *ANN*
S	Sigmoid Function
$i-h-j$	Input-Hidden-Output Layer of *ANN*
$e_j(n)$	Error signal at the output of the neuron j, at iteration n
$w_j(n)$	Weight coefficient at the output of the neuron j, at iteration n
η	Learning Rate parameter

$\delta_j(n)$	Local Gradient
S^2	Mean Square Error
R^2	Co-efficient of multiple determination
SE	Standard error Co-efficient
DF	Degree of freedom
F_0	Test Statistic for the hypothesis of no difference in treatment
P	It is the smallest level of significance that would lead to the rejection of the null hypothesis H_o.
m_m, c_m, k_m	Mass, damping co-efficient and stiffness of the machine tool
r_o, f_o, F_o	Static penetration rate, chip thickness and radial force
dr, df, dF	Variation in penetration rate, chip thickness and radial force
k_1	Chip thickness co-efficient
k_f	Cutting force co-efficient
K	Penetration co-efficient
T, N	Time period and Revolution per sec
μ	Overlap Factor
$G_{cp}(s)$	Transfer Function of the cutting process
$G_m(s)$	Transfer Function of the machine tool structure
$G_{mts}(s)$	Transfer Function of the machine tool system
$G_a(s)$	Transfer Function of the actuator
$G_{PID}(s)$	Transfer Function of the PID controller
$G_{feedback}(s)$	Transfer Function of the feedback loop
$G_{closed}(s)$	Transfer Function of the closed loop system
$\omega_n =$	Natural frequency
$\zeta =$	Damping Ratio

ω_d =	Damping Frequency
ε_v	The slope of the force versus cutting speed curve
ε_f	The slope of the force versus feed curve
ε_l	The slope of the feed force versus feed curve
δ	Logarithmic decrement

Chapter I

Introduction and Literature Survey

1.0 Introduction

The latest trend in the research in machining is towards the concept of unmanned machining. To achieve an implementable unmanned machining strategy one should have adequate knowledge of the machining processes, reliable sensors to monitor the process and control mechanism for diagnostic actions. The machining processes are inherently dynamic in nature due to various factors. Some of them can be mathematically modeled, but others are too uncertain. Thus simplifications are made while modeling the extremely complex machining processes. Research in the field of machining has been primarily done on single point turning process, as it is the basic metal removal processes. Once a model has been developed for turning operation, it can be implemented for other multipoint processes like drilling, milling or grinding.

For the concept of unmanned machining to be implemented the process parameter on the basis of which the process is to be controlled, has to be carefully decided. These parameters are the outputs of the machining processes, for example cutting forces, temperature, tool wear, surface roughness etc. All these parameters have to be monitored on-line that is when the metal removal operation is going on, so that in case of any

deviation from the desired output, diagnosis can be made before any major damage has been done.

In this work surface roughness had been selected as the criterion for the process control in turning operation. Surface roughness of the workpiece plays a significant role in the acceptance of the part for the purpose it is supposed to serve. Since in conventional processes, surface roughness is a post-machining that is an off-line operation, there is no means of controlling the surface roughness during machining. Thus we focus on the online process monitoring and control techniques.

1.1 Surface Roughness and related terminology

Solid surfaces, irrespective of their method of formation, contain irregularities or deviations from the prescribed geometrical form. The surfaces contain irregularities of various orders ranging from shape deviations to irregularities of order of inter atomic distances. No machining method, however precise, can produce a molecularly flat surface on conventional materials.

1.1.1 Surface Texture

Surface texture, shown in Fig. 1.1, is the repetitive or random deviation from the nominal surface that forms the 3D topography. Surface texture includes:

1) *Roughness:* Asperities in the form of surface roughness are formed by fluctuations in the surface of shorter wavelengths, characterized by hills (local maxima) and valleys (local minima) of varying amplitudes and spacing .They include the features which are intrinsic to production process such as traverse feed marks and other irregularities.

2) *Waviness:* It is the surface irregularity of longer wavelength and is referred to as macro-roughness. It may result from factors such as machine or workpiece defections, vibrations, chatter, heat treatment or warping strain.

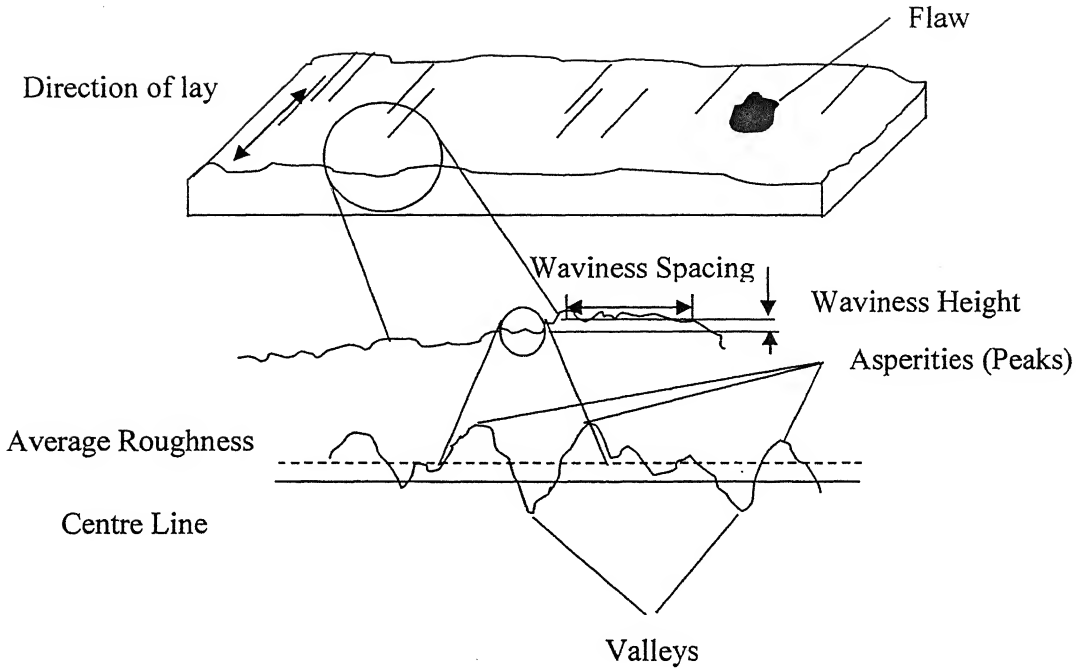

Figure 1.1: Surface Texture

3) *Lay:* It is the principal direction of predominant surface pattern, ordinarily determined by the production methods.

4) *Flaws:* They are the unintentional, unexpected interruptions in the texture.

1.1.2 Surface Roughness Parameters

Surface Roughness most commonly refers to the variation in the height of the surface relative to a reference plane. It is measured either along a single line profile or along a set of parallel line profiles (surface maps). It is usually characterized by one of the two statistical height descriptors advocated by ANSI and ISO. These are:

(i) *Centre Line Average (CLA, R_a)*: It is defined such that, the area between the profile and mean line above and below the mean line is equal. Therefore it can be mathematically represented as,

$$R_a = CLA = \frac{1}{L}\int_0^L |z - m| dx \tag{1.1}$$

where,

$$m = \frac{1}{L}\int_0^L z dx$$

(ii) *Standard Deviation or Variance (RMS Value, σ)*: It is the square root of the arithmetic mean of the square of the vertical deviation from the mean line. Mathematically it can be presented as,

$$\sigma^2 = \frac{1}{L}\int_0^L (z-m)^2 dx = R_a^2 - m^2$$

$$R_q^2 = RMS^2 = \frac{1}{L} \tag{1.2}$$

(iii) *Skewness (s_k) and Kurtosis (k) Statistical Height Descriptors:* They are defined as below,

$$s_k = \frac{1}{\sigma^3 L}\int_0^L (z-m)^3 dx \tag{1.3}$$

$$k = \frac{1}{\sigma^4 L}\int_0^L (z-m)^4 dx \tag{1.4}$$

(iv) *Five Extreme-Valued Height Descriptors:*

1) R_t Distance between Highest Asperity and Lowest Valley

2) R_p Distance between Highest Asperity and Mean Line

3) R_v Distance between Lowest Valley and Mean Line

4) R_z Distance between Average 5 Highest Asperities and 5 Lowest Valleys

5) R_{rpm} Distance between Average 5 Highest Asperities and Mean Line

1.1.3 Origin of Surface Roughness

The origin of poor surface finish in machining operations is caused by three broad phenomenons:

(i) The tool geometry and kinematics relative to the part, often induce feed marks.

(ii) Self excited and machine tool vibrations.

(iii) Surface plastic deformations resulting from a worn tool, BUE or material softening that occur especially at high temperature and insufficient cooling.

1.2. In-process Surface Roughness Measurement

In-process or online surface roughness measurement means that the surface roughness is measured during the cutting process. Thus the need is to measure the roughness of the freshly cut workpiece surface as soon as it is produced by the cutting process. Therefore the measuring head should move along with the tool post as in turning operation. This type of measurement is extremely productive for industries as surface roughness measurement is generally a post machining operation. The part whose surface roughness is greater than the prescribed roughness is to be rejected or re-machined, which reduces the productivity drastically.

1.2.1. Types of In-process Measurements

Various types of contact and non-contact measuring devices have been developed for in-process surface roughness as given in Fig. 1.2.

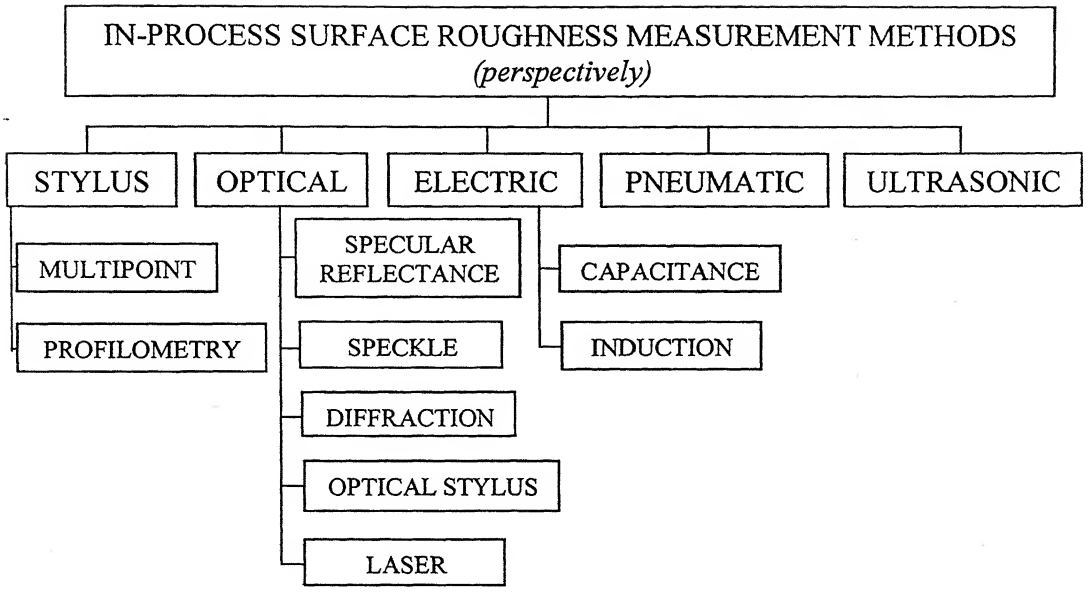

Figure 1.2: Various types of In-process surface roughness measurement

For on-line measurement of surface roughness contact methods were not feasible, so most of the attempts were made with non-contact methods. This is because the contact head of such instrument will wear out extremely fast under the dynamic cutting conditions.

1.2.2 Problems faced during online measurement of Surface Roughness

Direct surface roughness measurement is needed for machining control as there is no absolute, robust way to predict the roughness analytically or experimentally. There seem to be numerous factors that affect the surface roughness. Controllable process parameters include: feed, cutting speed, tool geometry and setup. Other factors which are harder to control include tool, workpiece, machine vibrations, tool wear and degradation, and workpiece variability.

1.2.3 Methods of Measurement

Due to the practical problems direct on-line measurement of surface roughness is difficult to achieve. For example non-contact type measuring devices like optical, pneumatic cannot be used when cutting fluid is used due to clouding. So indirect methods of measuring the on-line surface roughness have gained popularity. The different methods are discussed below.

1) *Direct method:* It involves the measurement of Surface Roughness directly through some mechanical stylus, opto-electrical sensor etc, as shown in Fig. 1.3(a).

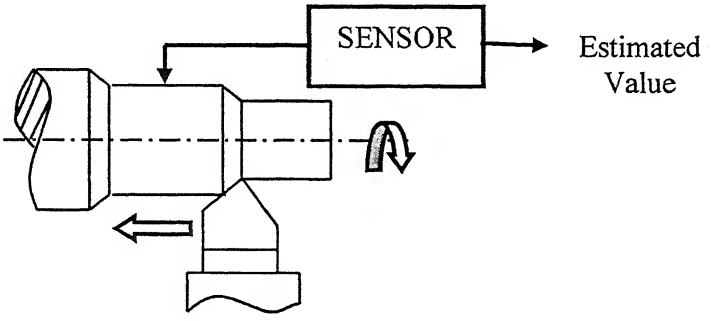

Figure 1.3(a): Direct method of on-line surface roughness measurement

2) *Indirect method:* In this method the surface roughness is estimated indirectly through some other characteristic like cutting force for example and a model. Thus difficult to measure characteristics can be measured more easily through other easily measured characteristic, shown in Fig. 1.3(b).

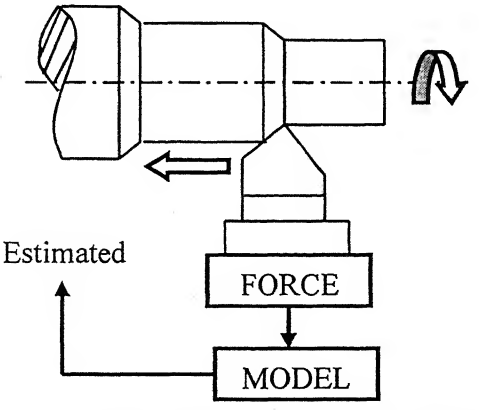

Figure 1.3(b): Indirect method of on-line surface roughness measurement

3) *Fusion method:* It is similar to indirect method except that more than one process characteristic is measured. The cutting speed, feed, depth of cut in terms of cutting temperature and radial and axial cutting force can be used for on-line measurement of surface roughness, using a fusion model, as shown in Fig. 1.3(c).

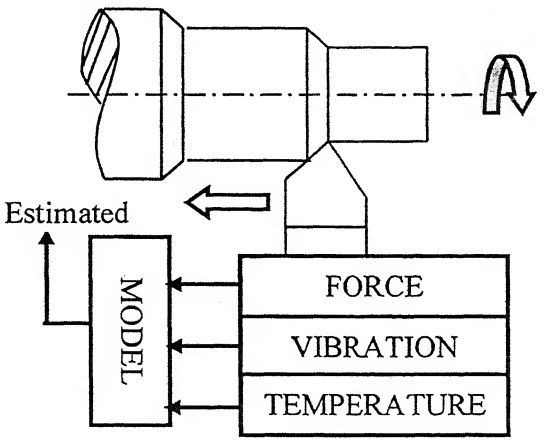

Figure 1.3(c): Fusion method of on-line surface roughness measurement

1.3 Literature Review

Preliminary work on on-line monitoring of machining had been reported in the year 1976 by Micheletti *et al* [1]. They had given an overview of the general characteristics required for sensors suitable for on-line monitoring. They gave the concept of direct and indirect measurement of tool wear. Direct measurements were made with the help of optical, electrical, radioactive or pneumatic sensors, which measured the tool wear directly and were mostly offline operations. On the other hand from the signals during measurements of cutting force, torque, vibration, roughness etc, tool wear was measured indirectly. The indirect measurement systems were shown to be more suited for on-line monitoring of tool wear.

In 1981, Shiraishi [2] developed a technique for on-line measurement of surface roughness which employed an optical method. He used double laser beam which made it possible to detect the surface roughness not only along the circumference but also along the feed direction. He also concluded that chipping and chattering can be detected sensitively along with both measurement directions and the maximum roughness value is always obtainable from the reading along the feed direction.

Coker and Shin, in 1994 [3], used an ultrasonic system for online monitoring and control of surface roughness. They developed a new system that utilized the reflected intensity of ultrasonic beams from the surface. The system was capable of measuring both surface roughness as well as tool wear experimentally. The on-line control of surface roughness was obtained by a geometric adaptive control scheme resulting in surface roughness within 10% of targeted value.

In the same line as Shiraishi's work [2], Lee *et al* [4] in 1987 developed an online surface roughness and form accuracy measurement technique for ground surface. They measured the surface roughness by analyzing the radiational pattern of a laser beam from the surface. They suggested that the technique can be implemented for industrial purpose and is capable of monitoring a surface roughness heights ranging from 0.10 to 6.0μm RMS value.

In 1987, Shiraishi [5] described a modified theory based on the work of Beckmann and Spizzichino in connection with R_{max} roughness of a turned surface. He concluded that the ratio of the two reflectances provides a good performance of surface roughness evaluation from the point of view of high sensitivity. He also stressed on the applicability of the system for on-line monitoring.

Choudhury *et al* [6] in 1995, used a bifurcated optical transducer along with a laser source for measuring wear online and also suggested the use of the same for surface roughness. The system can be effectively used for on-line monitoring in experiments. The bifurcated optical transducer is a Y-shaped optical fiber which has annular section at the

sensing head. The inner section was used for passing laser beam and the outer section for the beam reflected from the measured surface. In 1995 Jin et al [7] used an optical fiber system for indirect measurement of force by measuring the displacement occurring due to the forces during cutting. Zhang *et al* [8] in 1997 have also used a similar optical fiber sensor system for measurement of surface roughness.

Once the on-line surface roughness measurement technique has been obtained, the model for the cutting process has to be developed which will correlate the surface roughness along with the various input parameters. The choice of the input parameters and type of model have been decided based on the past research works.

Along with the development of sensors for on-line measurement of surface roughness, mathematical models were also developed to optimize the cost and the difficulty of on-line measurements of surface roughness in turning. Analytical models for the above had been developed by Vajpayee [9] in 1981. He also considered the effect of tool wear. The technique was based on the principle of overlapping of successive cuts. The analytical model gave more accurate relation to feed and nose radius of the cutting tool to surface roughness.

There are different types of mathematical techniques used for modeling the turning operation. They are mainly Regression Analysis [11-14], Artificial Neural Network [15-23], Fuzzy-Neural Network [24] and Abductive Network [26]. In Regression Analysis prediction models are generally used to predict one or more output parameters like force [10], temperature [14], surface roughness [11-14], etc.

Choudhury *et al* [11] developed a first and second order surface prediction models for turning EN24T steel utilizing surface response methodology. A factorial design technique has been used to study the effects of the main cutting parameters such as cutting speed, feed and depth of cut on surface roughness. They concluded that from the analysis of variance, the second order prediction model is more adequate.

Escalona *et al* [12] used variables like feed rate, tool nose radius and cutting speed to develop a regression model to relate them with surface roughness. They developed a multiple regression model for different types of steels and concluded that depth of cut has insignificant effect on surface roughness.

Chen *et al* [13] developed a multiple regression model, for in-process recognition of surface roughness for milling operation. They have developed eight different regression equations and with four input parameters like speed, feed, depth of cut and vibration average per revolution. The overall accuracy of their models was 81.7% and supported the use of regression techniques to model the dynamic machining processes. They also suggested that the number of experiments have to be increased greatly to drastically increase the accuracy of the regression models,. Thus they proposed the use of neural network and fuzzy sets as an alternative.

The inadequacy of the regression models made researchers look into other alternatives. Thus they started using newly developed concepts of neural, fuzzy and abductive networks.

In 1990 Rangwala and Dornfeld [15] have used neural network to integrate information from multiple sensors (acoustic emission and force) in order to recognize the occurrence of tool wear in a turning operation. According to them, the superior learning and noise suppression abilities of these networks enable high success rates for recognizing tool wear under a wide range of cutting conditions. They stated that the parallel computing ability of these networks offers the potential for application the monitoring and control of real time manufacturing environments which inherently have large process abnormalities.

The difficult to model tool condition monitoring was the field in machining where neural network was extensively used. Dimla *et al* [16] summarized that supervised as well as unsupervised neural network architectures have been applied in the Tool Condition Monitoring (TCM) problem with fairly similar results. The most widely used neural

network architecture was Multi Layer Perceptron due to their acceptable error prediction levels and its rate of convergence adequate in TCM problems.

Susič *et al* [17] developed an online estimation of surface roughness and surface hardness involved in sliding friction process. The information about the process was extracted from the acoustic emission (AE) signal generated by friction. The relationships between the AE signal and the surface properties were modeled empirically by an adaptive system comprised of a self-organizing neural network and the conditional average estimator which is capable of performing a mapping from AE spectrum to the surface parameters. The system performance was tested in the online pin-in-disk experiment for four different classes of surface roughness and/or pin hardness. The recognition reliability for placing given cases in correct class was found to be greater than 96% for the majority of the experiments. Their technique was effective for lower number of experimental samples too. They claimed that their method was better than the most frequently applied back propagation rule.

In 2003, Risbood *et al* [18] used a neural network model to predict the surface roughness within a reasonable degree of accuracy by taking the acceleration of the radial vibration of the tool holder as a feedback. They fitted different neural network models for dry and wet turning operations by HSS and carbide tools. They observed that during turning surface finish improves with increasing feed up to some value where it starts deteriorating with further increase in feed in carbide tools whereas in HSS tools such observations were not found. The accuracy of the prediction of surface roughness was around 20%. The performance of the developed neural network model was assessed by carrying out a number of experiments involving dry and wet cutting with HSS and carbide tools.

Sata *et al* [19] in 1985 have made an analysis of surface roughness generation in turning operation. They examined the turning operation using FFT analyzer and found that the roughness of the turned workpiece was composed of several periodical components, like the cutting tool feed component, the spindle rotation error component and the chatter

vibration error component. To examine the origin of these error components, a series of cutting tests were conducted with different spindle rotation arrangements and work piece materials. They stated that the relative displacement due to the tool and the workpiece modifies the surface roughness profile in the axial direction.

Jang *et al* [20] tried to correlate the surface roughness with cutting vibrations to develop an on-line roughness measuring technique. They developed an algorithm which utilized the relative cutting vibrations between the tool and the workpiece, which were measured through an inductance pick up filtered by an analogue band pass filter for a specific vibration component. The cutting vibration signals of a specific frequency were superimposed onto the kinematic roughness, which was calculated from the tool edge radius and fed rate. Experimental results showed good correlation between the simulated roughness obtained using the proposed algorithm and the roughness actually measured with a surface profilometer. Further they showed that the surface roughness along the work piece without chatter had specific frequency components that were determined by the feed marks in the lower frequency range and were closely related to the natural frequencies of the machine tool structure.

Lin and Chang [21] developed a surface topography simulation model for turning. The model incorporated the effects of the relative movement between tool and workpiece with the effects of tool geometry to simulate the resultant surface. The surface topography simulation model was used to study the effects of vibration on the surface finish profile. They found that the vibration ratio, the ratio between the vibration frequency and the spindle rotation speed, was a more important vibration parameter than the vibration frequency on the characterization of the surface finish profile.

Beauchamp *et al* [22] studied the collection and analyzed the surface roughness and tool vibration data generated by dry turning of mild steel samples at different feed, speed, tool nose radius, tool length and work piece length. A full factorial experimental design that allowed consideration of a three level interactions between independent variables, were conducted. Vibration analysis revealed that the dynamic force, related to the chip

thickness variation acting on the tool, is related to the amplitude of the tool vibration at resonance and to the vibration of the tool natural frequency while cutting. The analogy of the effect of the cutting parameters between the tool dynamic forces and surface roughness was also investigated. The results also showed the second order interactions between the cutting speed and the tool nose radius, along with third-order interaction between the feed rate, cutting speed and depth of cut are the factors with the greatest influence on the surface roughness and tool dynamic forces in this type of operation and parameter levels studied. The results showed that the depth of cut did not have significant effect on surface roughness, except when operating within built-up edge range. The feed rate and tool nose radius were the variables that produce the most important effects on the surface roughness followed by cutting speed.

Azouzi and Guillot [23] developed the relationships of the readily sensed variables in machining to surface roughness, and established its sensitivity to process conditions. Based on the experimental data and using statistical tools, they found that the cutting feed, depth of cut and two components of cutting force (radial and feed force components) provided the best combination to build a fusion model for on-line estimation of surface roughness. Surface roughness was assessed with an error varying from 2 to 25% under different process conditions. The paper also demonstrates the performance of neural network in situations where nonlinear mappings must be automatically acquired from the training data.

In 2001, Abouelatta and Mádl [24] studied the relation between the surface roughness and cutting vibrations in turning, and derived mathematical models for predicted surface roughness parameters based on the cutting parameters and machine tool vibration. Tool vibration was measured both in the radial and the feed direction. The surface roughness models depending on both cutting parameters and machine tool vibrations were more accurate than the models depending only on the cutting parameters. They concluded that the maximum height roughness parameter depends greatly on the rotational cutting speed.

In this work, the control of surface roughness has been implemented with the help of the correlation between the displacement of the cutting tool with respect to the workpiece in turning operation. This relative displacement was the effect of machine tool vibration as suggested by Tobias [25] that exciting forces during cutting process do not come from external sources but from the process itself. Tobias presented a model for thrust force for dynamic cutting and proposed a single degree of freedom chatter theory for the vibrating machine tool system including the effect of regeneration. Regeneration was considered to be caused by the variation of the uncut chip thickness when successive cuts overlap. He assumed a 'direct receptance' model of a single degree of freedom to approximate the machine tool structure. Though it had shown appreciable similarity with experimental results, but later Tlusty and Polacek [26] accepted models in which it is assumed that any mode participates not by its 'direct receptance', but by its 'cross receptance'. Thus the earlier assumption that the tool edge describes a straight linear motion was not the actual case, but it describes an elliptical path during chatter of the machine. Still the 'direct receptance' model is used as it is elegant in basic principle and fits to the control strategy with the help of a piezoelectric actuator along with the mode coupling coefficient.

Mie *et al* [27] established a nonlinear theoretical model to discuss the effects of the effect of tool geometry on the dynamic instability. They obtained a good correlation between the experimental results and the theoretical analysis for active suppression of machine tool chatter by on-line variation of tool geometry.

Choudhury *et al* [28] showed that the surface roughness can be improved by compensating the relative displacement between tool and workpiece. They used a bifurcated optical fiber for on-line measuring the vibration at the tool-workpiece interface. The signal was phase shifted, amplified and fed to a specially designed piezoelectric actuator supporting the tool. The closed loop feedback contour stabilized the machine tool-cutting process system by providing an equal and opposite force. From the results they concluded that there was significant improvement in the dynamic characteristics of the machine tool, resulting in considerably higher productivity and accuracy.

Choudhury *et al* [29] described a control system designed to improve the surface finish during turning by reducing the vibration of the machine tool. Vibration control was achieved by sensing the relative vibration between the tool and the work-piece, generating a force which tends to neutralize the excitation. The control system consisted of an optical sensor for measuring the relative displacement between the tool and the work-piece, and a tool actuator for the control action, the optical sensor being made from a bunch of bifurcated optical fibers, whilst the tool actuator was an electromagnetic device. The control system had been tested experimentally during turning under various cutting conditions. The improvement in surface finish was verified by comparing two identical surfaces, one machined with and the other without the designed feedback-control device. Results indicated that the amplitude of vibration decreased by 33% whilst the resulting improvement in the surface finish was about 22%. They concluded that the control device developed was quite simple and can be used in an industrial environment.

Tarng *et al* [30] explored the use of piezoelectric inertia actuator mounted in a cutting tool and acting as a tuned vibration absorber for the suppression of chatter in turning operations. They suggested that the piezoelectric actuator must have natural frequency equal to that of the cutting tool and should have a high damping ratio. Through experimental results they have shown that the chatter in turning can be greatly suppressed and the cutting stability increased six times by using their technique.

Lee *et al* [31] used a passive vibration control system using a dynamic vibration absorber mounted on a cutting tool which had been developed to suppress vibrations in turning operations. They showed that the dynamic response of the cutting tool can be greatly improved due to the presence of the dynamic vibration absorber attached to the cutting tool. Several experimental cutting tests have been performed, experimental results showing that the proposed vibration control strategy is practical and effective.

Pan *et al* [32] suggested that through active control damping can be increased in some selected frequency ranges chatter in machine tool can be reduced instead of increasing

the damping of the system, and is more economical and practical. They commented that in active chatter control of machine tools, the most effective way to suppress the chatter is to place the actuator as close as possible to the too tip. The flexibility effect of the tool shank made them propose two advanced control algorithms. These control algorithms brought about a reduced the chatter by 20dB.

Tewani *et al* [33] studied the use of an active dynamic absorber to suppress machine tool chatter in a boring bar. The vibration of the system was reduced by moving an absorber mass using an active device such as a piezoelectric actuator, which generated an inertial force counteracting the disturbance on the main system. An equivalent lumped mass model of a boring bar with active dynamic absorber was considered. A cutting process model that considered the dynamic variation of shear and friction angle, causing self-excited chatter during the cutting process, was applied to the lumped mass model. The theory of regenerative chatter was also applied to the model. Stability boundaries had been calculated for maximum permissible width of cut as a function of cutting speed. A comparison of the boundaries for chatter-free cutting operation of a plain boring bar, a boring bar with passive tuned dynamic absorber and a boring bar with active dynamic absorber was presented in this paper. The comparison shows that a substantial increase in the maximum permissible width of cut for stable cutting operation over a range of cutting speeds was obtained for a boring bar equipped with an active dynamic absorber. They also showed that the surface roughness improved due to the implementation of the active control.

Jang and Tarng [34] reported the use of a piezoelectric actuator to act as an active vibration damper on a cutting tool. The piezoelectric actuator with an inertial mass was attached to the controlled cutting tool. The actuator resonance could be well tuned over a wide frequency range by adjusting the size of the inertial mass, so that the actuator could provide an extremely large damping force to suppress undesired vibration of the cutting tool at the resonance frequency of the actuator. Experimental results were presented to illustrate the proposed method. Free vibration tests had shown that the damping ratio of the cutting tool could be increased about four times by using the active control technique

proposed in this study. In addition, when the cutting tool was excited by a harmonic disturbance, experimental results showed that the forced vibration on the cutting tool could be suppressed up to 90% with the aid of the piezoelectric actuator.

In their work, Potoçnik and Grabec [35] proposed a control strategy with an objective to improve the manufacturing quality, namely surface finish of the workpiece. Manipulation of the tool support, which was elastically coupled to the tool, was selected as a control variable. Using the proposed nonlinear model predictive control scheme they succeeded to achieve the control objective for the case of a cutting process simulated by a nonlinear analytical model. Consequently, they confirmed the assumption that the tool support manipulation can be used to improve the manufacturing quality. It was demonstrated that a relatively simple feedforward network with ten hidden neurons was applicable to the predictive control of the cutting process. The results show considerable improvement of the manufacturing quality obtained by model predictive control. The drawback of the method was the intensive computation performed during the optimization loop. For a real-time application in high-precision machining, a previously trained neural controller has been suggested to be implemented in hardware and then applied for autonomous control of the process.

Various control strategies had been proposed for the active control of vibration in recent past. Snyder and Tanaka [36] derived the architecture of a feedforward neural network based control system for active control of vibration. But they concluded that more work was required to improve the predictability and the consistency of the performance before the neural network controller could be implemented as a practical alternative to the current linear feedforward systems. Tewani *et al* [37] concluded that the disturbance rejection in optimal control strategy was most effective in reducing the amplitude of vibrations. But it was difficult to implement. The control system posed as a Linear Quadratic Regulator was easier to implement in practice, though it was not as efficient as optimal control strategy. They suggested that the optimal control strategy was also more effective than the acceleration feedback control. Marra *et al* [38] developed a robust control system to minimize the vibration response in machining to unknown disturbances.

Their method consisted of on-line identification of the system's state space equations couple with an H_∞ optimal controller design. This robust controller was used to eliminate vibrations in cutting operations of a boring bar with an active dynamic absorber. Robustness was demonstrated by varying the system's dynamic characteristics (i.e. changing the length to diameter ratio of the boring bar) without adjusting the calculated control parameters. The results obtained for the H_∞ case showed that it had a significant improvement over LQR method.

1.4 Problem Definition

The problem definition for this work can be broadly divided into two parts. First part includes the on-line monitoring and the modeling of surface roughness in turning operation. The second part includes the on-line control of surface roughness arising from the relative displacement between tool and workpiece.

The on-line monitoring of surface roughness was achieved with the help of a bifurcated optical transducer and a laser gun as a light source. The transducer being a displacement transducer in nature should pick up the radial component of vibration occurring during the cutting operation along with the surface roughness. Thus it was necessary to observe the on-line surface roughness and the vibration separately. Moreover the effect of various cutting parameters on surface roughness were planned to be investigated. For this both regression and neural network models were to be used and the significant parameters obtained from literature review were to be included. Design of experiment has to be used to reduce the total number of runs without affecting their individual significance. After selecting the input parameters and conducting experiments, regression and neural network models have to be developed. They have to be compared to study their suitability for modeling surface roughness. Various types of regression as well as neural network models have to be developed and compared with each other to select the most accurate one. The models thus selected have to be experimentally validated to find their accuracy of prediction.

In the second part, a control strategy was planned to be developed which can keep the surface roughness arising from the relative movement between the tool and the work piece minimum. This strategy has to be applied for the machine tool used for this work. For this a dynamic model for the cutting process has to be developed and the machine tool characteristics have to be determined. After the system identification, the controller has to be designed for a closed feedback loop. Through simulation the above proposed control strategy has to be implemented and results should be compared with the actual cutting process-machine tool system.

1.5 Layout of thesis

The documentation of the thesis work has been divided into the following chapters.

Chapter I: Introduction and Literature Survey

This chapter gives the introduction to on-line monitor and control of surface roughness in turning operation. The literature review is provided to give a brief idea of the level work previous research works that have been done in this particular field. The problem proposed in this work has been defined.

Chapter II: Theoretical Analysis

It deals with the theoretical analysis of the mathematical modeling used. The mathematical models include Regression models as well as Neural Network models. The theoretical backgrounds of Linear and Multiple Regression models have been dealt with along with Analysis of Variance (ANOVA) for the above models. Neural Network models have been extensively discussed including the various architectures, learning rules, training rules and back propagation algorithm are presented.

Chapter III: Experimentation

This chapter deals with the experimental set-up and the design of experiments used for carrying out the experiments. The various components designed as well as used are given along with their specifications. The steps of experimentation have also been included.

Chapter IV: Experimental Results and Discussion

This chapter deals with the results obtained from the experiments and developing the mathematical models from the experimental data. Both regression and neural network models have been developed and compared with each other. The best models have been validated with a set of validation data.

Chapter V: Vibration in turning operation and its control

This chapter deals with the causes of vibration in machine tool during the cutting operation and means of controlling it with the help of a piezoelectric actuator. The coefficients of the dynamic model for cutting process and characteristics of machine tool have been determined. Then the proposed control strategy had been developed for simulating a closed loop machine tool system along with the cutting process and the feed back control.

Chapter VI: Conclusion and Future Directions

The results and discussions of the on-line monitoring and modeling of surface roughness as well as its control are discussed in this chapter. Directions for future works are also included.

Chapter II

Theoretical Analysis

2.1 Mathematical modeling for machining processes

2.1.1 Introduction

The primary objective of modeling of machining operation is to develop a predictive capability of machining performance in order to facilitate effective planning of machining operations to achieve optimum productivity, quality and cost. Machining performance can be of two categories:

a) *Technical Aspects*, accuracy of shape and dimension and surface roughness and properties of subsurface layer of the work piece.

b) *Commercial Aspects*, useful for management such as machining time and cost, throughput time, the fraction of rejects etc.

2.1.2 Difficulties in modeling machining processes

Difficulties in modeling machining processes are largely attributed to the following factors:

1) Lack of fundamental understanding of the basic mechanism and interactions of cutting tool and work piece material even in the simplest case s.
2) The different purposes and the great variety and complexity of the real machining applications.

Robust and reliable models of machining operation are difficult to be formulated, owing to a variety of issues such as:

1) Large variety of machining processes
2) Large variety of input variables
3) Large variety of internal variables
4) Large variety of output variables
5) Work material properties are difficult to determine
6) Complex tool work piece material interface
7) Machining is a small scale operation
8) Process of chip formation is not uniquely defined
9) Large variety of chip types and chip formation
10) Large machining databases are required

Significant effort has been made towards understanding the complex interactions with the basic mechanism and their complex interactions, such that the complete and robust model may be obtained, ready for practical application. Analytical, numerical and AI based methods are amongst the most commonly used techniques for predictive modeling for machining operation for practical application, would consist of the following phases:

I) The development of models for machining variables
II) The development of models for machining performance
III) The development of models for obtaining optimal machining conditions

2.1.3 Purpose of modeling of machining operation

There are different reasons why models of metal cutting operation may be required. The most well known examples are:

1. Design of processes
2. Optimization of processes
3. Control of processes
4. Simulation of processes
5. Design of equipment

2.1.4 Different types of Models

The two types of model for the turning process, developed in this work were *Multiple Regression Models* and an *Artificial Neural Network (ANN) Model*. The outputs of both the models had been compared with the experimental values. Three as well as four input models, with inputs as *feed* (mm/rev), *speed* (m/min), *rake angle* (°) and amplitude (a) of displacement due to vibration between the tool and the workpiece. The surface roughness, R_a (μm) was the dependent output. The three and a four-input models developed, are shown in Fig. 2.1. In the three-input type as shown in Fig. 2.1(a), amplitude of vibration is not considered. In the four-input type the measured amplitude of vibration, which is an output of the cutting process, is taken as the fourth input parameter, as done by Chen [13] and Risbood [18].

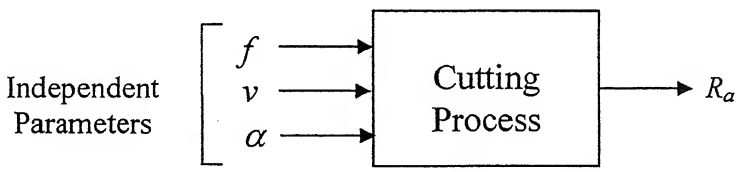

Figure 2.1 (a): Three-input model

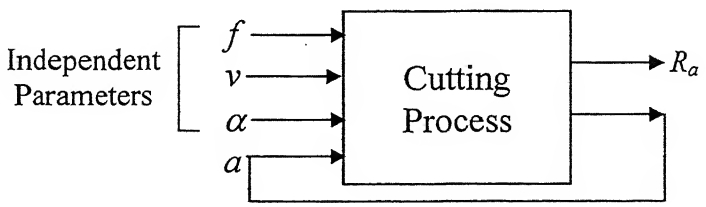

Figure 2.1 (b): Four-input model

2.2. Linear Regression Models

In general a linear regression model of a response variable (y) in terms of k independent or predictor variables is represented as follows,

$$y = \beta_0 + \beta_1 x_1 + \beta_2 x_2 + ... + \beta_k x_k + \varepsilon \quad (2.1)$$

where the terms x_1, x_2,...., x_k are independent or controllable variables, β_0, β_1,..., β_k are regression co-efficients and ε is a random error term. The regression co-efficients represents the effect of a particular independent variable on the response variable. For example β_1 measures the expected change in y per unit change in x_1, when the other variables are held constant. These types of models are known as *without interaction* models. If we consider the following model,

$$y = \beta_0 + \beta_1 x_1 + \beta_2 x_2 + ... + \beta_k x_k + \beta_{12} x_1 x_2 + \beta_{23} x_2 x_3 + ... + \varepsilon \quad (2.2)$$

we have now interaction terms, such as, with x_1 and x_2, x_2 and x_3, so on. These types of models are called *with interaction models.*

Another type of regression model is *response surface model.* A response surface model with two variables may be represented as follows,

$$y = \beta_0 + \beta_1 x_1 + \beta_2 x_2 + \beta_{11} x_1^2 + \beta_{12} x_1 x_2 + \beta_{22} x_2^2 + \varepsilon \quad (2.3)$$

which can be written in terms of linear multiple regression equation as given below,

$$y = \beta_0 + \beta_1 x_1 + \beta_2 x_2 + \beta_3 x_3 + \beta_4 x_4 + \beta_5 x_5 + \varepsilon \quad (2.4)$$

where $x_3 = x_1^2, x_4 = x_1 x_2, x_5 = x_2^2, \beta_3 = \beta_{11}, \beta_4 = \beta_{12}$ and $\beta_5 = \beta_{22}$.

Let us have n $(n>k)$ response variables say $y_1, y_2, y_3, ..., y_n$ and along with each observed response y_i, we will have an observation on each regressor variable and let x_{ij} denote the ith observation or level of variable x_j. We assume the error term, ε in the model has $E(\varepsilon)=0$ and $V(\varepsilon)=\sigma^2$ and that the $\{\varepsilon_i\}$ are uncorrelated random variables.

Writing the model equation in terms of the observations yields,

$$y_i = \beta_0 + \beta_1 x_{i1} + \beta_2 x_{i2} + \beta_3 x_{i3} + ... + \beta_{k-1} x_{ik-1} + \beta_k x_{ik} + \varepsilon_i \quad (2.5)$$

which can be written as

$$y_i = \beta_0 + \sum_{j=1}^{k} \beta_j x_{ij} + \varepsilon_i; \quad i = 1,2,3,...n \tag{2.6}$$

The method of least square chooses β's such that the sum of all the square errors between the observed and the calculated response variable ε_i, is minimized. Thus the least square function is given by

$$L = \sum_{i=1}^{n} \varepsilon_i^2$$
$$L = \sum_{i=1}^{n} \left(y_i - \beta_0 - \sum_{j=1}^{k} \beta_j x_{ij} \right)^2 \tag{2.7}$$

The function L is to be minimized with respect to $\beta_0, \beta_1, ..., \beta_k$. The least squares estimators, say $\hat{\beta}_0, \hat{\beta}_1, ..., \hat{\beta}_k$, must satisfy the following

$$\left. \frac{\partial L}{\partial \beta_0} \right|_{\hat{\beta}_0, \hat{\beta}_1, ..., \hat{\beta}_k} = -2 \sum_{i=1}^{n} \left(y_i - \hat{\beta}_0 - \sum_{j=1}^{k} \hat{\beta}_j x_{ij} \right) = 0 \tag{2.8}$$

and

$$\left. \frac{\partial L}{\partial \beta_j} \right|_{\hat{\beta}_0, \hat{\beta}_1, ..., \hat{\beta}_k} = -2 \sum_{i=1}^{n} \left(y_i - \hat{\beta}_0 - \sum_{j=1}^{k} \hat{\beta}_j x_{ij} \right) x_{ij} = 0, for\ j=1,2,...,k \tag{2.9}$$

Simplifying we get the least square normal equations, which are easier to solve by matrix algebra. Writing the model in terms of the observations, we get

$$y = X\beta + \varepsilon \tag{2.10}$$

where

$$y = \begin{bmatrix} y_1 \\ y_2 \\ . \\ . \\ y_n \end{bmatrix}_{(nx1)} ; \quad X = \begin{bmatrix} 1 & x_{11} & . & x_{1k} \\ 1 & x_{21} & . & x_{2k} \\ . & . & . & . \\ 1 & x_{n1} & . & x_{nk} \end{bmatrix}_{(nxk)} ; \quad \beta = \begin{bmatrix} \beta_0 \\ \beta_1 \\ . \\ . \\ \beta_n \end{bmatrix}_{(kx1)} \quad and \quad \varepsilon = \begin{bmatrix} \varepsilon_1 \\ \varepsilon_2 \\ . \\ . \\ \varepsilon_n \end{bmatrix}_{(nx1)}$$

Now form the above discussions we get the matrix form of the least square normal equation as:

$$X'X\hat{\beta} = X'y \tag{2.11}$$

and the fitted regression model as $\hat{y} = X\hat{\beta}$ (2.12)

In scalar notation, the fitted model is written as,

$$\hat{y}_i = \hat{\beta}_0 + \sum_{j=1}^{k} \hat{\beta}_j x_{ij}, \quad i = 1,2,3,\ldots, n \tag{2.13}$$

The difference between the observed (y_i) and the fitted value ($\hat{y}_i$) is denoted by e_i and given in the matrix form as, $e=y-\hat{y}$. Thus we find the unbiased estimator of the parameter β in the linear regression model, produced by the least square method, is given by the following equation as all the variables are known,

$$\hat{\beta} = (X'X)^{-1}X'y \tag{2.14}$$

Once we have obtained the un-biased coefficients, we now check the adequacy of the model with the help of a method known as the *analysis of variance*.

The test significance of a regression is a test to determine if there is a linear relationship between the response y and any of the regressor variables, $x_1, x_2, \ldots\ldots, x_k$. The appropriate hypotheses are:

$$H_0: \beta_1=\beta_2=\beta_3=\ldots\ldots=\beta_k=0 \tag{2.15}$$

$$H_1: \beta_j \neq 0, \text{ for at least one j} \tag{2.16}$$

Rejection of $H_1: \beta_j = 0$ implies that at least one of the regressor $x_1, x_2, \ldots\ldots, x_k$ contributes significantly to the model. The test procedure is a generalization of that used in simple linear regression. The total sum of squares S_{YY} is partitioned into sum of squares due to regression and a residual sum of squares, for example,

$$S_{YY} = SS_R + SS_E \tag{2.17}$$

and if $H_1: \beta_j = 0$ is true then, $SS_R/\sigma^2 \sim \chi_k^2$, where the number of degrees of freedom for χ^2 are equal to the number of regressor variables in the model. Also, it can be shown that the $SS_E/\sigma^2 \sim \chi_{n-k-1}^2$, and that SS_E and SS_R are independent. The test procedure for $H_0: \beta_j = 0$ is to compute

$$F_0 = \frac{SS_R/k}{SS_E/(n-k-1)} = \frac{MS_R}{MS_E} \tag{2.18}$$

and to reject H_0 *if* $F_0 > F_{\alpha,k,n-k-1}$. The procedure is usually summarized in an analysis of variance Table 2.1.

The set of computational formula for the sum of squares is given as below,

$$S_{YY} = y'y - \frac{\left(\sum_{i=1}^{n} y_i\right)^2}{n} \tag{2.19}$$

$$SS_E = yy' - \hat{\beta}X'y \tag{2.20}$$

and $SS_R = S_{YY} - SS_E$ gives,

$$SS_R = \hat{\beta}X'y - \frac{\left(\sum_{i=1}^{n} y_i\right)}{n} \tag{2.21}$$

Table 2.1: Analysis of Variance for significance of regression in Multiple Regression

Source of Variation	*Sum of Squares*	*Degrees of Freedom*	*Mean Square*	F_0
Regression	SS_R	k	MS_R	
Residual	SS_E	$n-k-1$	MS_E	MS_R/MS_E
Total	S_{yy}	$n-1$		

2.2.1 Modeling of surface roughness by Multiple Linear Regression equation

First a multiple regression Eq. (2.22) which excluded the interaction terms was developed by following the sequence in Fig. 2.2.

$$R_a = \beta_0 + \beta_1 f + \beta_2 v + \beta_3 d + \beta_4 A + \varepsilon \tag{2.22}$$

In addition to it another multiple regression model was developed, with two way interaction terms between independent variables.

$$R_a = \beta_0 + \beta_1 v + \beta_2 f + \beta_3 d + \beta_4 A + \beta_{11} v^2 + \beta_{22} f^2 + \beta_{33} d^2 + \beta_{44} A^2 + \beta_{12} vf + \beta_{13} vd + \beta_{14} vA + \beta_{23} fd + \beta_{24} fA + \beta_{34} dA + \varepsilon \tag{2.23}$$

The predicted R_a and experimental R_a were calculated and used for the selection of the more accurate model for the above modeling purpose. *Analysis of Variance* (ANOVA) was done to calculate the correlation, standard error, rms error and F-test values.

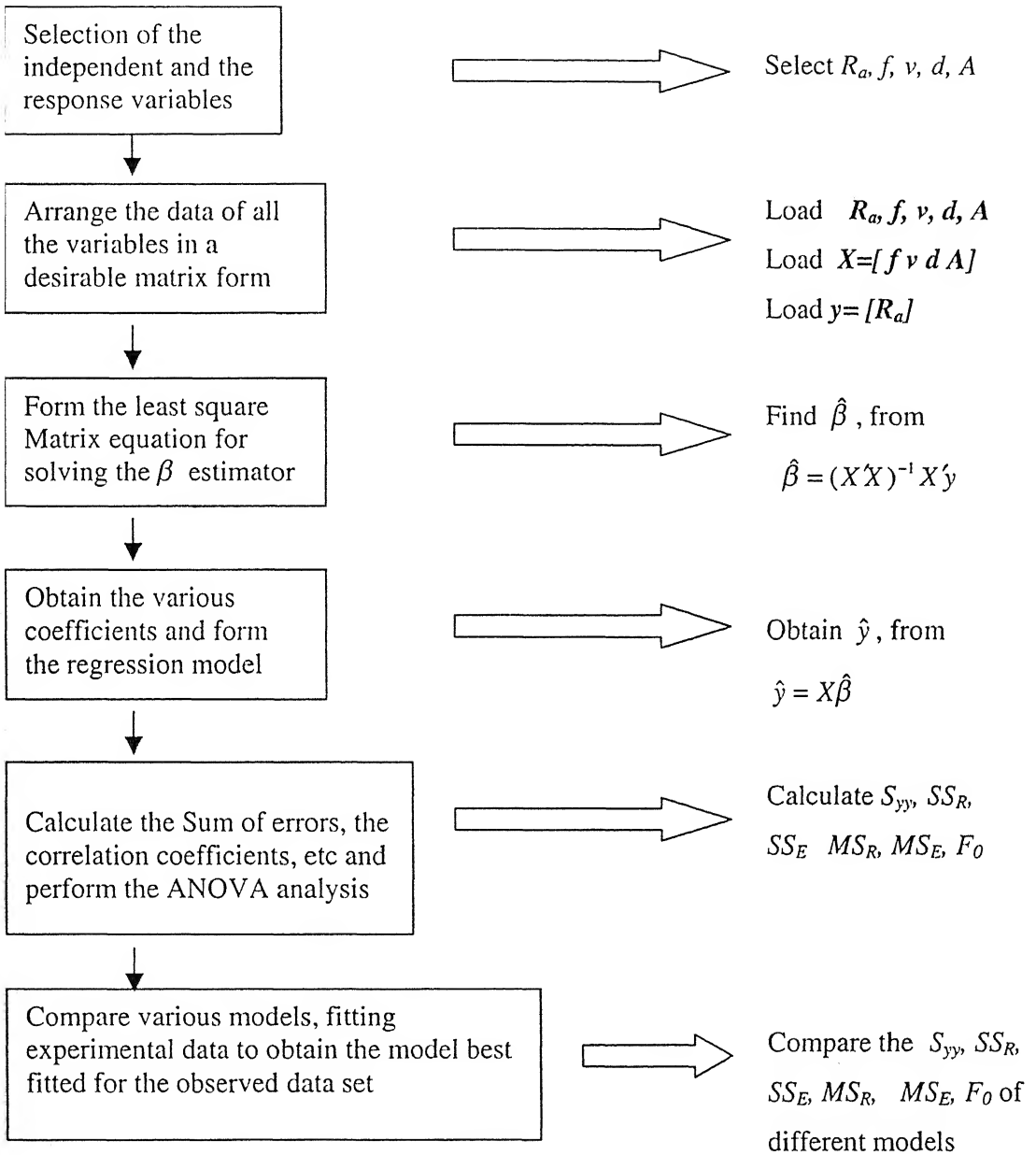

Figure 2.2: Statistical analysis procedure for multiple regression models.

2.3 Neural Network

2.3.1 Introduction

The Artificial Neural Network (*ANN*) consists of massive interconnections of simple processing units which simulates the human brain. These neurons have a pattern of connectivity among them and the knowledge can be represented by the strength of the connections, which is not fixed. Instead, the weights can be modified based on the experience, so the network can learn from its past experience, so as to simulate the human brain.

2.3.2 The General aspect of neural network

The general aspect of neural network is shown in the Fig. 2.3. There are a set of processing units (neurons) indicated by the dark circles in the figure. At each point of time, each unit has an activation value *a(t)*.This activation value is passed through a function to produce an output value *Y(t)*, which will pass through a set of unidirectional connections to other units in the system, so that

$$Y_i = F_i[a_i] \tag{2.24}$$

A real number associated with each connection called weight or strength *W (t)* of the connection, which determines, the amount of affect that the first unit has on the second one. Now all inputs with their weights are combined by some operator, usually addition, to yield

$$net_i = \sum W_{ij}(t) * Y_j(t) \tag{2.25}$$

The new activation value is now determined through a function '*f*', which is a function of the current activation value and the combined inputs, so that

$$a_i(t) = f_i(a_i(t); net_i) \tag{2.26}$$

A neural network learns by undergoing changes in the weight, as a function of experience.

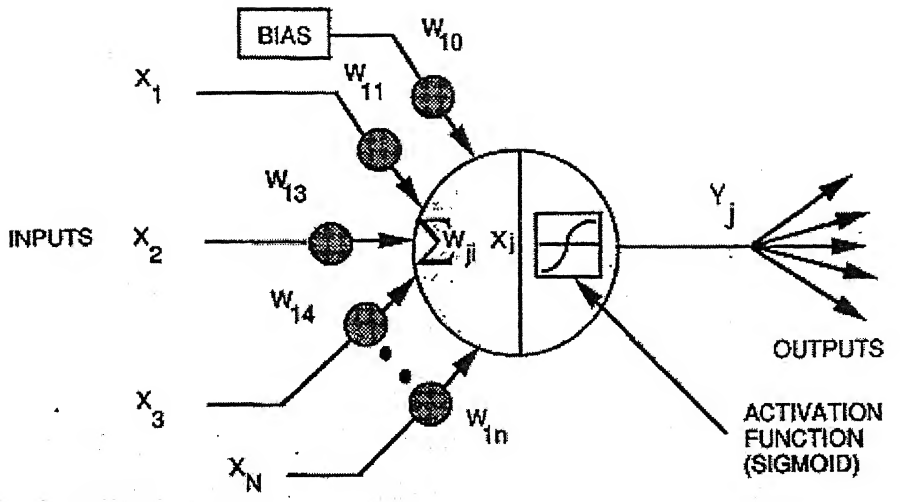

Figure 2.3: General representation of an ANN [43]

In their work Mc Clelland and Rumelhart [39] proposed eight aspects of a neural network. They are explained as below.

2.3.2.1 Set of Processing Units

The whole processing of a neural net is done by a set of processing units. Each unit receives inputs from its neighbors to compute an output value based on a function of the input it receives and to send the output to its neighbors. The system is inherently parallel. The processing units are divided into three kinds namely input, hidden and output units.

2.3.2.2 The state of activation

The state of the system at any time'*t*' is specified by a vector of *n* real numbers $a_n(t)$, which represents the pattern of activation over the set of processing units. Each element of the vector represents the activation of a unit at time'*t*'. Activation values may be continuous or discrete.

2.3.2.3 Output of the Units

Associated with each unit, u_i, there is an output function $F_i(a_i(t))$, which maps the current state of activation, a_i, to an output signal, $Y_i(t)$. So that $Y_i(t) = F_i(a_i(t))$ (2.27)

In some models 'F' is a threshold function or a stochastic function.

2.3.2.4 The pattern of connectivity

The pattern of connectivity of the system constitutes what a system knows and determines how it will respond to any arbitrary input. In many cases, the total input to the unit is simply the weighted sum of the separated inputs from each of the individual units.

2.3.2.5 The rule of propagation

This rule combines the output vector $Y(t)$, the output values of the units, with the connectivity matrices 'W' to produce a net input for each unit i.e.

$$net = W * Y(t) \quad (2.28)$$

2.3.2.6 Activation Rule

The net inputs of each type of impinging on a particular unit are combined with one another and with the current state of the unit to produce a new state of activation in accordance with a rule 'S'. We assume 'S' to be a sigmoid function, when *a (t)* is assumed to take on continuous values. In this case, an individual unit can saturate and reach a minimum or maximum value of activation.

2.3.2.7 Learning Rule

A learning rule is used to change the weights of interconnections. In principle there are three kinds of modifications,

a) The development of new connections

b) The loss of existing connections

c) The modifications of the strengths of connections that already exist.

There are many kinds of learning rules. Virtually all of them can be considered a variant of the Hebbian learning rule suggested by Hebb [40], in his classical book "Organization of Behavior (1949)".

2.3.2.8 Representation of the environment

This refers to a model of the environment in which this model exists. We often represent the environment as time-varying stochastic function over the space of input patterns.

2.3.3 Significance of Neural Networks in on-line monitoring

For better online monitoring of machining processes, it is necessary to have the knowledge of the dynamics of the cutting process which can be measured with the help of a response variable, but requires a mathematical model of the above. The formulations of these mathematical models may be based on either empirical analysis or physical models. The empirical models are limited by their nature and applicable only in some specific conditions. But the physical models are applicable in wider range but they are restricted by the difficulties in formulating the accurate models.

Intelligent evolution of sensor information is necessary to perform the monitoring problem, as it is difficult to have the actual physical model to describe the state of the process. Sensor feedback is essential if automated machines are to produce the correct size and surface finish. This problem can be solved by using neural networks which can find solutions for problems with unknown or complex internal relationships. A neural network takes an input numeric pattern and gives a numeric output pattern. Adaptation, or the ability to learn, is the most important property of neural networks and they work much like the human brain.

A neural network can be trained to map a set of input patterns onto a corresponding set of output patterns through training. During it the network gradually adapts the internal weights of the network, so as to reduce differences between actual network outputs, for a given set of inputs and the desired network outputs. Larger the training set, the more accurate is the estimation.

The concept of on-line control action might not be implemented effectively as due to inherent sensor and the controller delays, there will be delay in the control action(s). Thus one can use a trained neural network, and simulate the cutting process by simply giving input patterns and obtaining the output patterns, avoiding any time delay within the system. Thus neural network model is used as an estimator as well as a predictor.

2.3.4 Multiple-layer perceptrons

Multiple layered feedforward networks is an important type of neural networks, typically consisting of a set of sensory units that constitute the input layer, one or more hidden layers of computation nodes and an output layer. The input signal propagates through the network in the forward direction layer by layer basis. Multilayer perceptrons have been successfully been used [16] to solve many complex and diverse problems. Several learning procedures have been developed in ANN. Many of these learning methods are closely connected with a certain network topology, with the main categorization method distinguished by supervised and unsupervised learning. Among various existing learning methods, back propagation was adopted in this research work because of the following two reasons:

1) it is most representative and commonly used algorithm and relatively easy to apply
2) it has been proven to be successful in practical application

Specifically the error signal is generated by subtracting the desired (targeted) and the output response which is propagated in the backward direction, i.e. against the direction

of the synaptic connections. The synaptic weights are adjusted such that the error signal is minimized. The back propagation algorithm could be divided into two main process: learning and recalling corresponding to the backward and forward passes.

Learning Process:

Step 1: Given network parameters, set all the necessary parameters such as the number of input neurons (i), the number of hidden layers and the number of neurons included in each hidden layer (h), the number of output neurons(j), etc.

Step 2: Initialize the beginning weights and biases, setting their values randomly.

Step 3: Load the input vector **X** and the target output vector **T** of training example.

Step 4: Calculate and infer the actual output vector **Y**.

Step 5: Calculate the error term.

Step 6: Calculate the revised weight of the weight matrix and the revised bias of the bias vector.

Step 7: Adjust and renew the weight matrix and the bias vector

Step 8: Repeat step 3 through 7 until energy function is converged or the specified learning cycles (epochs) are completely executed.

Recalling Process:

Step 1: Set all the network parameters

Step 2: Read the weight matrix and the bias vector

Step 3: Load the input vector X of a testing example.

Step 4: Calculate and infer the actual output Y.

2.3.4.1 The Derivation of the back-propagation algorithm

The error signal at the output of the neuron, j, at iteration n is defined as:

$$e_j(n) = d_j(n) - y_j(n) \tag{2.29}$$

the sum of the squared errors is obtained as:

$$E(n)=\frac{1}{2}\sum_{j=1}^{r}e_j^2(n) \tag{2.30}$$

where r is the number of neurons in the output layer.

Consider a neuron, j, fed with the signal produced by the preceding layer of neurons. The net internal activity level, $v_j(n)$, produced at the neuron, j, is therefore

$$v_j(n)=\sum_{i=0}^{p}w_{ji}(n)y_j(n) \tag{2.31}$$

where p is the number of inputs fed to the neuron, j. Hence

$$y_j(n)=\phi(v_j(n)) \tag{2.32}$$

In the back propagation algorithm, a correction $\Delta w_{ji}(n)$, applied to the synaptic weights is proportional to the instantaneous gradient. This gradient can be expressed as:

$$\frac{\partial E(n)}{\partial w_{ji}(n)}=\frac{\partial E(n)}{\partial e_j(n)}\frac{\partial e_j(n)}{\partial y_j(n)}\frac{\partial y_j(n)}{\partial v_j(n)}\frac{\partial v_j(n)}{\partial w_{ji}(n)} \tag{2.33}$$

from Eq. 2.30,

$$\frac{\partial E(n)}{\partial e_j(n)}=e_j(n) \tag{2.34}$$

from Eq. 2.31,

$$\frac{\partial e_j(n)}{\partial y_j(n)}=-1 \tag{2.35}$$

from Eq. 2.32,

$$\frac{\partial y_j(n)}{\partial v_j(n)}=\phi'(v_j(n)) \tag{2.36}$$

$$\frac{\partial v_j(n)}{\partial w_{ji}(n)}=y_j(n) \tag{2.37}$$

Therefore,

$$\frac{\partial E(n)}{\partial w_{ji}(n)}=-e_j(n)\phi'(v_j(n))y_j(n) \tag{2.38}$$

The correction applied to the synaptic weights, $\Delta w_{ji}(n)$ is given by delta rule as:

$$\Delta w_{ji}(n)=-\eta\frac{\partial E(n)}{\partial w_{ji}(n)} \tag{2.39}$$

where η is the learning rate parameter. Therefore

$$\Delta w_{ji}(n) = \eta \delta_j(n) y_j(n) \tag{2.40}$$

where the local gradient is given by,

$$\delta_j(n) = e_j(n)\phi'(v_j(n)) \tag{2.41}$$

As the activation function used is hyperbolic tangent, we have

$$\phi(v_j(n)) = a\tanh(bv_j(n)) \tag{2.42}$$

$$= a\frac{1-\exp(-bv_j(n))}{1+\exp(-bv_j(n))}$$

$$= \frac{2a}{1+\exp(-bv_j(n))} - a$$

Differentiating we get,

$$\Rightarrow \phi'(v_j(n)) = \frac{2ab\exp(-bv_j(n))}{(1+\exp(-bv_j(n)))^2}$$

$$\Rightarrow \phi'(v_j(n)) = \frac{2ab}{(1+\exp(-bv_j(n)))}\left\{1-\frac{1}{(1+\exp(-bv_j(n)))}\right\}$$

$$= b\{a+\phi(v_j(n))\}\left\{1-\frac{a+\phi(v_j(n))}{2a}\right\}$$

$$= \frac{b}{2a}(a+\phi(v_j(n)))(a-\phi(v_j(n)))$$

$$= \frac{b}{2a}(a^2-\phi^2(v_j(n)))$$

$$= \frac{b}{2a}(a^2-y^2(n)) \tag{2.43}$$

In the Eq. 2.29, the *ej(n),* is straight forwardly known for the output layer neurons. But for the hidden layer neurons, this term is to be determined recursively in terms of the error signals of all the neurons to which it is connected.

From Eq. 2.41, $\delta_i(n) = -\frac{\partial E(n)\partial y_j(n)}{\partial y_j(n)\partial v_j(n)}$ (2.44)

from Eq. 2.32, $= -\frac{\partial E(n)}{\partial y_j(n)}\phi'(v_j(n))$

$$= \sum_k \frac{\partial e_k(n) \partial v_k(n)}{\partial v_k(n) \partial y_j(n)}$$

but since

$$e_k(n) = d_k(n) - y_k(n) = d_k(n) - \phi(v_k(n))$$

we have,

$$\frac{\partial e_k(n)}{\partial v_k(n)} = -\phi'(v_k(n))$$

and since

$$v_k(n) = \sum_{j=0}^{q} w_{kj}(n) y_i(n) \quad \Rightarrow \frac{\partial v_k(n)}{\partial y_j(n)} = w_{kj}(n)$$

Therefore

$$\frac{\partial E(n)}{\partial y_j(n)} = -\sum e_k \phi_k'(v_k(n)) w_{kj}(n)$$

$$= -\sum \delta_k(n) w_{kj}(n)$$

Hence, the local gradients for the hidden layer neurons can be written as:

$$\delta_j(n) = \phi_j'(n) v_j(n) \sum \delta_k(n) w_{kj}(n)$$

$$= \frac{b}{2a}(a^2 - y_i^2(n)) \sum w_{jk}(n) \delta_k(n) \tag{2.45}$$

Summarizing, the relations developed, may be written as:

1. The correction $\Delta w_{ji}(n)$=(learning rate parameter, η)x(local gradient, δ) x(input signal of neuron, j, $y_j(n)$)
2. For the output layer neurons,

$$\delta_j(n) = \frac{b}{2a}(a^2 - y_i^2(n)) e_j(n) \tag{2.46}$$

3. For the hidden layer neurons,

$$\delta_j(n) = \frac{b}{2a}(a^2 - y_i^2(n)) \sum w_{jk}(n) \delta_k(n) \tag{2.47}$$

2.3.4.2. Activation function

An example of a continuously differentiable nonlinear activation function, commonly used in multilayer perceptrons is, *sigmoidal* nonlinearity; two forms shown in Fig. 2.4 and are described as,

1. *Logistic Function:* This form of sigmoidal nonlinearity in its general form is defined by ,

$$\varphi_j(v_j(n)) = \frac{1}{1+exp(-av_j(n))} \quad a>0 \text{ and } -\infty < v_j(n) < \infty \tag{2.48}$$

where $v_j(n)$ is the induced local field of neuron, j.

2. *Hyperbolic tangent function:* Another commonly used form of sigmoidal non-linearity is the hyperbolic tangent function, which is in the form of as defined as,

$$\varphi_j(v_j(n)) = a\tanh(bv_j(n)), \quad (a,b)>0 \tag{2.49}$$

where a and b are constants. In reality, the hyperbolic tangent function is just the logistic function rescaled and biased.

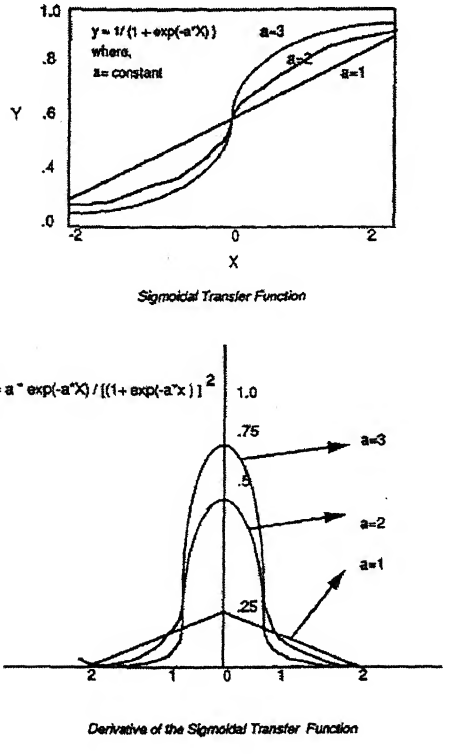

Figure 2.4: Sigmoidal Activation function and its derivative

2.3.4.3. Rate of learning

The back propagation algorithm provides an approximation to the trajectory in weight space computed by the method of steepest descent. The smaller we make the learning rate parameter η, the smaller the changes to the synaptic weights in the network will be from one iteration to the next, and the smoother will be the trajectory in the weight space.

2.3.4.4. Modes of training

One complete presentation of the entire training set during the learning process is called an epoch. For a given training set, back propagation learning may proceed in one of the following ways:

1. **Sequential Mode:** This mode is also called as the on-line, pattern or stochastic mode. In this mode of operation weight updating is performed after the presentation of each training example. Let an epoch consists of N training examples (patterns) arranged in the order$(x(1),d(1)),\ldots\ldots(x(N),d(N))$.

2. **Batch Mode:** In the batch mode of back propagation learning, weight updating is performed after the presentation of all the training examples that constitute an epoch.

From an "*on-line*" operational point of view, the sequential training is preferred to batch one, because it requires less local storage for each synaptic connection and making it less likely for the back propagation algorithm to be trapped in a local minimum.

2.3.4.5. Stopping Criterion

In general, the back propagation algorithm cannot be shown to converge, and there are no well-defined criteria for stopping its operation. Rather, there are some reasonable criteria, each with its own practical merit, which may be used for termination of the synaptic

weight adjustments. The unique properties of the local or global minimum considered for formulating a termination criterion are:

1. The back propagation algorithm is considered to have converged when the Euclidean norm of the gradient vector reaches a sufficiently small gradient threshold.

2. The back propagation algorithm is considered to have converged when the absolute rate of the change of the average squared error per epoch is sufficiently small.

3. The learning process is stopped when the generalization performance is adequate or when it is apparent that the generalization performance has peaked, where the network is tested for its generalization performance.

2.3.5 Model Strategy

There are many *ANN* models used for the modeling of machining processes, characterized by different topology. One has the freedom of choosing the input patterns, the output patterns, the network architecture, the activation function, strategy of training etc.

2.3.5.1 On-Line Monitor Model

A neural network model was used as an on-line model for the machining processes. First, an appropriate architecture for the network was determined. Both three input (3-6-1, 3-7-7-1 and 3-6-2) and four input (4-6-1) fully connected feed forward neural network were used. A back propagation neural network algorithm was implemented. The schematic diagram of a [4-6-1] ANN is shown as in Fig. 2.5. Each of the nodes corresponds to a single input parameter, and similarly each output node is uniquely associated with one of the output parameters. The four input parameters from the proposed network are: *speed (v)*, *feed (f)*, *rake angle (α)* and *amplitude of vibration (a)*. The output parameter is the surface roughness (R_a). The model architecture is shown in Fig. 2.5.

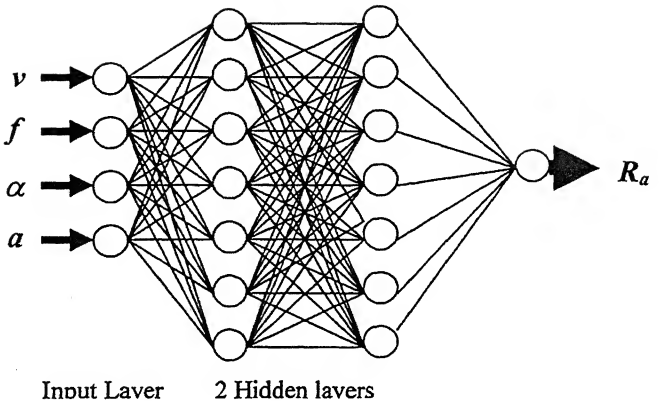

Figure 2.5: Schematic diagram of the *ANN* model developed

Once the architecture was decided, the *ANNs* were trained on the training examples (or patterns), where each pattern was a set of input and output parameters, which were obtained from experiments. All the values of patterns were normalized, so that the data should lie between the same limits, i.e. 0 and 1. It is very difficult to converge to a set of weights and the sigmoid function will get saturated if the parameters are not normalized.

After normalized, the network weights and node thresholds were randomized. Training involved presenting the patterns to the network, calculating the error, propagating the error back through the network (using the back propagation algorithm), and then modifying the weights by small increments to reduce error to zero. This process was repeated until the network was stabilized (i.e. the weights do not change).

2.3.6 Implementation of the ANN Model

The data collected from the experiments were used to train neural nets with the help of *MATLAB*. The software provides various training, learning and transfer functions. A gradient descent with momentum weight/bias learning function was used which calculated the weight change for a given neuron from the neuron's input and error. A network performance function was used which measures performance according to the

sum of squared errors. The transfer functions used for each neurons was Hyperbolic Tangent function, as shown in Fig. 2.6, which is computed as, $n = \frac{2}{\left(1+e^{-2n}\right)^{-1}}$ (4.50)

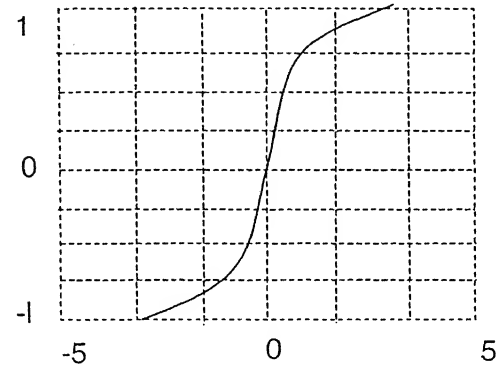

Figure 2.6: Plot of a Hyperbolic Tangent Transfer Function

Various training functions were used, which could train any network as long as its weight, net input, and transfer functions have derivative functions. Some of the functions are discussed below.

1) TRAINLM: It is a network training function that updates weight and bias values according to Levenberg-Marquardt optimization. Backpropagation is used to calculate the Jacobian of performance with respect to the weight and bias variables.

2) TRAINGD: It is a network training function that updates weight and bias values according to gradient descent. Backpropagation is used to calculate derivatives of performance with respect to the weight and bias variables x. Each variable is adjusted according to gradient descent

3) TRAINGDX: It is a network training function that updates weight and bias values according to gradient descent momentum and an adaptive learning rate. Backpropagation is used to calculate derivatives of performance with respect to the weight and bias variables. Each variable is adjusted

according to gradient descent with momentum. For each epoch, if performance decreases toward the goal, then the learning rate is increased by the factor. If performance increases by more than a specified value, the learning rate is adjusted by a factor and the change, which increased the performance, is prevented.

4) TRIAINGDA: It is a network training function that updates weight and bias values according to gradient descent with adaptive learning rate. Backpropagation is used to calculate derivatives of performance with respect to the weight and bias variables. Each variable is adjusted according to gradient descent. At each epoch, if performance decreases toward the goal, then the learning rate is increased by the factor. If performance increases by more than a specified value, the learning rate is adjusted by the factor and the change, which increased the performance, is prevented.

5) TRAINRP: It is a network training function that updates weight and bias values according to the resilient backpropagation algorithm (RPROP). Backpropagation is used to calculate derivatives of performance with respect to the weight and bias variables. Each variable is adjusted such that the if an element of gradient changes sign from one iteration to the next then the corresponding element of the variable is deceased by a fixed value. Or else it is increased by some different value.

6) TRAINOSS: It is a network training function that updates weight and bias values according to the one step secant method. Backpropagation is used to calculate derivatives of performance with respect to the weight and bias variables. A parameter 'a' is selected to minimize the performance along the search direction. A line search function is used to locate the minimum point. The first search direction is the negative of the gradient of

performance. In succeeding iterations the search direction is computed from the new gradient and the previous steps and gradients.

7) TRAINSCG: It is a network training function that updates weight and bias values according to the scaled conjugate gradient method. The scaled conjugate gradient algorithm is based on conjugate directions, but this algorithm does not perform a line search at each iteration.

8) TRAINBFG: It is a network training function that updates weight and bias values according to the BFGS quasi-Newton method. Backpropagation is used to calculate derivatives of performance with respect to the weight and bias variables. A parameter is selected to minimize the performance along the search direction. A line search function is used to locate the minimum point. The first search direction is the negative of the gradient of performance. In succeeding iterations the search direction is computed the gradient and an approximate Hessian matrix.

In all the training functions the training stopped when any of these conditions occur:

- The maximum number of *epochs* (repetitions) is reached.
- The maximum amount of *time* has been exceeded.
- Performance has been minimized to the *goal.*
- The performance gradient falls below minimum *gradient.*
- Validation performance has increased more than a factor times since the last time it decreased (when using validation).

Chapter III

Experimentation

3.0 Introduction

The basic aim of the experimentation was to implement the on-line monitoring of surface roughness and develop mathematical models to represent the cutting process, namely Regression and Neural Network models. The parameters *Speed (v), Feed (f), Rake Angle (α) and Amplitude of Vibration (a)* were selected as the input. There are numerous outputs to a cutting process that can be of considerable research interest, such as cutting force, tool wear, cutting temperature, surface roughness etc. In this particular work, average surface roughness *(R_a)* was measured. From the experiments the effect of the selected input parameters on R_a value was observed and models were developed to predict the output for known inputs and compared with each other.

The average surface roughness *(R_a)* was measured both during and after the cutting process. In the first case R_a was measured by a bifurcated opto-electrical transducer, while the cutting process was taking place. The arrangement for the above is shown in Fig. 3.13. The transducer was placed diametrically opposite to the cutting tool such that it was able to measure the freshly generated surface during turning operation. As R_a was

measured while the cutting was taking place it is referred as *On-line measurement of surface roughness*. The working of the bifurcated opto-transducer and the physics behind it is discussed in details in the section 3.2.2.1.

The output obtained from the transducer discussed above, was in terms of a voltage signal which depended on the surface roughness value. Thus there calibration of the output voltage signal with the actual R_a had to be made. This was achieved through the measurement of R_a, with the help of a Taylor-Hobson, Surtronic surface profiler. This measurement was done after the cutting process was over. Thus this post-machining measurement is referred as *Off-line measurement of surface roughness.*

Experiments were conducted with three independent variables. They are speed (v), feed (f) and Rake Angle (α). The measured parameters were average surface roughness (R_a) (on-line and off-line) and amplitude of vibration (a) in the displacement mode.

A scientific approach to planning of experiments was incorporated in order to perform the experiments most effectively. Thus statistical design of experiments, defined as the process of planning of experiments so that the appropriate data could be collected which may be analyzed by statistical method resulting in valid and objective conclusion; was used.

3.1 Three factors, three level of experiments

Three factors (v, f, α) in three levels (0, 1, 2) were chosen to carry out the experiments. A full factorial design was carried out, performing a total number of twenty seven experimental runs.

3.1.1 3^k Factorial Design

3^k factorial design is the most commonly used factorial design having three levels for each 'k' factors. The three levels may be referred to as Low (0), Intermediate (1) and

High (2). If there are three factors (*A, B, C*) under study and each factor is at three levels arranged in a factorial experiment, this constitutes a 3^3 factorial design. The experimental layout and treatment combination notations are shown in Fig. 3.1 below.

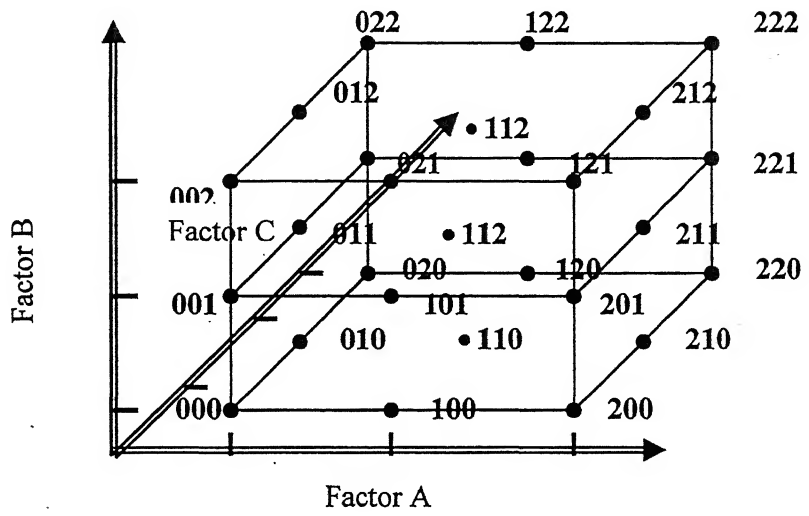

Figure 3.1: Treatment Combination in a 3^k Design

3.1.2 Levels of the parameters

The levels of the input parameters were selected from machine tool handbooks, the machine capabilities, experience and preliminary tests. They are given in Table 3.1

Table 3.1: Different levels of the Independent Cutting Parameters

Levels	*Cutting Speed (m/min)*	*Feed (mm/rev)*	*Rake Angle(°)*
-1	18.6	0.050	-10
0	22.6	0.069	0
+1	26.6	0.088	10

Depth of cut was kept constant at 0.3 mm, as it has been reported [12] that it has insignificant effect on the surface roughness generated.

3.2 Experimental Set up and procedures

A HMT make Engine Lathe [Appendix A] was selected to carry out the experimentation. The ranges of the levels of the input parameters as well as the diameter of the work piece were set on the basis of the particular machine tool capabilities.

3.2.1 Stages in experimentation

A number of experiments were carried out and the stages of experimentation may be given as follows:

1. Experimentation to calibrate the bifurcated opto-transducer for measuring on-line surface roughness.

2. Experimentation to measure surface roughness (R_a), both on-line as well as offline, and amplitude of vibration (a) to obtain data as per the design of experiments with three independent factors: speed (v), feed (f) and rake angle (α), to develop a neural network and a regression model.

3. Experimentation to validate the mathematical and neural network models, by measuring the surface roughness.

3.2.2 Experimental Set-up

The roughness of a reflecting surface dictates the amount of reflected light from a light source, was used to develop an optical sensor for monitoring the surface roughness. The

light source was mounted just on the opposite side of the tool so that the light got reflected as much as possible from the freshly formed surface only. The light source was rigidly fixed to the tool post of the lathe machine, and it moved parallel to the axis of work piece while turning, keeping the distance between them constant. The intensity of the reflected light could be sensed and the surface roughness could be correlated to the change in the light intensity.

The optical sensor acts like a displacement transducer, the obtained on-line roughness signal was not equal to the off-line surface roughness R_a, as it had the radial vibration signal combined to the surface irregularities i.e. the offline surface roughness as well as the vibration generated due to the tool-workpiece interaction. Thus the tool-workpiece vibration was sensed using an accelerometer, and the on-line, off-line surface roughness signals along with the vibration signal were obtained.

3.2.2.1 Optical sensor

The basic components of the optical sensor system included the optical fiber transducer, the sensing and amplification circuit and a recorder to measure the signals.

3.2.2.1.1 Optical Fiber

The advent of efficient and cost effective optical fiber technology for telecommunication requirements resulted in the development of a new generation physical measurement transducers. The fiber optics transducers are generally classified as intensity modulated, interferometric and polarization-based and wave length modulated devices. Of these, intensity modulated devices are commonly used ones. Fig. 3.2 shows the cross section of the step index multimode fiber [10]. These fibers are made of cylindrical core, typically 50 μm in diameter, surrounded by a cladding whose reflective index is less than that of core. The numerical aperture of the fiber in the air is given as:

$$NA = \sin\theta_c = \sqrt{n_1^2 - n_2^2} \qquad (3.1)$$

where n_1 and n_2 , are the reflective indices of the core and the cladding material respectively and θ_c is the angle of incidence at the core-cladding interface at the critical angle for the total internal reflection. The input ray consequently propagates along the fiber with no reflection losses.

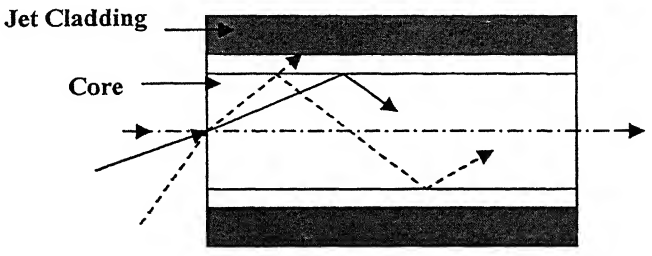

Figure 3.2: Sectional view of a step index multimode fiber [10]

Another important parameter of the optical fiber transducer is that the spatial resolution also known as the distance resolution. In the optical time domain reflectometer (OTDR), a rating based on the shortest distance along the length of an optical wave-guide (as an optical fiber) that the OTDR can distinguish on its display screen (usually CRT) is called spatial resolution. It is the measure of how close together the two events or faults can be distinguished as separate events.

Usually the sensor consists of a bifurcated fiber bundle with one leg connected to a photo-detector and the other to a light source (preferably monochromatic). At the face of merger of the two bundles the fibers from the two legs are mixed such that, it forms an annular ring, with the inner section supplying the light and the outer ring supplying the reflected light back to the photodiode.

The basis for the operating mechanism is the interaction between the source and the field of view of the detector fibers. A simplified illustration of this effect is shown in the Fig. 3.3. At the contact or zero gap, the whole amount of light passes through the source fibers, strikes the work-piece surface and is reflected back into the same source fibers,

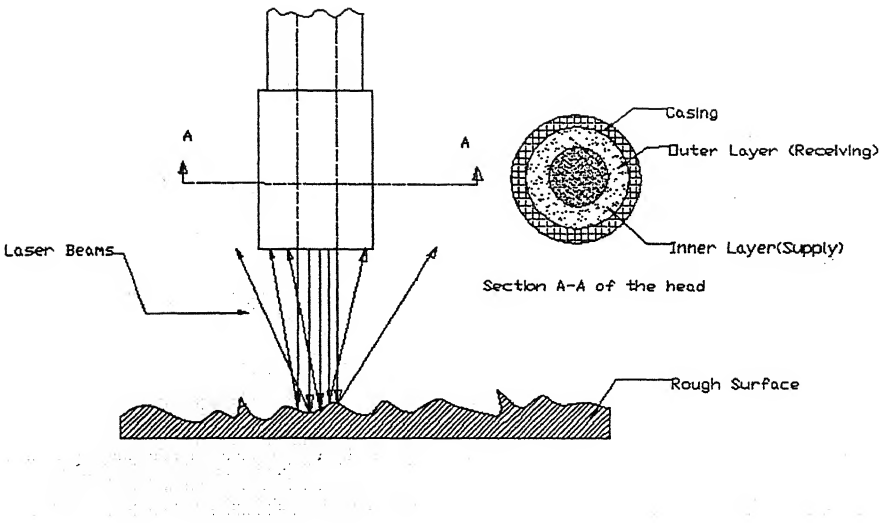

Figure 3.3: Operating principle of the optical fiber

almost no light get reflected into the sensing fibers and hence produces nearly zero output voltage. An increase in the probe to target distance will result in some distance from the work piece surface. Depending upon the surface roughness of the job, the intensity of the light captured by the receiving fibers will increase or decrease (scattering effect). As an optical fiber has an aperture angle, that is, an angle beyond which the rays are not transmitted, there will be a preferred stand-off distance at which the light intensity from the transmitting fibers to the receiving fibers reflected from the surface, will be maximum. As the sensor is placed further back, the cone of light emanating from the fiber is coupled outside the receiving fibers and consequently the light intensity at the detector is reduced. For the experiments performed in this work, a bifurcated bundle of optical fibers, concentric traverse inside (CTI) grouping of the fibers at the merger points, was selected.

3.2.2.1.2 Sensing and Amplification Circuit

Photodetection involves measuring the incident lights in terms of an electrical signal. There are three basic forms of photodetection. They may involve the photoemission, photoconduction and the photovoltaic actions. Photoemission involves incident light that

frees electrons from the detector surface. This usually occurs in a vacuum tube. With photoconduction the incident light on a photosensitive material causes the photodetector to alter its conductance. In the photovoltaic action, a voltage is generated when the light strikes the sensitive material of photodetector.

The most popular photodetector is a single junction photodiode. A photodiode is the optical version of the standard diode. It is constructed of a P-N junction photons of light energy are absorbed into the device and the Hole-Electron pairs are generated. This pairs are combined at different depths within the diode depending upon the energy level of the photon. A wide, thin surface area is used to ensure the maximum absorption. Current flow is dependent on the amount of radiation absorbed. Photodiodes operate in the photoconductive mode with reverse DC bias applied. This is also called as the current mode. Current is extracted as a measure of the applied radiant energy. Signal current flows through a load resistor, R_1, in the photoconductive circuit, as shown in the Fig. 3.4 below. A detector material is specially selected so that when it is exposed to light rays, it will absorb the light energy.

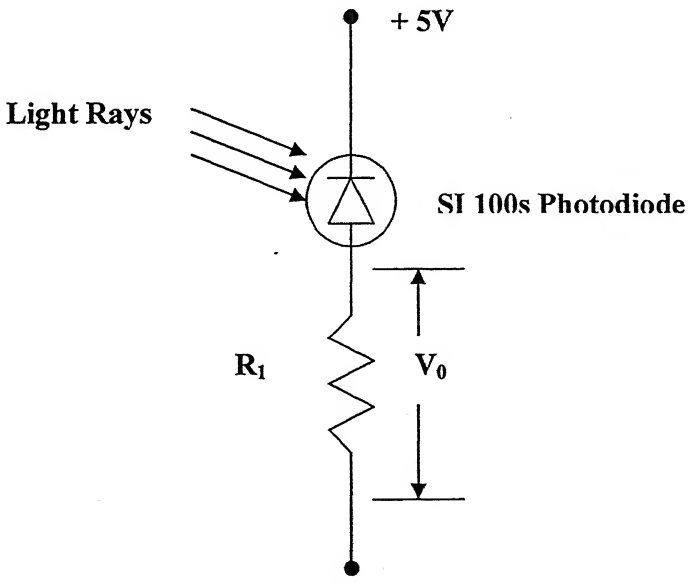

Figure 3.4: Photodiode circuit

In the present work, a SI 100s photodiode with responsivity of 0.4 A/W at 632.8 nm wavelength is used. The specifications are shown in the Appendix. A 10 mW continuous He-Ne Laser gun is used as the light source.

As the output voltage available from the photodiode is in terms of a few milli-volts, a pre-amplification circuit is required before using the signals. A two stage pre-amplification circuit has been designed and fabricated using a special purpose operational amplifier OP-07. The circuit is shown in Fig. 3.5.

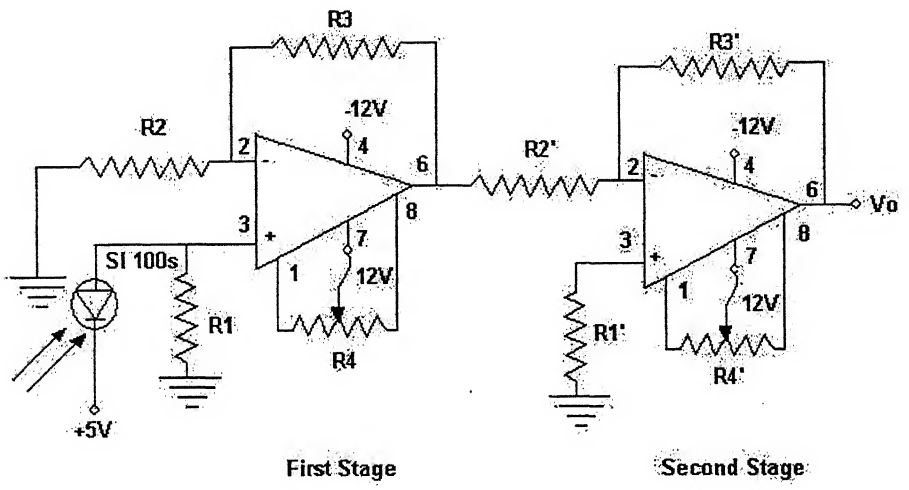

Figure 3.5: Sensing and Amplification circuit

An operational amplifier amplifies the difference between the voltage signals at the two inputs, and can operate either inverting or non-inverting mode. The voltage developed across the load resistor of the photodiode, R_1, is fed as one input to the op-amp, the other input is grounded with the other resistor, R_2; R_3 being the feedback resistor. Required factor of gain is obtained by using the appropriate values of two resistors, R_3 and R_2. Initially with the two inputs of the op-amp shorted and grounded, the output is set to zero using the variable resistor R_4, this is called the input offset voltage correction. This is done carefully before using the circuit otherwise the op-amp will be driven into saturation region giving a constant output voltage for any input signal. The gain in every stage of the circuit in the present work is calculated as follows:

Gain at every stage,

$$G = 1 + \frac{R_3}{R_3} \tag{3.2}$$

$$V_0 = G(V_3 - V_2) \tag{3.3}$$

$$= (1 + \frac{R_3}{R_3})(I_P R_1) \tag{3.4}$$

$$= (1 + \frac{R_3}{R_3})\rho P R_1 \tag{3.5}$$

3.2.2.2 Accelerometer

In an effort to find the effect of vibration on the surface roughness we have measured the vibration between the tool and the work-piece interface with the help of an accelerometer. The accelerometer used for the experiments is a piezoelectric-type. The specifications of the accelerometer and the charge-amplifier are given in Table 3.2. The design diagram of the accelerometer is given in Fig. 3.6.

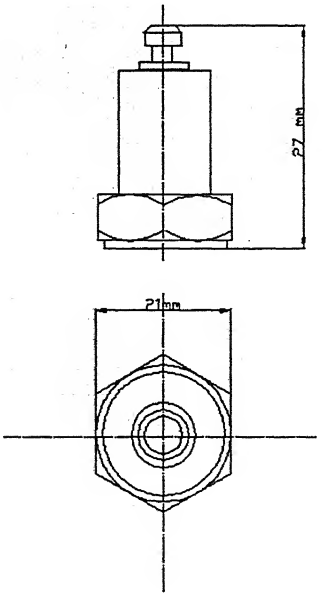

Figure 3.6: Dimension of the Bruël & Kjær 820361 Accelerometer

Table 3.2: Specifications of Accelerometer and Charge Amplifier

Make:	Bruël & Kjær 820361
Material:	Piezo-electric Type PZ23
Charge Sensitivity:	0.990 pC/ms^2
Voltage Sensitivity:	0.909 mv/ ms^2
Capacitance:	1089pF

The accelerometer has a magnetic base with the help of which it was mounted to the tool post, as shown in Fig. 3.7 below. The measurement was taken in the displacement mode with a gain of 100mV/unit, where a unit corresponded to 1mm of displacement. The accelerometer was mounted on the tool post to measure the radial displacement of the tool relative to the workpiece, due to the vibration between the two.

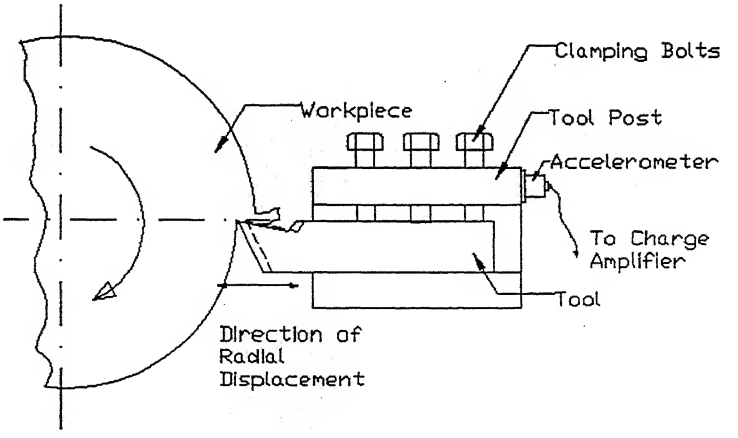

Figure 3.7: The mounting of the accelerometer

3.2.3 Experimentations

In the present work the, the surface roughness was monitored continuously, through out the turning operation, with the help of an optical transducer. The optical transducer consisted of bifurcated optical fiber, laser gun as the light source and a photo-diode as a

detector along with an amplification circuit. The accelerometer was connected to the tool post to sense the vibration between the tool and workpiece interactions. The workpiece of original dimension of $\phi 80x750mm$ was divided into nine sections of equal lengths, such that the diameter of all the sections can be maintained to a particular value and thus the speed can be accurately be same for all of them, as shown in Fig. 3.8. The other parameters feed and rake angles were changed, the speed remaining constant. A schematic diagram of the experimental setup is given in Fig. 3.9 and photographs of the set up in Fig. 3.10.

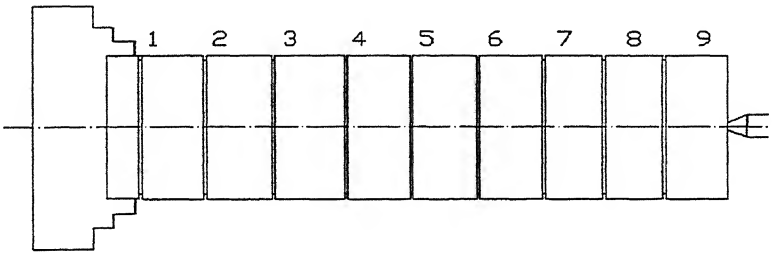

Figure 3.8: The Sections made on the workpiece to keep the cutting speed constant

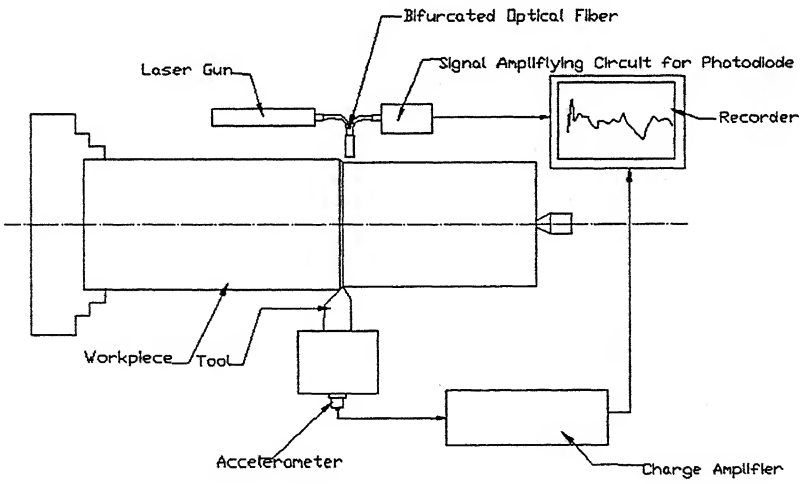

Fig. 3.9: Schematic Diagram of Experimental Set up

The Y shaped optical fiber was held on the diametrically opposite side of the cutting tool. The optical fiber was fixed in such a way that it's tip is at a certain distance from the workpiece surface and its axis normal to the same. The cone of illumination was

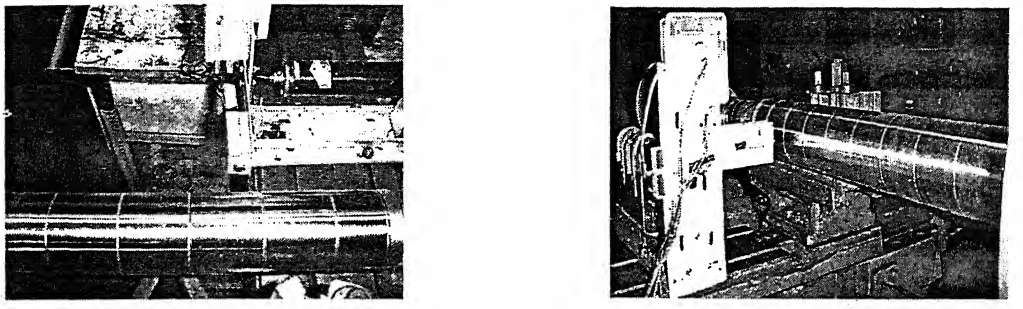

Fig. 3.10: Photograph of the Experimental Set-up

adjusted such that it was incident on and reflected back from the freshly produced work surface. The optical fiber had a core of 3 mm diameter and the cladding of 5 mm diameter. The core and the cladding were coupled with brass sleeves at the ends. A 10 mW continuous laser gun was used as the light source. He-Ne laser guns have the advantage of being handy over the solid state lasers. The model (105-1) of Uniphase Inc. was used. The power of the laser beam should be such that it does not drive the photodiode into the saturation region and yet provide the signals of sufficient strength. It was necessary to ensure that the laser beam produced was of a constant intensity throughout the experiments. A brass coupling (I) as shown in the Fig. 3.11 (a) was used to connect the source fibers to the sensors to the laser gun. This was to ensure that there was no relative motion between the source fibers and the laser gun.

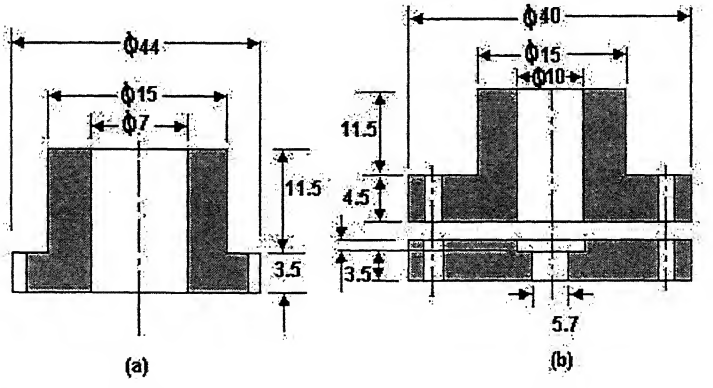

Fig. 3.11: Brass sleeves (a) Coupling I (b) Coupling II (All dimensions in mm)

The sensing fibers were connected to the photodiode using another brass coupling (II) as shown in Fig 3.11 (b), to ensure that the light coming to the photodiode is the light from

he laser gun only this coupling was also necessary to avoid any relative movement between the sensing fibers and the photodiode. This setup ensured that any change in the output signal was only due to the change in the intensity of the reflected light.

3.2.3.1. Experimentation to observe the effect of the stand off distance on the output of the optical transducer

The bifurcated optical transducer is a displacement transducer in nature. Thus the standoff distance of the face from the workpiece surface was an important factor to be considered. A set of experiments were conducted to obtain the stand-off characteristics of the transducer, as sown in Fig 3.12. It can be observed from the characteristic curve that as the standoff distance was increased the voltage output at the photodiode also increased until a certain maximum value after which it remained constant. As the standoff distance increased, initially the amount of reflected light also increased, but beyond certain distance it started decreasing, as there was hardly any reflection.

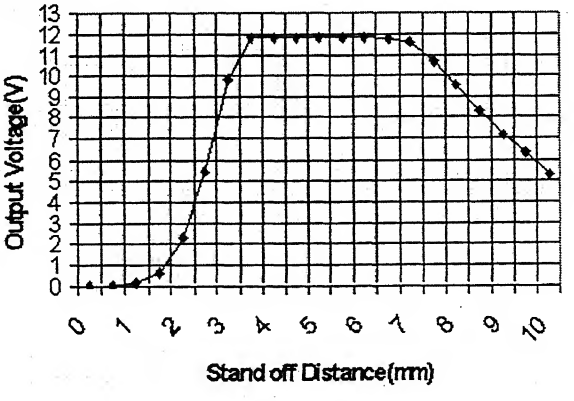

Fig. 3.12: The plot of Output Voltage against Stand off Distance

The workpiece was held stationary between the chuck and the revolving center on the tailstock. Feed was given to the tool carriage, on which the bifurcated optical transducer was mounted. The voltage output of the photodiode through the signal amplifying circuit, was recorded on a Omniscribe-Millivolt recorder. The roughness (R_a) in μm was measured with the help of a Taylor-Hobson, Surtronic surface profiler. The details of the above experimentation are provided in the next chapter.

Chapter IV

Result and Discussions

This chapter deals with the result of the experiments conducted. The effect of independent parameters on the surface roughness, in turning operation had been investigated. Then various Regression models have been developed and compared. Analysis of Variance (*ANOVA*) had been performed for all the models. Various Artificial Neural Network (*ANN*) models were also developed and compared. The Regression and *ANN* models were compared for the same validation data set.

4.1 On-line Measurement of Surface Roughness

The *on-line* surface roughness was measured during the cutting process with the help of the bifurcated optical fiber transducer. The setup for the above had been discussed in section 3.2.3. The output voltage signal was obtained from the amplifier, used along with the above transducer and this signal is referred as '*On-line surface roughness*'. After the cutting operation had taken place, the surface roughness was measured with a Taylor-Hobson, Surtronic surface profiler. This surface roughness is referred as the '*off-line surface roughness*'.

Calibration of the opto-transducer was done by measuring the *off-line* as well as the *on-line*

surface roughness of the same surface for a fixed stand off distance. The voltage signal obtained from the above transducer was plotted against the actual surface roughness values measured with the help of the surface profiler that is *off-line* R_a. Assuming reasonable linearity of the calibration relation a best fit line was obtained, the *on-line* surface values were obtained by extrapolation. A calibration plot was made using the *off-line* data as shown in Fig. 4.1 and the calibration equation as given in Eq. (4.1).

$$Ra = -2.9489V + 40.512 \tag{4.1}$$

where

V= The output voltage of the optical transducer, plotted in the recorder.

The *on-line* measurement, i.e. when the cutting operation was taking place, included the measurement of two values. They were the amplified signal from the optical transducer that is the *on-line* surface roughness and the amplitude of vibration from the accelerometer. After a particular cut had been completed, *off-line* measurements of the roughness were taken with help of a digital surface profilometer.

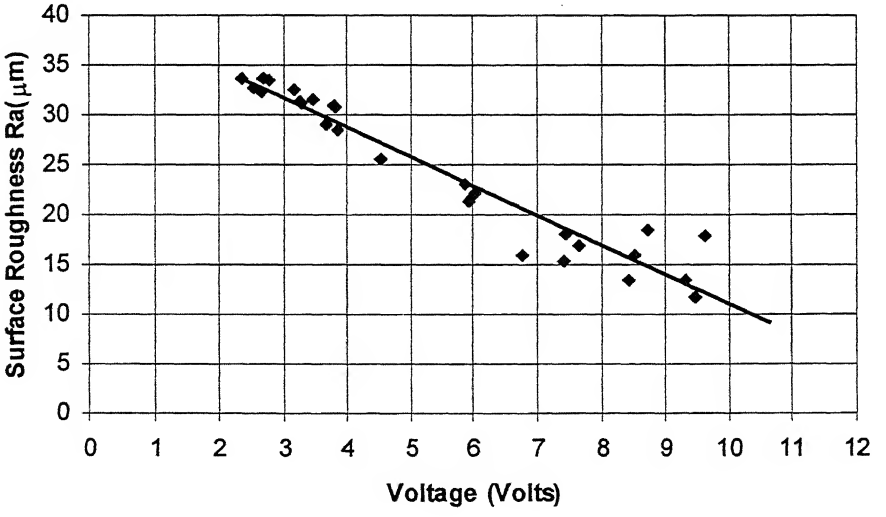

Figure 4.1: Calibration Chart for the Optical Transducer

4.2 Result of experimentation on the measurement of the surface roughness and vibration

The parameters speed (v), feed (f) and rake angle (α) had been selected for conducting the experiments. A three-factor three level i.e. 3^3 Factorial design had been chosen. The three natural or independent parameters were coded in terms of three levels -1 (Low), 0 (Intermediate) and +1 (High). The relationship between the natural and the coded variables are given in the Table 4.1. They are calculated as below,

$$Coded\ Variable = \frac{(Actual\ Value - Mean\ Value\ of\ Working\ Range)}{(Maximum\ Value - Mean\ Value\ of\ Working\ Range)} \qquad (4.2)$$

Table 4.1: Natural and Coded Variables

Coded	*Speed*		*Feed (mm/rev)*	*Rake Angle (^{0})*
	R.P.M	*(mm/min)*		
-1	80	18.6	0.050	-10
0	100	22.6	0.069	0
+1	125	26.6	0.088	+10

Thus the measured parameters were both *on-line* and *off-line* surface roughness and the amplitude of vibration between the tool and the work piece. The data collected from the experimentation are given in Table 4.2. The *on-line* surface roughness data and the vibration signal readings were in terms of voltages which were converted in μm with the help of calibration charts (Fig. 4.1) and conversion factors of the amplifier and recorders.

Table 4.2: Experimental Data Set

Expt #	Speed (m/min)	Feed (mm/rev)	Rake Angle (Degrees)	On-Line Ra (μm)	Off-Line Ra (μm)	Vibration ($\pm\mu$m)
1	-1	-1	-1	17.36	22.17	10.50
2	-1	0	-1	21.49	28.97	11.80
3	-1	+1	-1	32.08	31.33	12.85
4	-1	-1	0	29.98	31.13	22.70
5	-1	0	0	28.57	33.70	12.50
6	-1	+1	0	28.04	32.3	16.70
7	-1	-1	+1	22.82	15.87	15.00
8	-1	0	+1	24.00	21.30	32.50
9	-1	+1	+1	26.06	30.90	25.00
10	0	-1	-1	34.97	28.46	11.00
11	0	0	-1	31.99	30.80	16.67
12	0	+1	-1	33.82	32.53	18.50
13	0	-1	0	34.17	23.00	5.08
14	0	0	0	32.70	31.60	12.17
15	0	+1	0	30.43	33.73	14.33
16	0	-1	+1	30.57	25.60	14.00
17	0	0	+1	31.37	33.37	17.00
18	0	+1	+1	33.20	32.70	20.17
19	+1	-1	-1	13.59	17.80	9.83
20	+1	0	-1	17.39	18.50	16.04
21	+1	+1	-1	17.60	18.00	10.58
22	+1	-1	0	17.22	16.00	8.17
23	+1	0	0	19.57	16.90	22.96
24	+1	+1	0	18.30	16.70	15.83
25	+1	-1	+1	12.79	13.50	7.58
26	+1	0	+1	13.03	13.40	6.17
27	+1	+1	+1	13.23	11.80	21.46

Both the optical transducer and the accelerometer are displacement pick-ups. The signal from the accelerometer represents the displacement due to the vibration at the tool-workpiece interaction, during a cutting operation. Whereas the signal obtained by the opto-transducer in

:ase of *on-line* measurement, is the combination of the displacement due to the surface rregularities as well as vibration. The Fig. 4.2 shows the plot of *on-line* R_a, *off-line* R_a and lisplacement due to vibration (a) in the radial direction. Thus it can be interpreted that the /ibration generated during the cutting process had an affect on the *on-line* roughness. It can ›e stated that the *on-line* surface roughness lies within the sum of *off-line* surface roughness ınd the vibration generated in the cutting process which may have either positive or negative ımplitude, as given in Eq. 4.3.

$$\left(R_a^{\,Off-Line} - a_{Vibration}\right) \leq R_a^{\,On-Line} \leq \left(R_a^{\,Off-Line} + a_{Vibration}\right) \tag{4.3}$$

vhere,

$R_a^{\,Off-Line}$ = Displacement due to Surface Roughness

$a_{Vibration}$ = Amplitude of Vibration in the Displacement Mode

$R_a^{\,On-Line}$ = Displacement due to On-line Surface Roughness Measurement

The amplitude of vibration was calculated by measuring five maximum peaks ınd troughs of the displacement signal obtained from the accelerometer.

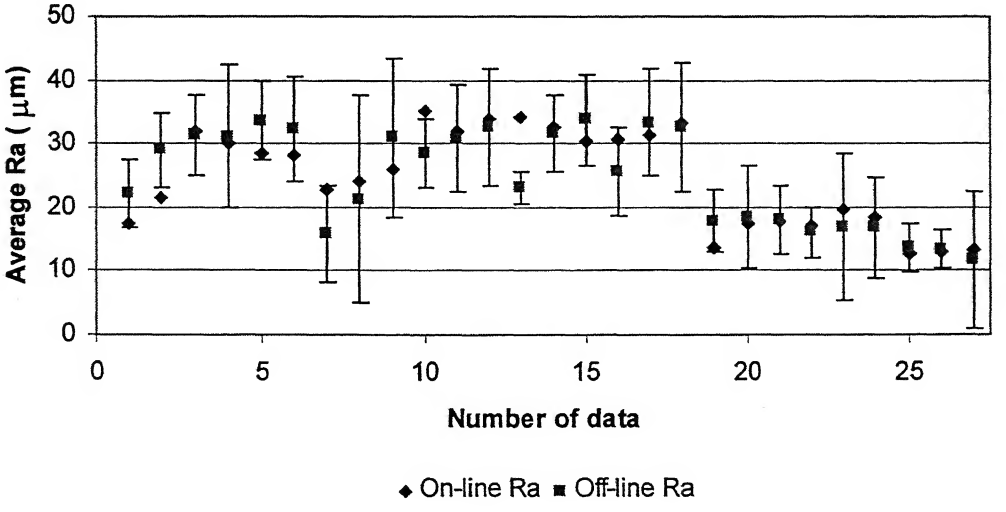

Figure 4.2: Comparison of the on-line and off-line surface roughness data along with the amplitude of vibration.

4.2.1 Effect of the independent parameters on Surface Roughness

From literature [17-24] and known empirical formulae it has been stated that surface roughness depends on speed and feed to a great extent. Thus the three independent parameters selected were speed (v), feed (f) and rake angle (α). Amplitude of vibration was also considered to investigate the effect of the input parameters on the surface roughness.

4.2.1.1 Effect of Speed on Roughness at Different Feeds

Fig. 4.3 below shows effect of speed on average surface roughness in terms of R_a value. The rake angle (α) was kept constant at -10°. The surface roughness was observed to decrease with increase in speed, after an initial increase, which may be accounted for the formation of built-up edges. The roughness also worsened with increase in the feed, due to the formation of feed marks.

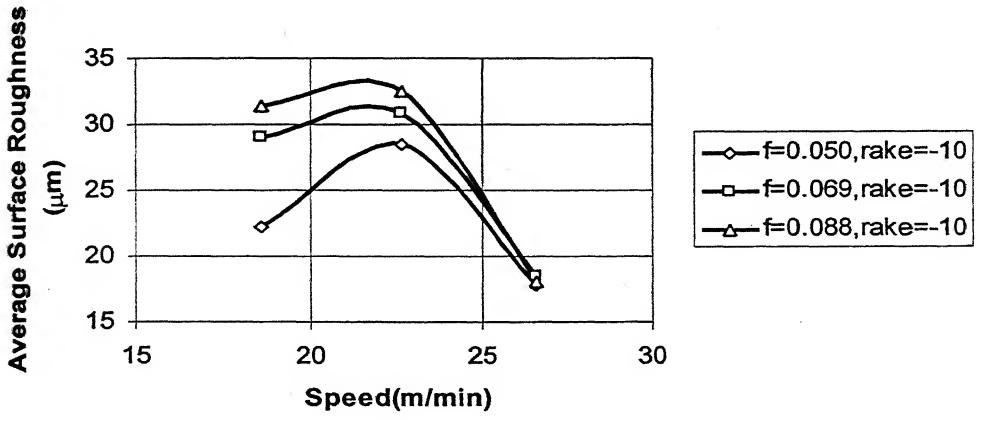

Figure 4.3: Effect of Speed on Roughness at Different Feeds

4.2.1.2 Effect of Speed on Roughness at Different Rake Angles (α)

Fig. 4.4 shows that, as the speed was increased at a constant feed, the surface roughness decreased. It also decreased with the increase in rake angle, α. This can be accounted for the

decrease in cutting force with the increase in α.

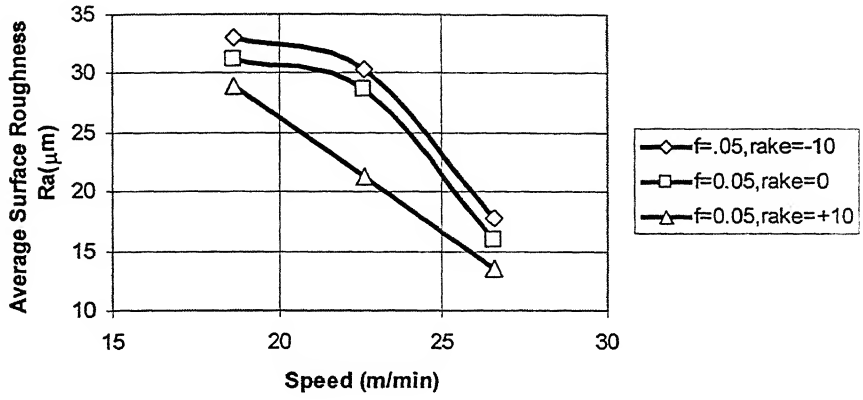

Figure 4.4: Effect of Speed on Roughness at Different Rake Angles

4.2.1.3 Effect of Feed on Surface Roughness, at Different Speeds

Fig. 4.5 shows that, with the increase in the feed the surface roughness increased. But this happened more prominently for lower speed. At higher speed the surface starts improving with the increase in the feed. This is due to the fact the HSS tool gets worn out very fast while machining the hard EN24 workpiece. So the worn-out and blunt tool tip removes less metal and does not deteriorate the surface finish of the machined surface as much.

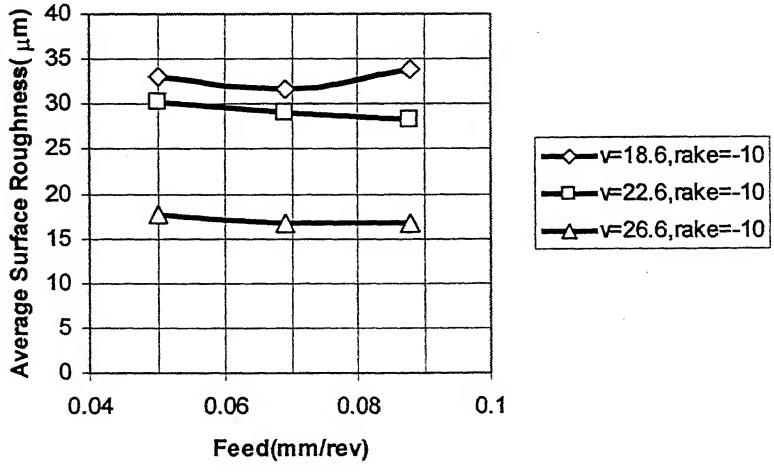

Figure 4.5: Effect of Feed on Roughness at Different Speeds

4.2.1.4 Effect of Feed on Roughness at Different Rake Angles

Fig. 4.6 shows that the surface roughness initially increased with the increase in the speed but then there was hardly any increase, at higher rake angles. The wear in the tool causing the tip to get blunt and the decrease in the cutting force at higher values of α, can be accounted for such observations.

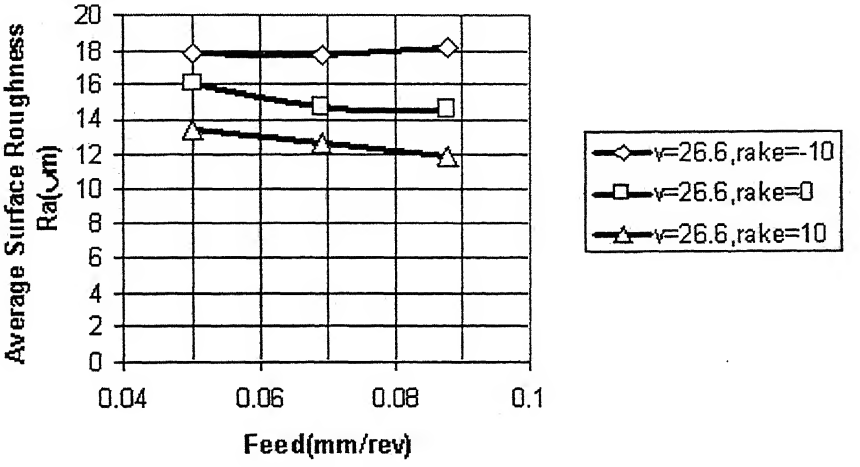

Figure 4.6: Effect of Feed on Roughness at Different Rake Angles

4.2.1.5 Effect of Rake Angles on Roughness at Different Speeds

Fig. 4.7 shows that the surface roughness decreases with the increase in the rake angle (α), from -10^0, 0^0, $+10^0$. Decreasing cutting force and more space for chip accommodation are the main reasons for such observations.

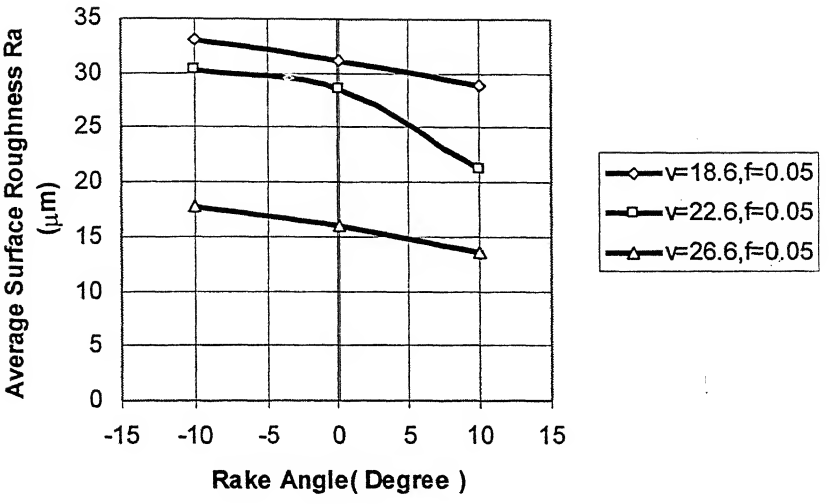

Figure 4.7: Effect of Rake Angle on Roughness at Different Speeds

4.1.1.6 Effect of Rake Angle on Roughness at Different Feeds

The analysis of this plot is same as the last one, the surface roughness decreasing with increasing rake angle. The changes in the roughness at various levels of feed are due to the shorter ranges of the feed levels and blunting of the tool tips.

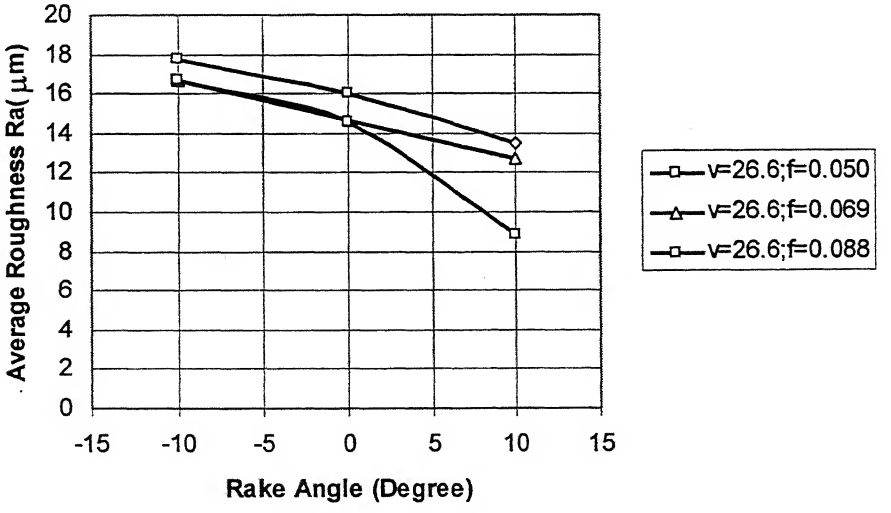

Figure 4.8: Effect of Rake Angle on Roughness at Different Feeds

4.3 Regression Analysis

In this work several regression models have been developed with the help of *MINITAB* software, and the error in the prediction have been evaluated. The different models used, are as follows:

1) *Three Regressor Model*
    a) Multiple Linear Regression Model
    b) Second Order Surface Response Model

2) *Four Regressor Model*
    a) Multiple Linear Regression Model
    b) Second Order Surface Response Model

From the 27 experimental data sets, 21 were used to develop the regression models and the other 6 were used to calculate the error in the prediction of the above models. Analysis of Variance (ANOVA) was also made to identify the most significant contributors to the surface roughness.

4.3.1 Three Regressor model

In these models three inputs have been considered. They are speed (v), feed (f) and rake angle (α). The response is surface roughness in terms of R_a value.

4.3.1.1 Multiple Linear Regression Model

This model is in the simple form given below:

$$R_a = \beta_0 + \beta_1 v + \beta_2 f + \beta_3 \alpha + \varepsilon \qquad (4.4)$$

where, β_0= Constant

β_1= Coefficient of Speed (v)

β_2= Coefficient of Feed (f)

β_3= Coefficient of Rake Angle (α)

ε = Random Error

The *Regression* equation along with the Analysis of Variance (*ANOVA*), for the above model is given as below:

a) Regression Analysis

$$R_a = 44.3 - 1.40\,v + 172\,f - 0.153\,\alpha \qquad (4.5)$$

Table 4.3: Regression Co-efficients of Eq. (4.5)

Predictor	*Coefficient*	*SE Coefficient*	*T-Values*	*P-Values*
Constant	44.27	11.67	3.79	0.001
V	-1.39	0.4024	-3.47	0.003
F	172.31	84.73	2.03	0.058
α	-0.15	0.161	-0.95	0.357

$S = 5.878$ $R^2 = 54.6\%$ $R^2\ (adj) = 46.6\%$

where

SE= Standard Error of Co-efficients

S= The estimated standard deviation about the regression line, S^2= Mean Square Error

T-Value=Test Static Value

P-Value=It is the smallest level of significance that would lead to the rejection of the null hypothesis H_o.

R^2=Co-efficient of Multiple Determination= ($SS_{Regression}$) / (SS_{Total})

$R^2\ (adj) = 1 - \left| \dfrac{SS_{Error}/(n-k-1)}{SS_{Total}/(n-1)} \right|$ where n= Number of Experiments or Replicates

k= Number of Regressor

b) Analysis of Variance

Table 4.4.A: Results of ANOVA of Eq. (4.5)

Source	*DF*	*SS*	*MS*	F_o	$F_{.05,3,17}$	*P*
Regression	3	707.22	235.74	6.82	3.20	0.003
Residual Error	17	587.40	34.55			
Total	20	1294.62				

Table 4.4.B: Significance of Individual Coefficients of Eq. (4.5)

Source	*DF*	*Seq SS*
V	1	551.13
F	1	125.05
α	1	31.04

where *DF*=Degree of Freedom

SS= Sum of Squares

MS= Mean Squares= (Sum of Squares/Degree of Freedom)

F= Test Statistic for the hypothesis of no difference in treatment means $= \frac{MS_{Rgression}}{MS_{Error}}$

As $F_o > F_{.05,3,17,}$ signifies that at least one of the regressor variables contributes significantly to the above model. The residual plot of the regression model given in Eq. (4.5) is given in Fig. 4.9.

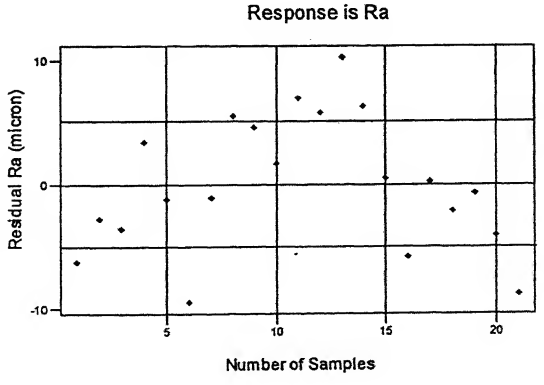

Figure 4.9: Plot of Residual for Eq. (4.5)

c) Error in Prediction:

Six experiments were chosen for validating the above *Regression* model developed (Eq. 4.5), and the predicted values were plotted along with experimental values as shown in Fig. 4.10. The experimental and the predicted R_a values for validation along with error are given in Table 4.5.

Table 4.5: Validation Data Set and Prediction Error of Eq. (4.5)

Expt #	*Speed (m/min)*	*Feed (mm/rev)*	*Rake Ang (Degrees)*	*Ra (μm)*	*Ra (Pred) (μm)*	*Error (μm)*	*Error (%)*
1	18.6	0.05	0	31.13	26.86	4.27	13.72
2	18.6	0.069	10	21.3	28.60	7.30	34.26
3	22.6	0.088	-10	32.53	29.33	3.20	9.85
4	22.6	0.05	10	25.6	19.73	5.87	22.93
5	26.6	0.069	-10	18.5	20.46	1.96	10.58
6	26.6	0.088	0	16.7	22.20	5.50	32.91

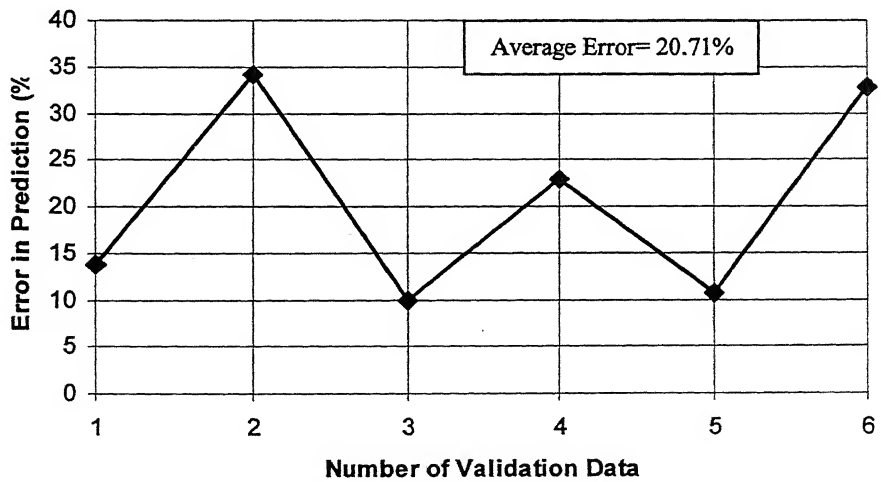

Figure 4.10: Plot of Error in Validation for Eq. (4.5)

4.3.1.2 Second Order Response Surface Model

This model in the simple form given below:

$$R_a = \beta_0 + \beta_1 v + \beta_2 f + \beta_3 \alpha + \beta_4 v^2 + \beta_5 f^2 + \beta_6 \alpha^2 + \beta_7 vf + \beta_8 v\alpha + \beta_9 f\alpha + \varepsilon \qquad (4.6)$$

The *Regression* equation along with the Analysis of Variance (*ANOVA*), for the above model is given as below:

a) Regression Analysis

The regression equation is

$$R_a = -326 + 25.5\,v + 2298\,f + 0.015\,\alpha - 0.531\,v^2 - 8457\,f^2 - 0.0067\,\alpha^2 - 42.4\,vf - 0.0198\,v\alpha + 4.06\,f\alpha \qquad (4.7)$$

Table 4.6: Regression Co-efficients of Eq. (4.7)

Predictor	*Coefficient*	*SE Coefficient*	*T-Values*	*P-Values*
Constant	-325.69	46.70	-6.97	0.000
V	25.546	3.730	6.85	0.000
F	2298.1	569.8	4.03	0.002
α	0.0147	0.5707	0.03	0.980
V^2	-0.53133	0.07872	-6.75	0.000
F^2	-8457	3489	-2.42	0.034
α^2	-0.00667	0.01259	-0.53	0.607
Vf	-42.42	11.17	-3.80	0.003
$V\alpha$	-0.01980	0.02123	-0.93	0.371
$F\alpha$	4.060	4.469	0.91	0.383

$S = 2.567$ $\quad R^2 = 94.4\%$ $\quad R^2\ (adj) = 89.8\%$

b) Analysis of Variance

Table 4.7.A: Result of ANOVA of Eq (4.7)

Source	*DF*	*SS*	*MS*	F_0	$F_{0.05,9,11}$	*P*
Regression	9	1222.13	135.79	20.61	2.90	0
Residual Error	11	72.48	6.59			
Total	20	1294.61				

Table 4.7.B: Significance of Individual Coefficients of ANOVA of Eq. (4.7)

Source	*DF*	*Seq SS*
V	1	551.13
F	1	125.05
α	1	31.04
V^2	1	370.12
F^2	1	25.06
α^2	1	13.71
Vf	1	95.02
$V\alpha$	1	5.56
$F\alpha$	1	5.44

As $F_o > F_{.05,9,11,}$ signifies that at least one of the regressor variables contributes significantly to the above model. The residual plot of the regression model given in Eq. (4.7) is given in Fig. 4.11.

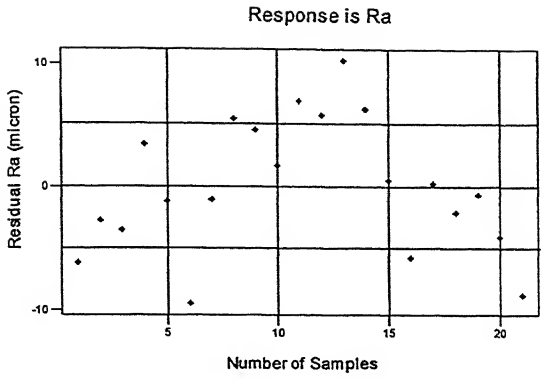

Figure 4.11: Plot of Residual for Eq. (4.7)

c) Error in prediction

Six experiments were chosen for validating the above *Regression* model developed (Eq. 4.7), and the predicted values were plotted along with experimental values as shown in Fig. 4.12. The experimental and the predicted R_a values for validation along with error are given in Table 4.8.

Table 4.8: Validation Data Set and Error for Eq. (4.7)

Expt #	*Speed (m/min)*	*Feed (mm/rev)*	*Rake Ang (Degrees)*	*Ra (μm)*	*Ra Pred (μm)*	*Error (μm)*	*Error (%)*
1	18.6	0.05	0	31.13	18.92	12.21	39.22
2	18.6	0.069	10	21.3	27.08	-5.78	27.12
3	22.6	0.088	-10	32.53	31.58	0.95	2.93
4	22.6	0.05	10	25.6	21.97	3.63	14.19
5	26.6	0.069	-10	18.5	18.71	-0.21	1.13
6	26.6	0.088	0	16.7	14.07	2.63	15.76

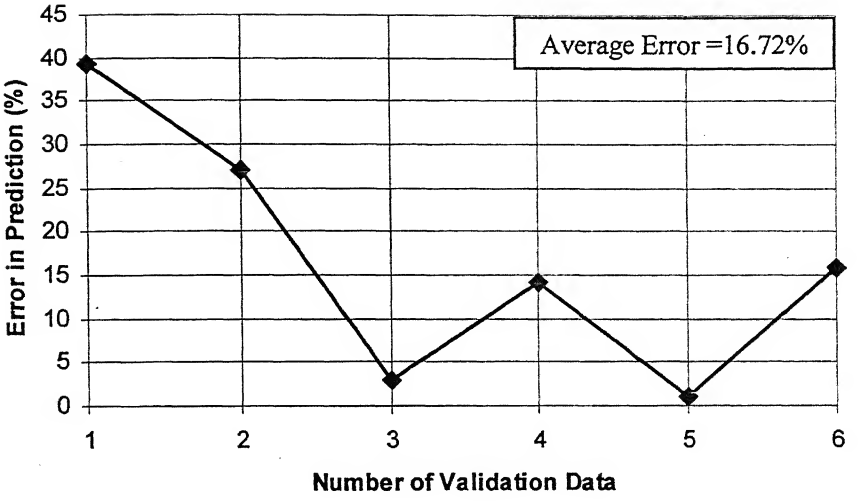

Figure 4.12: Plot of Error in Validation for Eq. (4.7)

4.3.2 Four Regressor model

In these models four inputs have been considered. They are speed (v), feed (f), rake angle (α) and vibration amplitude (a). The response is surface roughness in terms of R_a value.

4.3.2.1 Multiple Linear Regression Model

This model is in the simple form given below:

$$R_a = \beta_0 + \beta_1 v + \beta_2 f + \beta_3 \alpha + \beta_3 a + \varepsilon \qquad (4.8)$$

The *Regression* equation along with the Analysis of Variance (*ANOVA*), for the above model is given as below:

a) Regression Analysis

The regression equation is

$$R_a = 59.4 - 2.05v + 99.3f - 0.185\ \alpha + 0.0831a \qquad (4.9)$$

Table 4.9: Regression Coefficients for Eq. (4.9)

Predictor	*Coefficient*	*SE Coefficient*	*T-Values*	*P-Values*
Constant	59.37	12.93	4.59	0.000
V	-2.0529	0.4854	-4.23	0.001
f	99.29	85.15	1.17	0.261
α	-0.1847	0.1481	-1.25	0.230
A	0.08311	0.04008	2.07	0.055

$S = 5.379$ $R^2 = 64.2\%$ $R^2\ (adj) = 55.3\%$

b) Analysis of Variance

Table 4.10.A: Results of ANOVA for Eq. (4.9)

Source	*DF*	*SS*	*MS*	*F*	$F_{0.05,4,16}$	*P*
Regression	4	831.66	207.92	7.19	3.01	0.002
Residual Error	16	462.95	28.93			
Total	20	1294.61				

Table 4.10.B: Significance of Individual Coefficients of Eq. (4.9)

Source	*DF*	*Seq SS*
v	1	551.13
f	1	125.05
α	1	31.04
a	1	124.45

As $F_o > F_{.05,4,16,}$ signifies that at least one of the regressor variables contributes significantly to the above model. The residual plot of the regression model given in Eq. (4.9) is given in Fig. 4.13.

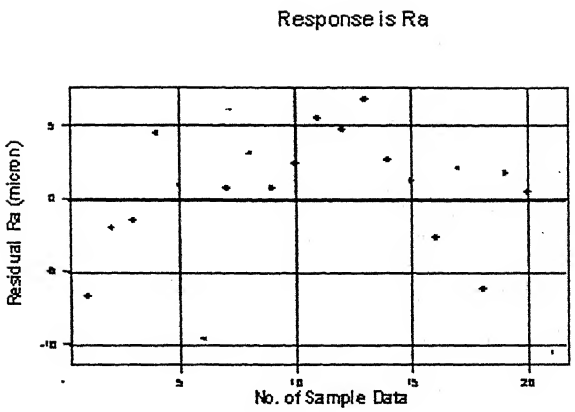

Figure 4.13: Plot of Residual for Eq. (4.9)

c) Error in Prediction

Six experiments were chosen for validating the above *Regression* model developed (Eq. 4.9), and the predicted values were plotted along with experimental values as shown in Fig. 4.14. The experimental and the predicted R_a values for validation along with error are given in Table 4.11.

Table 4.11: Validation Data Set and Error for Eq. (4.9)

Expt #	*Speed (m/min)*	*Feed (mm/rev)*	*Rake Ang (Degrees)*	*Vib (μm)*	*Ra (μm)*	*Ra Pred (μm)*	*Error (μm)*	*Error (%)*
1	18.6	0.05	0	22.7	31.13	28.12	3.01	9.66
2	18.6	0.069	10	32.5	21.3	28.97	7.67	36.02
3	22.6	0.088	-10	111	32.53	32.88	0.35	1.08
4	22.6	0.05	10	84	25.6	23.17	2.43	9.51
5	26.6	0.069	-10	96.25	18.5	21.57	3.07	16.60
6	26.6	0.088	0	95	16.7	21.50	4.80	28.76

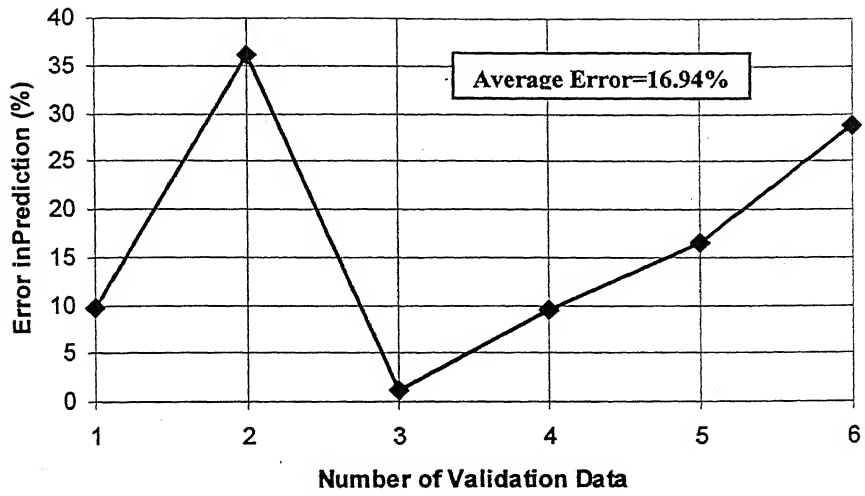

Figure 4.14: Plot of Error in Validation for Eq. (4.9)

4.3.2.2 Second Order Response Surface Model

This model is in the simple form given below:

$$R_a = \beta_0 + \beta_1 v + \beta_2 f + \beta_3 \alpha + \beta_4 v^2 + \beta_5 f^2 + \beta_6 \alpha^2 + \beta_6 a^2 + \beta_7 vf + \beta_8 v\alpha + \beta_9 \quad (4.10)$$
$$f\alpha + \beta_{10} va + \beta_{11} fa + \beta_{12} \alpha a + \varepsilon$$

The *Regression* equation along with the Analysis of Variance (*ANOVA*), for the above model is given as below:

a) Regression Analysis

The regression equation is

$$R_a = -78 + 4.2\,v + 1748\,f - 0.092\,\alpha + 0.802\,a - 0.082\,v^2 - 7438\,f^2 - 0.0276\,\alpha^2 - 0.00086\,a^2 - 23.9\,vf - 0.0216\,v\alpha - 0.0224\,va + 2.36\,f\alpha - 1.32\,fa + 0.00484\,\alpha a \quad (4.11)$$

Table 4.12: Regression Co-efficients for Eq. (4.11)

Predictor	*Coefficient*	*SE Coefficient*	*T-Values*	*P-Values*
Constant	-346.32	46.9	-7.38	0.000
V	26.485	3.342	7.92	0.000
f	1648.3	493.3	3.34	0.006
α	-1.3062	0.7504	-1.74	0.107
A	4.668	1.483	3.15	0.008
V^2	-0.53263	0.06893	-7.73	0.000
f^2	-4373	4192	-1.04	0.317
α^2	-0.02633	0.01281	-2.05	0.062
A^2	-0.05078	0.02271	-2.24	0.045
Vf	-34.05	13.99	-2.43	0.031
$V\alpha$	0.02564	0.02907	0.88	0.395
va	-0.09234	0.05349	-1.73	0.11
$F\alpha$	6.783	6.297	1.08	0.303
Fa	-12.24	13.08	-0.94	0.368
αa	0.00842	0.02268	0.37	0.717

$S = 2.363$ $R^2 = 97.4\%$ $R^2\ (adj) = 91.4\%$

b) Analysis of Variance

Table 4.13.A: Results of ANOVA of Eq. (4.11)

Source	*DF*	*SS*	*MS*	*F*	$F_{0.05,14,6}$	*P*
Regression	14	1261.115	90.08	16.13	3.96	0.001
Residual Error	6	33.498	5.583			
Total	20	1294.613				

Table 4.13.B: Significance of Individual Coefficients of Eq. (4.11)

Source	*DF*	*Seq SS*
V	1	551.133
f	1	125.045
α	1	31.039
A	1	124.446
V^2	1	246.277
f^2	1	27.942
α^2	1	12.255
A^2	1	41.391
vf	1	69.855
$V\alpha$	1	0.021
va	1	8.089
$F\alpha$	1	4.398
fa	1	0.014
αa	1	19.209

As $F_o > F_{.05,\ 14,\ 6}$, signifies that at least one of the regressor variables contributes significantly to the above model. The residual plot of the regression model given in Eq. (4.11) is given in Fig. 4.15.

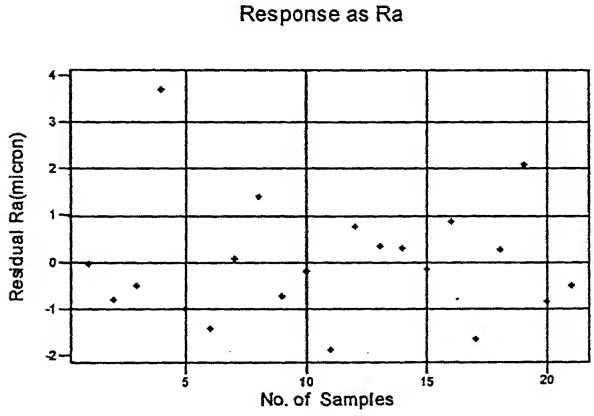

Figure 4.15: Plot of Residual for Eq. (4.11)

c) Error in Prediction

Six experiments were chosen for validating the above *Regression* model developed (Eq. 4.11), and the predicted values were plotted along with experimental values as shown in Fig. 4.16. The experimental and the predicted R_a values for validation along with error are given in Table 4.14.

Table 4.14: Validation Data Set and Error for Eq. (4.11)

Expt #	*Speed (m/min)*	*Feed (mm/rev)*	*Rake Ang (Degrees)*	*Vib (μm)*	*Ra μm)*	*Ra Pred (μm)*	*Error (μm)*	*Error (%)*
1	18.6	0.05	0	22.7	31.13	25.14	5.99	19.26
2	18.6	0.069	10	32.5	21.3	30.44	9.14	42.90
3	22.6	0.088	-10	111	32.53	28.66	3.87	11.89
4	22.6	0.05	10	84	25.6	26.75	1.15	4.50
5	26.6	0.069	-10	96.25	18.5	17.76	0.74	3.99
6	26.6	0.088	0	95	16.7	16.77	0.07	0.40

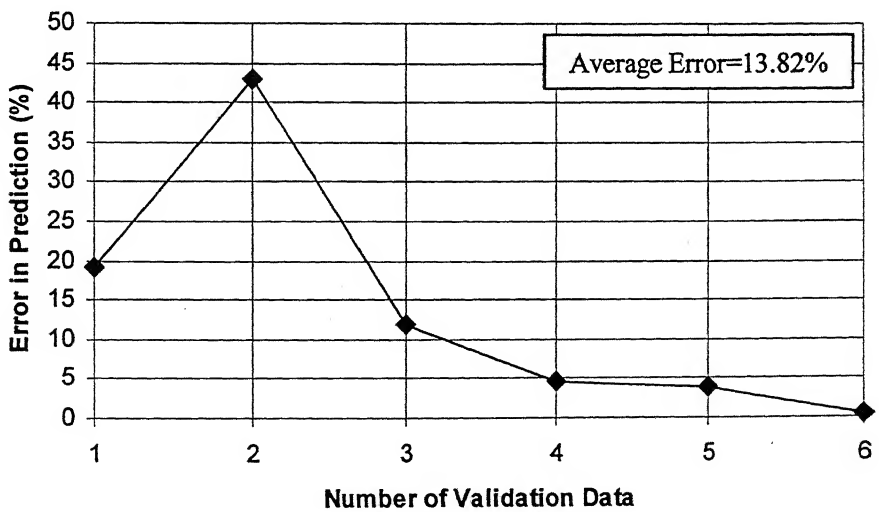

Figure 4.16: Plot of Error in Validation for Eq. (4.11)

4.3.3 Comparison between the various Regression Models

The four regression models developed in the above section were used to predict the surface roughness, using the same set of validation data. The Table 4.15 shows that the average error was minimum when a four regressor second order surface response model was used.

Table 4.15: Comparison of Prediction Error of various Regression models

No.	*No. of Regressor*	*Regression Model*	*Avg. Error (%)*
1	3	Multiple Linear Regression	20.71
2	3	Second Order Surface Response	16.72
3	4	Multiple Linear Regression	16.94
4	4	Second Order Surface Response Model	**13.82**

4.4 Neural Network Model

The data collected from the above experiments were used to train Artificial Neural Network (*ANN*) with the help of *MATLAB*. Total twenty one data were used for training in sequential mode and the other data, were used for validation. The validation data were same as those used for *Regression* models.

4.4.1 Neural Network Architecture

The architecture of the neural network is intimately linked with the learning algorithms used to train the network. Thus it plays an important role in predicting the output. Three different network architectures had been developed for this purpose. They are:

4.4.1.1 [3-6-1] Network Architecture

The *ANN* had three inputs viz. *Speed (v), Feed (f) and Rake Angle* (α) and *Average Surface*

Roughness (R_a) as the target output. It had a single hidden layer with six neurons.

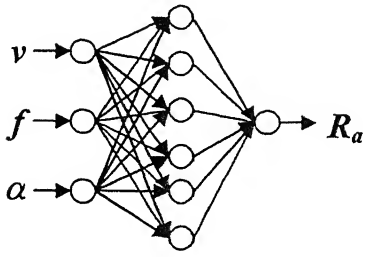

Figure 4.17: The architecture of [3-6-1]

4.4.1.2 [3-6-2] Network Architecture

The *ANN* had three inputs viz. *Speed (v), Feed (f) and Rake Angle (α). Average Surface Roughness (R_a) and Vibration (a)* were the target outputs. It had a hidden layer with six neurons.

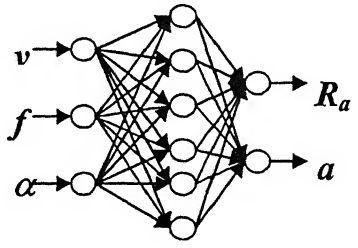

Figure 4.18: The architecture of [3-6-2]

4.4.1.3 [3-7-7-1] Network Architecture

The *ANN* had three inputs viz. *Speed (v), Feed (f) and Rake Angle (α). Average Surface Roughness (R_a)* was the target outputs. It had two hidden layers with six neurons each.

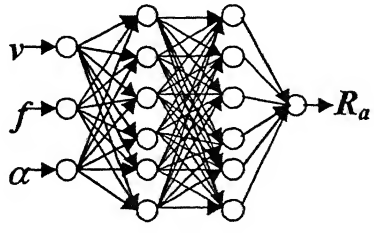

Figure 4.19: The architecture of [3-7-7-1]

4.4.2 Comparison between the various available algorithms

Some of the training functions (Section 2.3.6) were able to train the *ANN* with the same training and validation data, as the type of data and the architecture affects the training function to be used. All the *ANNs* were trained for 50000 epochs, with a goal of making the sum square error to be zero which was measured by a network performance function. The steady state error in some of the training functions were getting unstable like TRAINLM, TRAINGDX, for some architecture so were not included in the comparison. The results are given in Table 4.16 the first six networks, having the minimum error between the predicted and the validation target data, for the same set of data were selected for further analysis. The following Fig. 4.20 and 4.21 gives the plot of the training and the prediction capabilities of the selected networks respectively.

Table 4.16: Comparison of Error and Performance of Various Training Functions and Network Architecture

Training Function	*Architecture*	*Performance*	*Error (%)*
BFGS quasi-Newton	[3-6-1]	2.78×10^{-3}	17.39
Resilient	[3-6-1]	3.12×10^{-7}	28.43
One Step Secant	[3-6-1]	7.26×10^{-4}	29.21
Adaptive Gradient Descent	[3-7-7-1]	9.61×10^{-4}	35.29
Gradient Descent	[3-7-7-1]	0.82×10^{-3}	38.58
Adaptive Gradient Descent	[3-6-2]	1.83×10^{-3}	41.29
Gradient Descent	[3-6-1]	7.16×10^{-4}	69.06
Scaled Conjugate Gradient	[3-6-1]	7.23×10^{-9}	75.22

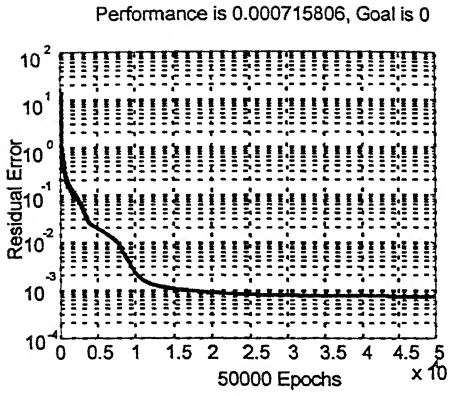

Figure 4.20.A: Gradient Descent

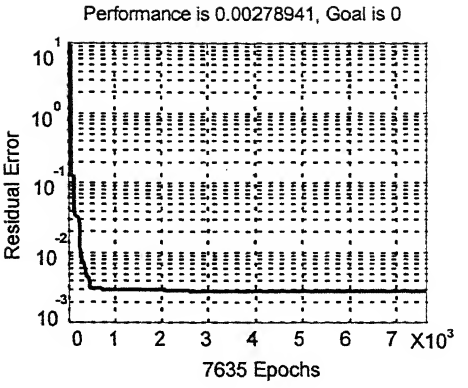

Figure 4.20.B: BFGS quasi-Newton

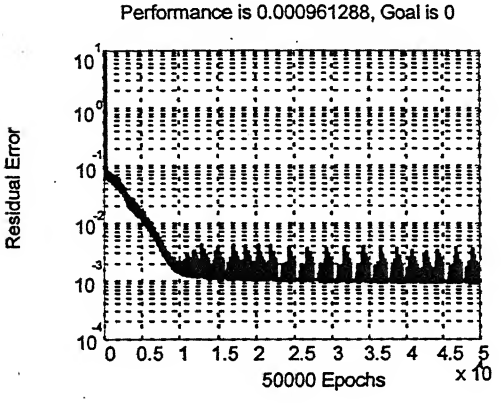

Figure 4.20.C: Adaptive Gradient Descent

(With two-Hidden Layers)

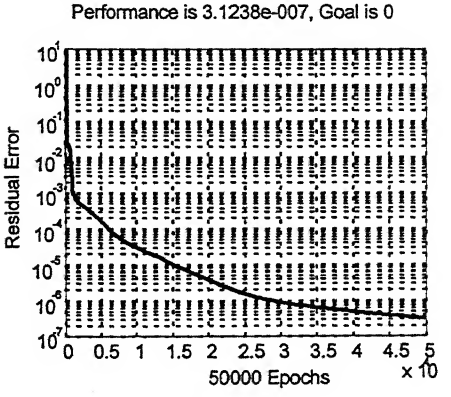

Figure 4.20.D: Resilient

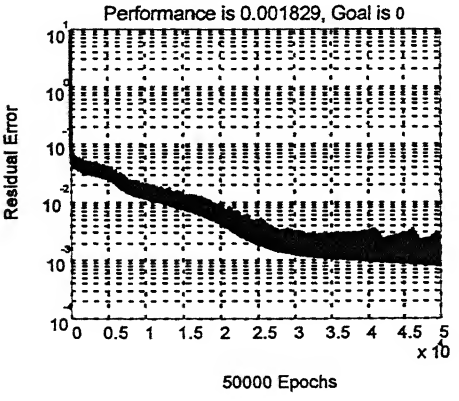

Figure 4.20.E: Adaptive Gradient Descent

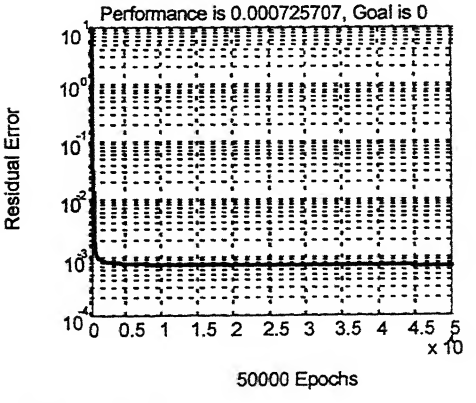

Figure 4.20.F: One Step Secant

Figure 4.20: The Plot of Residual Error versus No. of Epochs

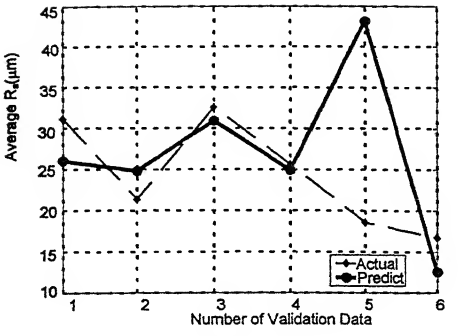

Figure 4.21.A: Gradient Descent

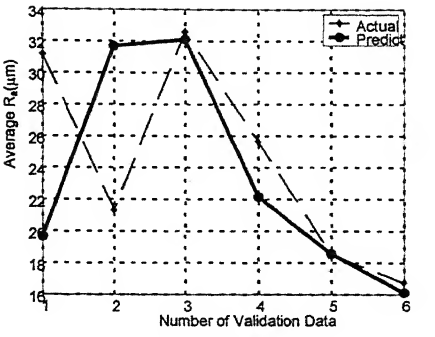

Figure 4.21.B: BFGS quasi-Newton

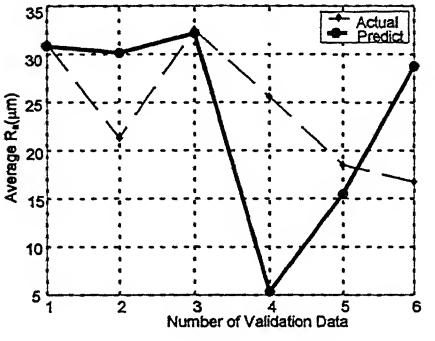

Figure 4.21.C: Adaptive Gradient Descent (With two-Hidden Layers)

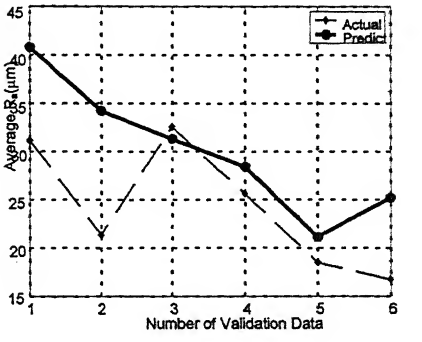

Figure 4.21.D: Resilient

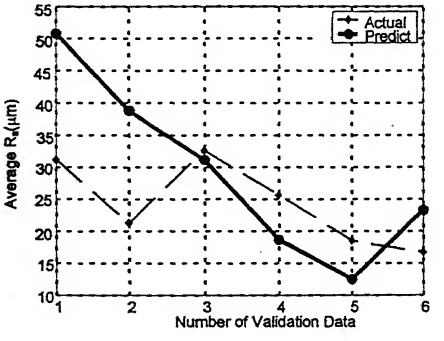

Figure 4.21.E: Adaptive Gradient Descent

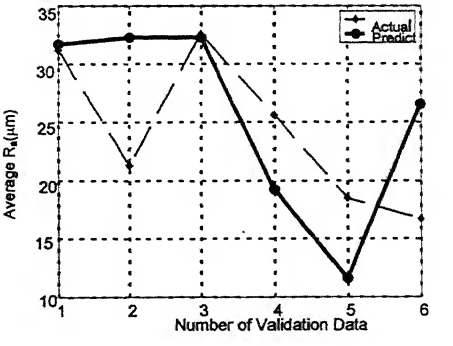

Figure 4.21.F: One Step Secant

Figure 4.21: Comparison between the Predicted and the Actual values

4.4.3 [4-6-1] Network Architecture

The *ANN* had four inputs viz. *Speed (v), Feed (f), Rake Angle (α) and Vibration (a), Average Surface Roughness (R_a)* being the target output. Chen [13] had used the measured vibration as an input to the neural network. But the measured vibration is also dependent on the other independent inputs *v, f and* α. Ideally for being able to use vibration as an independent input, one must control the vibration supplied to the process. The actuator and the tool holder developed as given in Appendix A and B respectively, can be used for supplying the vibration independently into the system.

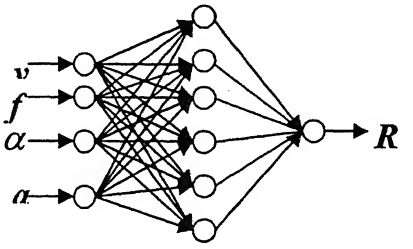

Figure 4.22: The architecture of [4-6-1] *ANN*

The various training functions (Section 2.3.6) used along with the [4-6-1] architecture is shown in Fig. 4.23. The comparison between the prediction capabilities of networks trained in different ways are given in the Fig. 4.24. The Table 4.16 gives the error (%) of these networks.

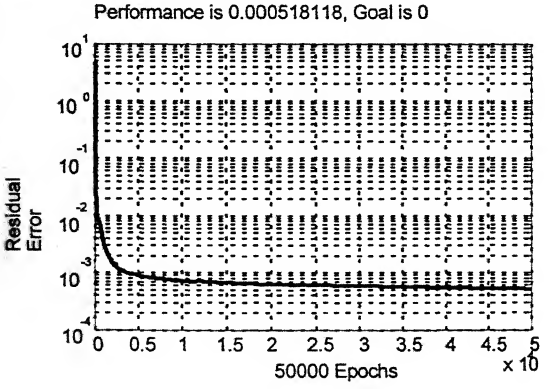

Figure 4.23.A: Resilient

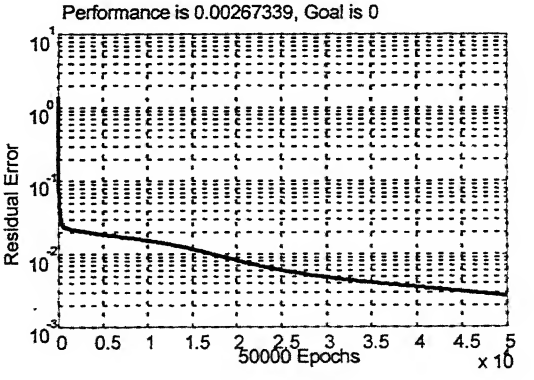

Figure 4.23.B: Gradient Descent

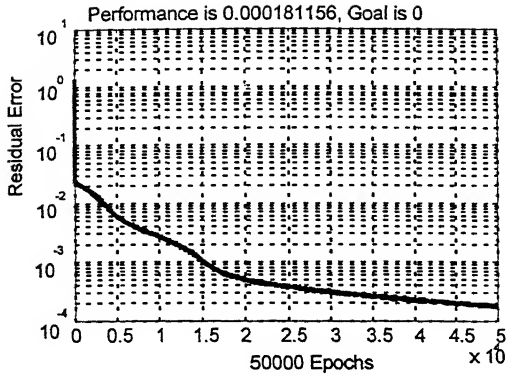

Figure 4.23C: Gradient Descent X

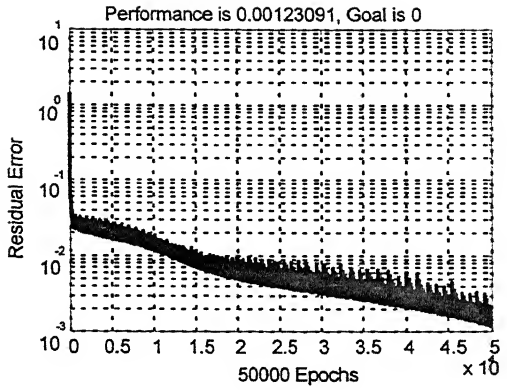

Figure 4.23.D: Adaptive Gradient Descent

Figure 4.23: The Plot of Residual Error versus No. of Epochs

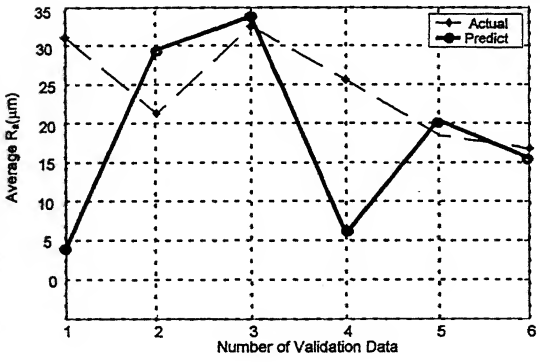

Figure 4.24.A: Resilient

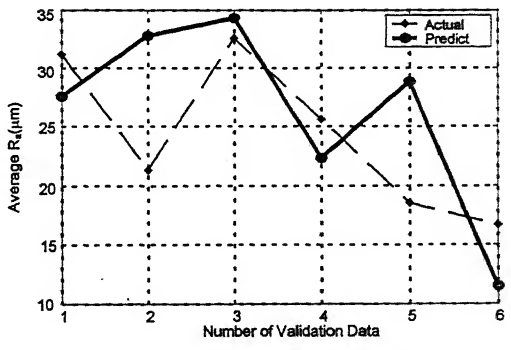

Figure 4.24.B: Gradient Descent

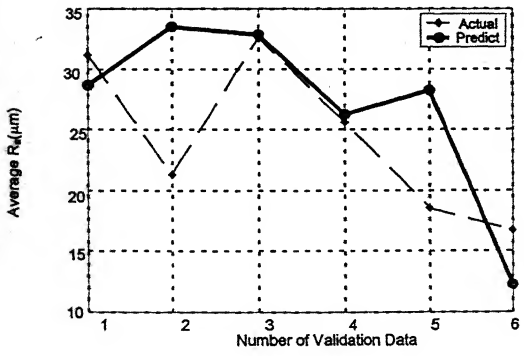

Figure 4.24.C: Gradient Descent X

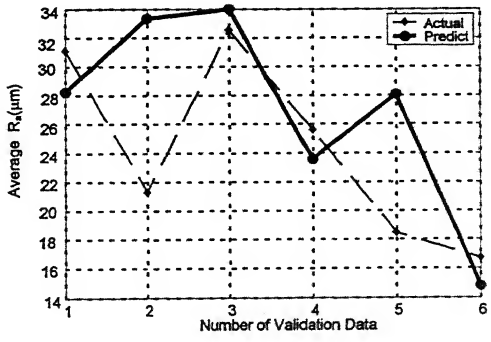

Figure 4.24.D: Adaptive Gradient Descent

Figure 4.24: Comparison between the Predicted and the Actual values

The Table 4.17 shows the comparison between the prediction errors (%) of the four [4-6-1] *ANN* with [3-6-1] *ANN* for the same set of validation data. Thus it was observed that most of the *ANNs* with four inputs were able to predict the surface roughness more accurately than those with three inputs.

Table 4.17: Comparison of Prediction Error between [3-6-1] and [4-6-1]

Training Function	***Architecture***			
	[3-6-1]		***[4-6-1]***	
	Performance	***Error (%)***	***Performance***	***Error (%)***
Resilient	3.12×10^{-7}	28.43	5.18×10^{-4}	46.56
Adaptive Gradient Descent	1.83×10^{-3}	41.29	1.23×10^{-3}	**23.55**
Gradient Descent	53.82×10^{-3}	69.06	2.67×10^{-3}	28.47
Gradient Descent X	------	-----	1.81×10^{-4}	24.74

4.5 Experimental Results

Results obtained from experiments and *Regression* as well as *ANN* models are discussed below.

The optical transducer used to measure *on-line* surface roughness also picks up vibration signal from the cutting process, but there is a close relation between the *on-line* and *off-line* surface roughness making the above transducer fit for '*On-line Monitoring of Surface Roughness*'. The simple yet robust arrangement makes it suitable for industrial implementation.

Speed and *feed* have significant effects on *surface roughness*. When amplitude of vibration was included then it also had a significant effect.

The most accurate *Regression* model developed was the four input second order model with an average error of 13.8%. This confirmed that the assumption of considering vibration as an input parameter made by Chen [13] was effective for modeling surface roughness.

Various types of *ANN* architectures and learning algorithms give rise to different levels of prediction capabilities. The network architecture had a significant effect on the type of training function used, for the same set of data. A [3-6-1] *ANN* with BFGS quasi Newton training function was the most accurate three layered ANN model, in predicting the surface roughness with an average error of 17.39%. But it could not be used for a four input ANN model, as the training got unstable.

Two hidden layer *ANN* gave more accurate models for training functions of the same type. The adaptive gradient descent learning algorithm with a 4-6-1 structure gave a minimum error of 23.55% which was the most accurate four layered ANN model developed in this work, as compared to 41.29% for architecture of [3-6-1].

Regression models had better predicting capability for the particular experimental data than *ANN* models. This can be mainly accounted for the inaccuracy of data collected, the number of experiments and the range of the input parameters selected.

The predicting capability of the mathematical model suggested that they might not be useful for simulating the cutting process, so a more complete model is desired which will take into account a number of other parameters on which surface roughness depends, for example tool overhang, nose radius, depth of cut etc.

Chapter V

Vibration due to regenerative chatter and its control

5.1 Introduction

The need for more accurate and reliable machine tools is the main thrust of today's research. This has necessitated that their design to be made not only from the static consideration but also considering their dynamic instability. Any vibration between the tool and the workpiece leads to inaccuracies in the workpiece. Thus a proper insight to the vibrations occurring in the machine tools is required.

During the machining operation, both static and dynamic forces act on the machine tool structure. The dynamic loads may be having periodic or impact characteristics and may act in either of the following manners:

1) dynamic behavior caused entirely by the acting load (*Forced Vibrations*)
2) dynamic behavior initiated by the acting load (*Free Vibrations*)
3) dynamic behavior through the interaction between machine tool structure and cutting process (*Self-excited Vibrations*)

Chatter is described as the most common phenomena of dynamic instability in machine

tools in one or more forms of self excited vibrations, leading to relative movement between tool and work piece in the radial direction. The main sources of vibration are as follows:

1) inhomogenities in the work piece material
2) built-up edges in cutting tools
3) unbalanced and distributed forces in the drives
4) intermittent cutting (like milling)
5) transmission of vibration from the ground which vibrates due to other sources
6) generation of vibration from the cutting process itself, commonly known as the machine tool chatter.

The effect of vibration may be categorized as follows:

1) the effect of vibration on the machine tools
2) the effect of vibration on the cutting conditions
3) the effect of vibration on the workpiece
4) the effect of vibration on the cutting tool

In this particular study we have focused on the effect of vibration on workpiece and cutting conditions. It had been planned to improve surface finish by controlling vibration. We have considered machine tool chatter to be the source of the vibration which causes the undue relative movement between the tool and the workpiece in the radial direction.

5.2 Machine Tool Chatter

Machine tools can vibrate due to the cutting process itself under some particular conditions. In these cases, exciting force does not come from an external source, but belongs to the cutting process itself. These types of vibrations are self-excited and commonly known as machine tool chatter.

ıbility due to chatter may arise due to one or both of the following reasons:

1) Introduction of negative damping coefficient either through the cutting process itself or through interaction with the system parameters.
2) Instability through directional effects on modal responses.

: most important characteristic property of chatter is that it is not induced by external iodic forces, but rather the forces that bring it into being and maintain are generated in vibratory process itself i.e. the dynamic process itself, as can be shown in Fig. 5.1. re δx and δF are the change in displacement between tool and workpiece and change cutting force, respectively.

r free vibration of a single degree of freedom system as shown in Fig. 5.2, the equation motion is given by ,

$$m\ddot{x} + c\dot{x} + kx = 0 \tag{5.1}$$

here m, c ,k are mass, damping coefficient and stiffness of the equivalent system spectively.

$$\dot{x} = \frac{dx}{dt} \text{ and } \ddot{x} = \frac{d^2x}{dt^2}$$

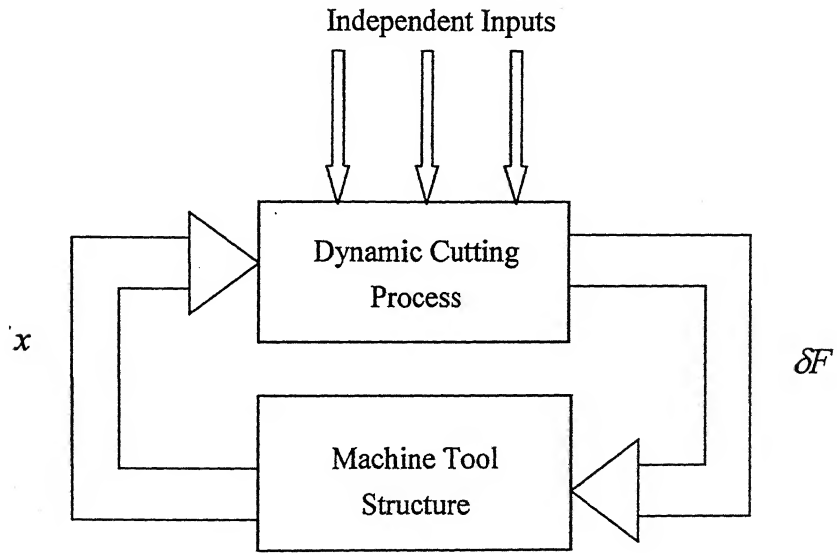

igure 5.1: Schematic diagram of Self-excited Machine Tool Vibration

If $c > 0$, the system is a damped one and is dynamically stable and the amplitude of x is exponentially decreases with time as shown in Fig. 5.3(a). If $c = 0$, free undamped vibration occurs at the threshold of stability. When $c < 0$, the system is a self-excited one and is dynamically unstable and the amplitude of x increases exponentially with time as shown in Fig. 5.3(b).

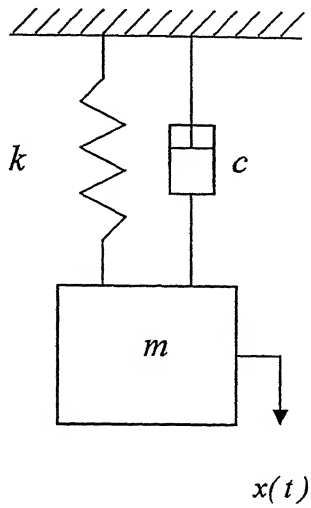

Figure 5.2: Single Degree of Freedom, Mass-Spring-Dashpot

Similarly when an external force $F(t)$ acts on the system, which depends on the relative velocity, the following equation may be written,

$$m\ddot{x} + c\dot{x} + kx = F(t) \tag{5.2}$$

and $$F(t) = A + B\dot{x}$$

$$\therefore m\ddot{x} + (c - B)\dot{x} + kx = A \tag{5.3}$$

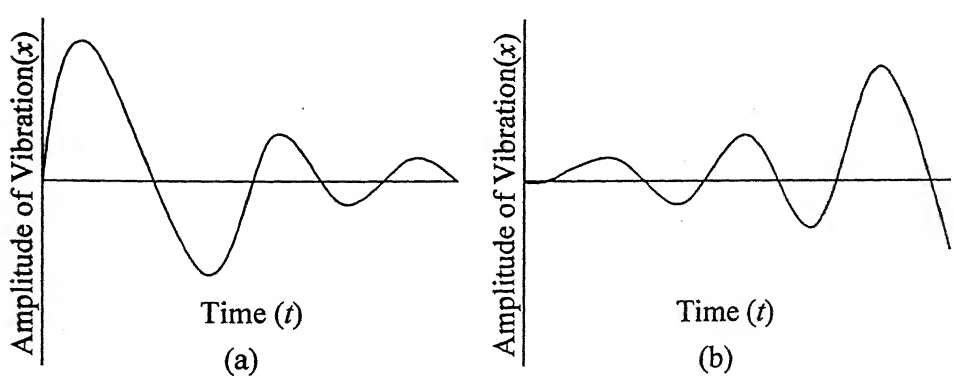

Figure 5.3: (a) Damped Vibration (b) Self-excited Vibration

Though in dynamically unstable systems the amplitude of vibration should grow indefinitely but actually that does not occur. At large amplitudes the nonlinearity of the system becomes more and more prominent and the growth of the amplitude is restricted by that.

In machine tools self-excited vibrations occur at a frequency close to the natural frequency of the undamped system. Many models have been proposed by researchers for analyzing self-excited vibration in machine tools. The main models are given in Fig. 5.4.

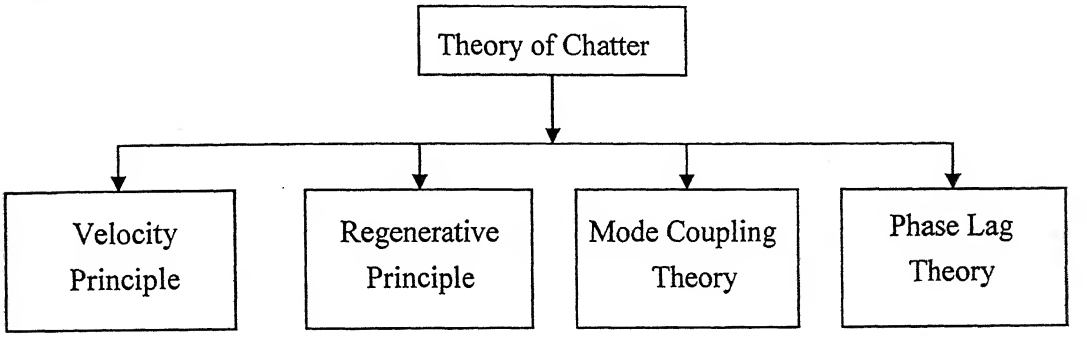

Figure 5.4: The various types of models for self-excitation vibration in machine tools

In this present work a *Regenerative Principle* model along with the concept of coupling coefficient, for orthogonal cutting was used, which is discussed in details in the following sections.

There are several factors that are responsible for machine tool chatter. The primary causes of chatter can be categorized as forced, self-excited and regenerative vibrations. Forced vibrations can result from an imbalance of rotating members of the machine tool or impacts due to a multi-tooth cutter. Self-excited and regenerative chatter are dependent on the relative motion between the tool and the workpiece. Self-excited chatter can be due to the variation of the friction force on tool rake as a result of dynamic variation of shear and friction angle. The friction force can be a strong function of the relative motion of the tool and the workpiece. Regenerative chatter develops when the cutting pattern in the previous tool pass affects the chip thickness and, therefore, the cutting force during the current tool pass. For certain conditions of cutting speed, overlap between the two

successive tool passes, tool geometry and the transfer function characteristics of the machine tool, the cutting process can become unstable and develop machine tool chatter.

5.3 Purpose of vibration control

Machine Tool chatter is an undesirable phenomenon. Its adverse effects include undesirable noise, poor surface finish of the workpiece, reduced dimensional accuracy and reduced machine tool life. In this work the main focus is on the control of surface roughness in turning operation. The effect of machine tool chatter on surface roughness is minimized by active control of vibration i.e. by introducing vibration from external source. A suitable vibration control mechanism is developed which can be used *on-line* to minimize the surface roughness.

5.4 Strategies of vibration control

The vibration control in machine tools can be achieved with the help of isolation techniques, for which two types of control mechanism are used. They are as follows.

5.4.1 Passive Control

In Passive Control of vibration the vibration energy is simply absorbed by a damper storing or dissipating the energy. It does not supply any vibration to the system. The simplest passive damper is shown in Fig. 5.5. Examples of passive vibration control are steel or rubber springs and various types of pads.

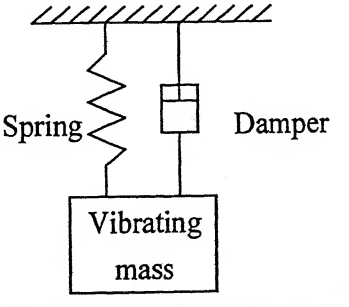

Figure 5.5: Passive Vibration Control

5.4.2 Active and semi-active Control

Active vibration isolation involves the use of an active system to reduce the transmission of vibration from one body to another. A broader definition would also include the reduction of vibration of machine or a structure by an active vibration absorber. A constant force source that is independent of the dynamics of the machine, simplifies the complex analysis and the result obtained are indicative of what can be achieved in many practical cases.

The objective of active vibration control is to reduce the vibration in a mechanical system by automatic modification of the system's structural response. An active vibration control system can take many forms, but the important components of any vibration control system are a sensor (to detect the vibration), an electronic controller (to suitably manipulate the signal from the detector) and an actuator (which influences the mechanical response of the system). Types of actuators used in active vibration control can be broadly classified into those which are fully-active and those which are semi-active as shown in Fig. 5.6 (a) and (b) respectively. Fully active actuators are able to supply mechanical power to the system, examples being electromagnetic shakers, piezoelectric ceramics, magnetostrictive and electrohydraulic devices. Actuators of these types can be used to generate a secondary vibration response in a linear mechanical system, which could reduce the overall response by destructive interference with the original response of the system caused by the primary source of vibration.

Semi-active actuators behave as essentially passive elements i.e. they can only store and dissipate energy. Their use in the active control stems from the fact that their passive mechanical properties can be adjusted by the application of control signal and such systems are thus sometimes called 'adaptive'. Semi-active actuators can be constructed using electrorheological fluids or shape memory alloys.

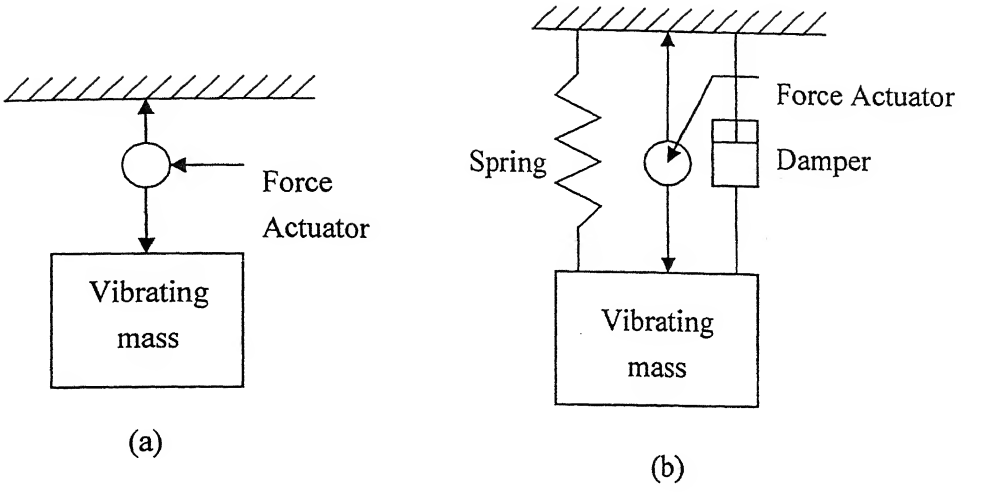

Figure 5.6: (a) Active Vibration Control; (b) Semi-active Vibration Control

5.5 Implementation of vibration control in turning operation

In this work we had focused on the control of surface roughness in orthogonal turning operation. Surface roughness measurement as well as control are considered as offline and post machining operations. A bifurcated optical transducer was used to monitor the on-line surface roughness, while the turning operation was taking place. Now the control of the same had to be achieved. Vibration caused by regenerative chatter leading to relative movement between tool and workpiece, was selected as the control action. An active control of vibration was implemented to minimize the above vibration. This was achieved by an active vibration control system. The proposed control system consisted of an accelerometer, PID controller and a piezoelectric displacement actuator. The simulation of the above control mechanism gave an insight to the *on-line* control of surface roughness in turning with the help of the active vibration control.

To achieve the *on-line* active control of vibration it is desirable to model the dynamic cutting process, the machine tool vibration and the actuator with the help of experimentation. After developing the above models the proposed PID controller can be designed accordingly. The modeling is discussed in the subsequent sections.

5.5.1 Dynamic model of the cutting process in turning

Chatter theory deals with metal cutting under non-steady state conditions, i.e., in the presence of vibration. The static cutting process model is not enough, thus a dynamic cutting model for turning operation was incorporated. The main difference between the static and the dynamic model is that in the later the cutting forces change at every instant. This leads to the relative movement of the tool and workpiece.

5.5.1.1 Static cutting process model in turning

In the static cutting process, as shown in Fig. 5.7, the static cutting force (F_o) dependent on two parameters f_o (feed in mm/rev) and V_o= (Cutting speed in mm/s), as penetration rate (r_o) in mm/s, $r_o=f_oN$ i.e. r_o can be expressed in terms of f_o. Thus F_o is given by,

$$F_o=\psi_o(f_o,V_o) \tag{5.4}$$

which can be written as,

$$dF_o = k_f f_o + k_v V_o \tag{5.5}$$

where $k_f = \left(\frac{\partial F_o}{\partial f_o}\right)_{dV=0}$ and $k_v = \left(\frac{\partial F_o}{\partial V_o}\right)_{df=0}$ are the parameters that can be found out for any cutting process from experimental data.

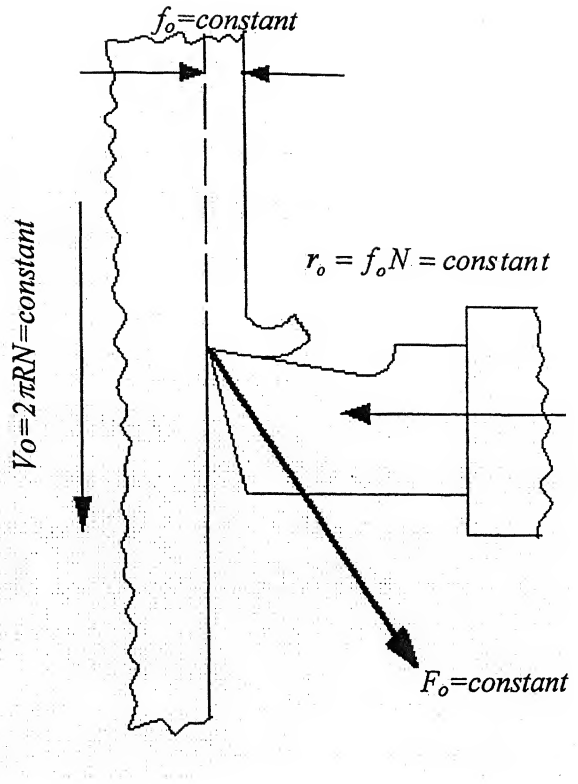

Figure 5.7: Static cutting process

5.5.1.2 Dynamic cutting process model in turning

As shown in Fig. 5.8, in dynamic cutting all the parameters namely rate of penetration (r), feed (f) and speed (V) do not remain constant but they start varying as given in Eq. (5.6). f and r can no longer be expressed in terms of each other. This may occur due to various reasons, for example, inclusion of a hard grain in the workpiece, vibration in the machine tool frame, tool wear etc.

$$\begin{aligned} V &= V_o + dV \\ f &= f_o + df \\ r &= r_o + dr \end{aligned} \tag{5.6}$$

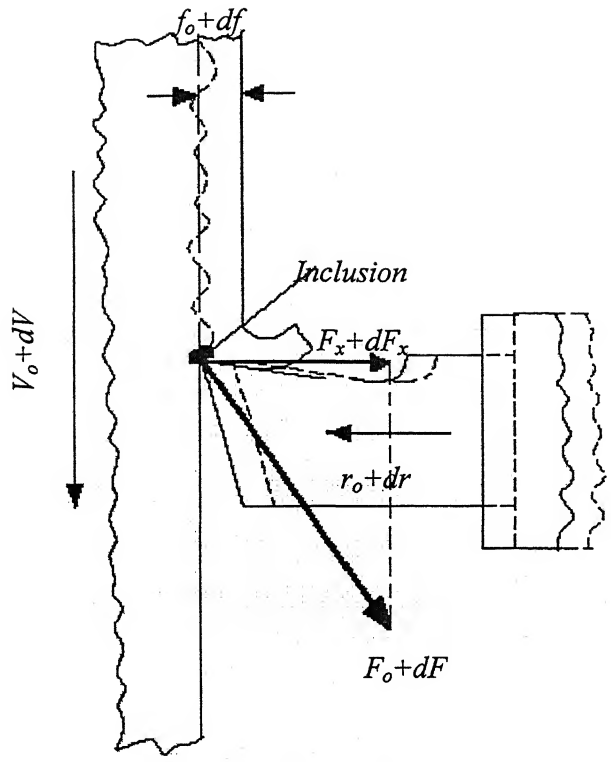

Figure 5.8: Dynamic cutting process

Thus the dynamic cutting force is then expressed as

$$F=\psi(f,V,r) \tag{5.7}$$

which can be written as,

$$dF = k_1 df + k_2 d + k_3 dr \tag{5.8}$$

The parameters k_1, k_2 and k_3 can be expressed as,

$$k_1 = \left(\frac{\partial F}{\partial f}\right)_{dV=dr=0}, \; k_2 = \left(\frac{\partial F}{\partial V}\right)_{df=dr=0} \text{ and } k_3 = \left(\frac{\partial F}{\partial r}\right)_{dV=df=0}$$

The above parameters are to be determined by experiments only. As for example while determining k_1, the feed has to be changed by df, but the V and r have to be kept constant, which is not possible as $dr=df.N$. But the coefficients of the equation for the dynamic cutting force variation Eq. (5.8) are tied to the co-efficients of the static equation, Eq.

(5.5). The equation [24] for the dynamic cutting-force variation can be expressed as

$$dF = k_1 df + \frac{(k_f - k_1)}{N} dr + \left[k_V - (k_f - k_1)\frac{f_o}{V_o} \right] dV \qquad (5.9)$$

where

k_1= Chip thickness co-efficient

k_f= Cutting force co-efficient

$(k_f - k_1) = K$= Penetration co-efficient

$[K_v - (k_f - k_1) f_o / V_o]$= Cutting speed co-efficient

Experiments were conducted to obtain the values of the co-efficients (k_s, k_v and k_1) in the equation of the dynamic cutting force, given by Eq. (5.9). The above co-efficients were determined experimentally through the process of system identification as shown in section 5.5.4.1.

5.5.2 Modeling of the Machine Tool Vibration (Tool-W/p interaction)

The single degree of freedom chatter theory should be considered for cases where the rigidity of the tool and the support is relatively small in one direction, so as to allow the tool to vibrate in one direction only. Otherwise the tool motion will not be straight and two degree of freedom theory will have to be used for analyzing the problem.

In this work the relative displacement between the tool and the workpiece had been simulated so that it can be compensated with a displacement in opposite phase with the help of a piezo-electric actuator. Therefore only a single degree of freedom model had been incorporated along with a coupling coefficient.

5.5.2.1 Single Degree of Freedom Model

The dynamic cutting force element dF_x acts on the machine frame and forces the machine tool frame into vibration; this effects a change in the relative position of the cutting edge, which in turn leads to a further change in dF. The disturbance forces the machine tool to

vibrate with different modes of vibration. The natural mode, however determines the relative motion of the cutting edge with reference to the work and is therefore partly responsible for deciding the form and characteristic of the dynamic cutting force element dF. In this work we have considered a situation in which the natural mode of vibration is of the frame permits vibration in a direction perpendicular to the cutting speed.

Since the machine tool frame has distributed elasticity and mass, it possesses an infinite number of natural modes of vibration along with a direction of principal vibration. Provided the natural frequencies of the frame are not very close to each other, it is permissible [24] to imagine the frame replaced by a number of elementary vibratory systems, consisting of an equivalent mass (m), an equivalent damper (c) and an equivalent spring (k). An equivalent system for machine tool with single degree of freedom model for the machine tool is shown in Fig. 5.9.

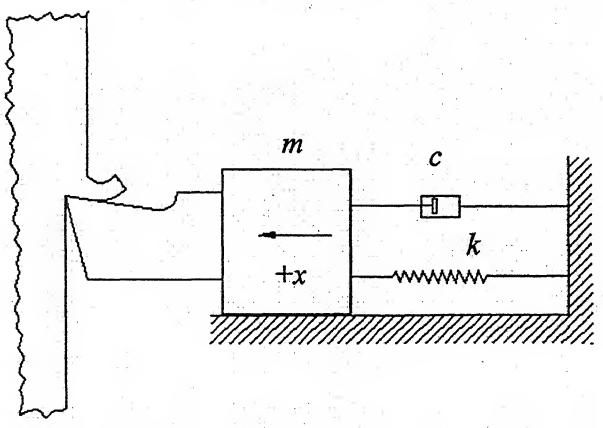

Figure 5.9: The equivalent system for the machine tool with one degree of freedom

The following steps were carried out for the analysis of the chatter process

1) It was assumed that the steady-state cutting process had been disturbed by a relative vibration x occurring between the tool and the workpiece having the direction of the principal vibration.
2) The influence of x on the cutting process was investigated and the cutting-force element dF_x found.

3) From dF_x the equivalent damping of the dynamic cutting process was calculated and added to the frame damping.
4) Cutting conditions for which the overall damping obtained in this way was negative were unstable and would cause chatter

Considering a chatter type in which the amplitudes x lie in the plane perpendicular to the cutting direction, regardless of whether the amplitudes are co-directional with the feed or perpendicular to it. In this type of chatter the cutting speed (V) is not directly influenced by the vibration x. It may of course happen that the load on the machine changes during the cutting process, and that this may setup vibration in the in the driving gear train which in turn can lead to an alteration in the cutting speed. For the purpose, however this possibility is ignored and $dV=0$ is used in Eq. (5.9). This assumption will be justified in due course in the agreement obtained between the theoretical and the experimental results. From Eq. (5.9), therefore the dynamic force element dF_x can be written as,

$$dF_x = k_1 df + \frac{(k_s - k_1)}{N} dr \tag{5.10}$$

Thus it can be said that dF_x depends only on the change in the chip thickness df and the change in the rate of penetration dr. Thus it is also necessary to understand the way in which they change in the process. The dynamic instability can occur only due to the change in the chip thickness df, and the variation rate of penetration dr always exerts a stabilizing influence [25].

5.5.3 Effect of Chip thickness Variation (Regenerative effect)

The chip thickness variation effect occurs with single edged tools when the cutting edge of the tool traverses a surface on the work from which it has taken a previous cut. The Fig. 5.10 shows a cutting tool at time t. Under disturbance free conditions this edge would remove a chip of constant thickness f_o. As a result of vibration $x(t)$ the surface of the chip to me removed is not flat but has a wavy form as indicated by *curve 1*, in Fig.

5.10. The surface of the chip has in fact been removed at an earlier time $(t\text{-}T)$, where T is the time for one revolution and given by $1/N$. At this time the vibration x was already present and from time $t=0$ onwards the cutting edge in actual contact moves along *curve 2* and hence the instantaneous chip thickness will be given by (f_o+df). In turning, however it is possible for successive cuts not to overlap, as is true, for example, for screw cutting. To provide this type of cutting, the overlap cutting factor μ has been introduced. The chip thickness variation can be expressed by

$$df = x(t) - \mu x(t-T) \tag{5.11}$$

where the value of μ is selected as $\mu \leq 1.0$ for turning operation.

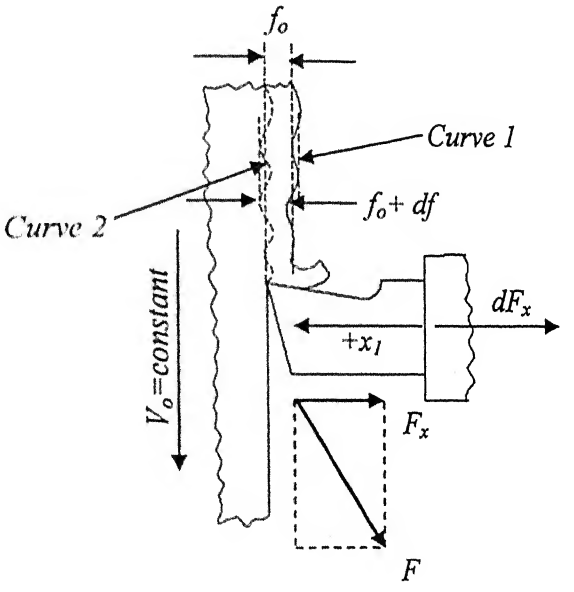

Figure 5.10: Chip-thickness variation effect occurring during cutting

5.5.4 Effect of variation in Penetration rate

The effect of penetration rate is defined as $r_o=f_oN$, where f_o and r_o are the values of feed and penetration rate in static condition. As r_o varies, it no longer remains a function of f_o. Its variation dr is then defined as disturbance velocity (dx/dt) superimposed on the feed rate.

The change in the penetration rate can be easily be found because if the variation $x(t)$ is superimposed on the nominal feed f_o, the rate of penetration associated with it will

change from $r_o=f_oN$ to r_o+dr, where $dr=dx/dt$.

Thus substituting ds and dr in terms of $x(t)$ in Eq. (5.9), we get

$$dF_x = k_1[x(t)-\mu x(t-T)]+(\frac{k_f-k_1}{N})\frac{dx}{dt}$$

$$dF_x = k_1[x(t)-\mu x(t-T)]+(\frac{k_f-k_1}{N})\dot{x} \qquad (5.12)$$

5.5.5 Transfer function of the Cutting Process

The model represented by Eq. (5.12), can be shown as in Fig. 5.11

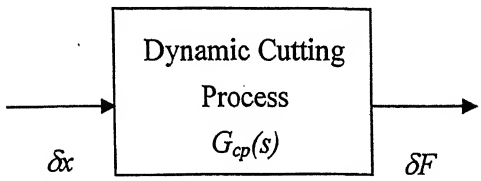

Figure 5.11: The model of the dynamic cutting process

Simplifying Eq. (5.12) we get,

$$dF_x = k_1x(t)-\mu k_1x(t-T)+(\frac{k_f-k_1}{N})\dot{x}$$

Taking Laplace transform, we get

$$dF_x(s) = k_1(s)-\mu k_1e^{-Ts}x(s)+(\frac{k_f-k_1}{N})s \qquad (5.13)$$

The transfer function is given by,

$$G_{cp}(s) = \frac{dF_x}{x(s)} = k_1-\mu k_1e^{-Ts}+(\frac{k_f-k_1}{N})s \qquad (5.14)$$

5.5.6 Transfer function of the Machine Tool

The dynamic force dF_x, given in Eq. (5.12) acts on the elastic frame of the machine and induces vibration in it. The machine thus vibrating, one of its natural modes is

represented by an equivalent elementary vibrating system consisting of the equivalent elements mass (m_m), damping (c_m) and spring (k_m) as shown in Fig. 5.9. These system parameters can be determined by the response of the machine, which is discussed in section 5.6.1.2.

Thus the equation of motion of the equivalent vibratory system consisting of the tool and work piece interface, shown in Fig. 5.9 can be represented as

$$m\ddot{x}_1 + c\dot{x}_1 + kx_1 = 0 \tag{5.15}$$

This is now acted on by a force element dF_x and hence the equation of motion for the mode of vibration concerned is now given by the following equation and can be represented by Fig. 5.12,

$$m\ddot{x}_1 + c\dot{x}_1 + kx_1 = -dF_x \tag{5.16}$$

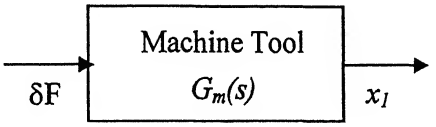

Figure 5.12: Model of the Machine Tool

Taking the Laplace transform of the above equation we get

$$-dF_x(s) = m_m s^2 x_1(s) + c_m s x_1(s) + k_m x_1(s)$$

Therefore the transfer function is given by,

$$G_m(s) = \frac{x_1(s)}{dF_x(s)} = -\frac{1}{m_m s^2 + c_m s + k_m} \tag{5.17}$$

In practical systems for example the tool-work piece interfaces in lathe, the system parameters (m_m, c_m, k_m) are distributed more or less uniformly. But these systems also possess large number of natural frequencies and consequently the resonance curve of such system shows a number of resonance peaks. Now if such a system vibrates near one of its natural frequencies, it is possible to replace by an idealized model consisting of an elementary vibratory system.

To find the values of the system parameters m_m, c_m ,k_m the system was therefore set into vibration by a known impulse force with the help of a Bruel and Kjaer Impact Hammer, [Appendix D]. The amplitude of acceleration at the point along the line of application of force acts was recorded by an Onno-Soki make accelerometer and a FFT Analyzer [Appendix E]. Both the time domain as well as frequency domain response of the input impulse force and the output amplitude of vibration were obtained with the help of Fast Fourier Transform (*FFT*). The impulse force used for exciting the work piece and the tool post system in the radial direction [Appendix F], in time as well as in frequency domain as shown in Fig. 5.13. The corresponding acceleration response in frequency and time domain are shown in Fig. 5.14. The arrangements and responses of other directions of loading and sensing are given in Appendix F and G respectively.

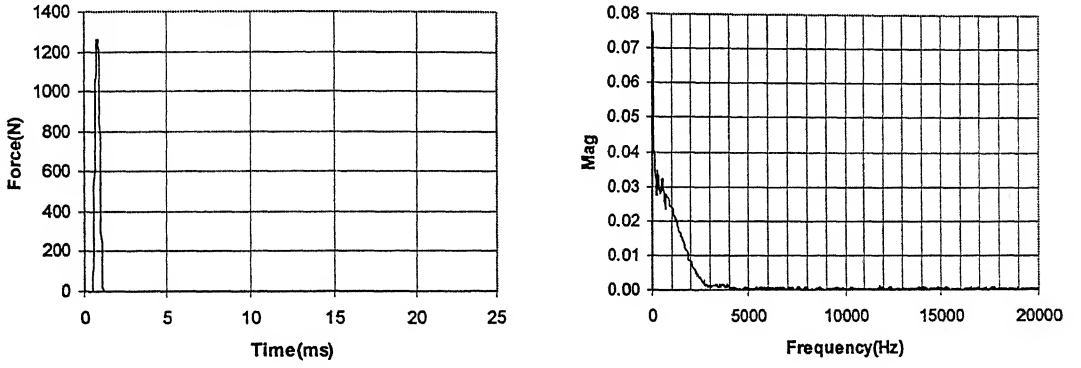

(a) (b)

Figure 5.13: Time (a) and frequency (b) response of the Impulse Force

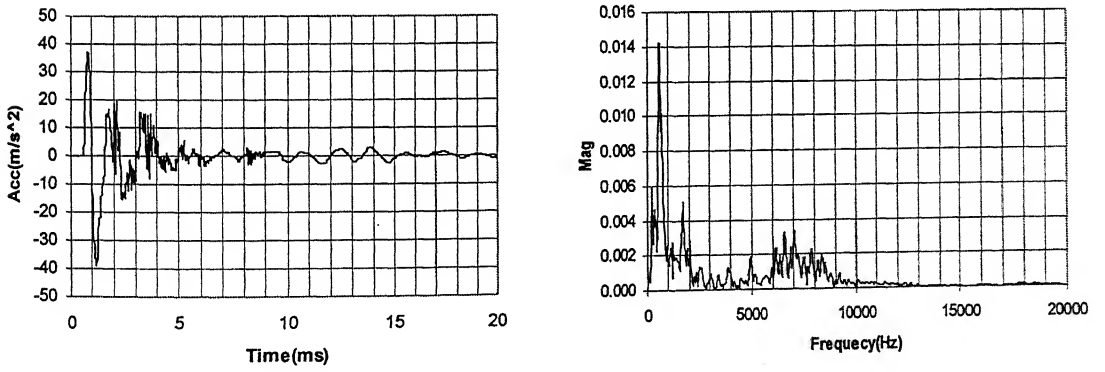

(a) (b)

Figure 5.14: Time (a) and frequency (b) response of the acceleration of vibration

The system parameters are found out by the following way:

We know that for a unit impulse loading we have the impulse response for a second order mass-damper-spring system

$$m\ddot{x}(t)+c\dot{x}(t)+kx(t)=\delta(t) \tag{5.18}$$

where,

$x(t)$= Response to the Impulse Loading

$\delta(t)$= Dirac delta function, defined as,

$$g(t)=\begin{cases}\dfrac{1}{m_m\omega_d}e^{-\zeta\omega_n t}\sin\omega_d t & t\geq 0\\ 0\end{cases} \tag{5.19}$$

where

$g(t)$= Response to the Impulse Loading=$x(t)$ of Eq. (5.18)

$$\omega_d=(1-\zeta^2)^{1/2}\omega_n,$$

ω_n =Natural Frequency, ζ =Damping Ratio.

The values of ζ and ω_n are determined in section 5.6.1.2

1) Mass (m_m) is given by fitting the experimental data in Eq. (5.19),

$$k_m=\omega_n^2 m_m$$

2) Spring *constant* (k_m) is given by,

$$m_m=k_m/\omega_n^2 \tag{5.20.a}$$

3) Damping(c_m) is given by,

$$c_m=2m\zeta\omega_n \tag{5.20.b}$$

5.5.7 Modeling of the actuator

The actuator proposed for this work was made of a stack of piezoelectric tablets. Specifications of the above are given in Appendix B. The principle of the actuator can be explained with the help of Fig. 5.15. Each tablet has a positive and a negative polarity on

either of its sides. When a potential difference is created by supplying a voltage V, due to the piezoelectric property the stack expands and displacement is obtained at the free end. When the potential difference is removed the stack regains its actual shape. This phenomenon can be used to obtain a vibratory motion, by supplying a pulse power supply.

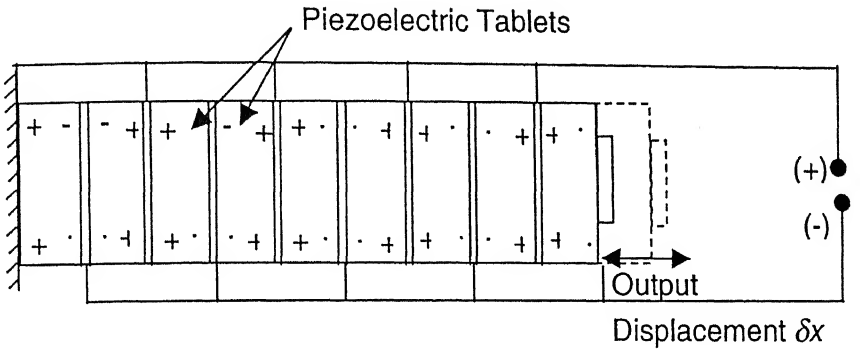

Figure 5.15: Piezoelectric Actuator

It can be seen that when the input to the stacks is a voltage V, the output is a displacement δx. Thus the actuator was modeled with the following equation and can be represented by Fig. 5.16,

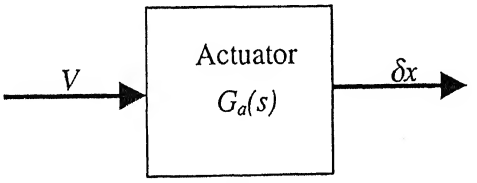

Figure 5.16: Representation of the actuator

$$\delta x = K_a V \tag{5.21}$$

where K_a is the gain of the actuator. Taking the Laplace transform we have

$$\delta x(s) = K_a V(s)$$

and the transfer function as

$$G_a(s) = \frac{\delta x(s)}{V(s)} = K_a \tag{5.22}$$

5.6 Controller Design

The machine tool system consists of the cutting process and the machine tool structure as shown in Fig. 5.17.

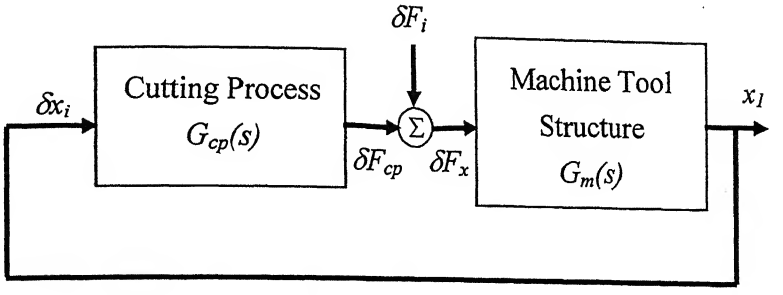

Figure 5.17: Interaction of machine tool structure and cutting process

where δx_i = The chip thickness variation as shown in Fig. 5.10

δF_x = The variation in the cutting force as shown in Fig. 5.10

x_l = The displacement of the machine tool structure due to δF_x as shown in Fig. 5.10

δF_i = The variation in the radial force due to the initial cutting conditions f and r.

δF_{cp} = The variation in the radial force due to regenerative chatter as shown in Fig. 5.10.

The proposed control system for the suppression of the displacement of the cutting edge in turning operation has the following components along with the machine tool system. They are:

1) The Actuator
2) The Vibration pickup along with a Proportional Integral Derivative (PID) Controller

The closed loop system will have all the above four components as shown in Fig. 5.18.

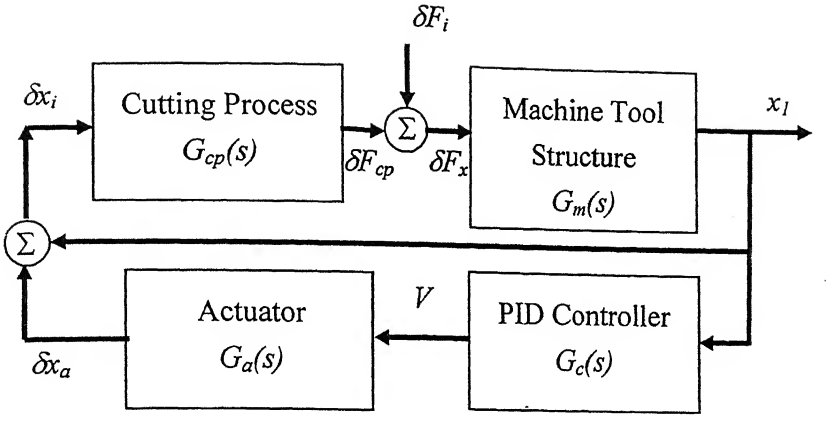

Figure 5.18: The closed-loop feedback control system

where

δx_a = Displacement provided by an actuator

V = Voltage supplied to the actuator by the controller

The steps followed for the design of the control system are shown in Fig. 5.19, below.

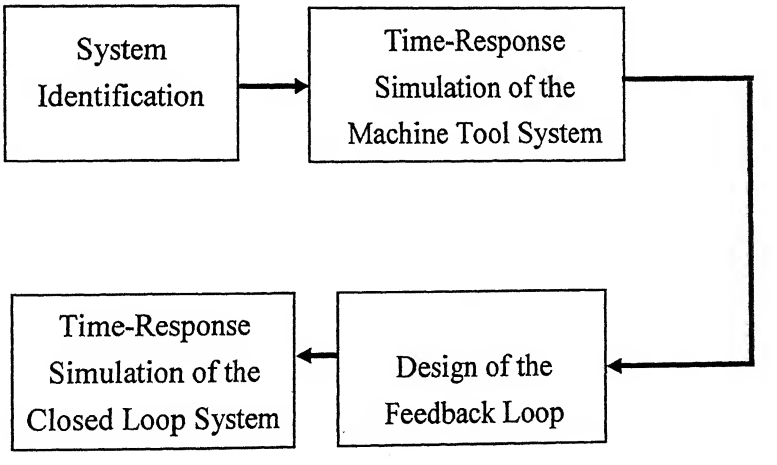

Figure 5.19: Steps of the design of the proposed control system

5.6.1 System Identification

In the proposed control system, system identification included the determination of the

system parameters of the cutting process, the machine tool structure and the actuator.

5.6.1.1 System Identification of the Cutting Process

In this step the coefficients of Eq. (5.14), k_v ,k_f and k_I were experimentally determined as given in the following sections.

5.6.1.1.1 Experimental determination of k_v

From the definition $k_v = \left(\frac{\partial F_o}{\partial V_o}\right)_{df=0}$, experiments were conducted to measure force at different cutting speeds at a fixed feed. The graph obtained shown in Fig. 5.20. From the graph k_v was obtained as given by, $k_v = tan\varepsilon_v$, where ε_v is the slope of the force versus cutting speed curve.

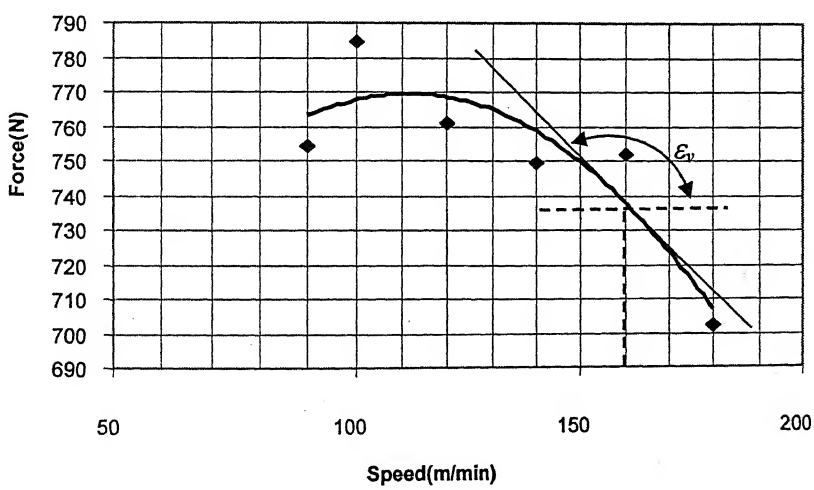

Figure 5.20: Determining the co-efficient k_v

5.6.1.2 Experimental determination of k_f

From the definition, $k_f = \left(\frac{\partial F_o}{\partial f_o}\right)_{dV=0}$ experiments were conducted to measure force at different feeds and at a constant cutting speed. The graph obtained is shown in Fig. 5.21. From the graph k_f was obtained as given by $k_f = tan\,\varepsilon_f$, where ε_f is the slope of the force versus feed curve shown in Fig. 5.21.

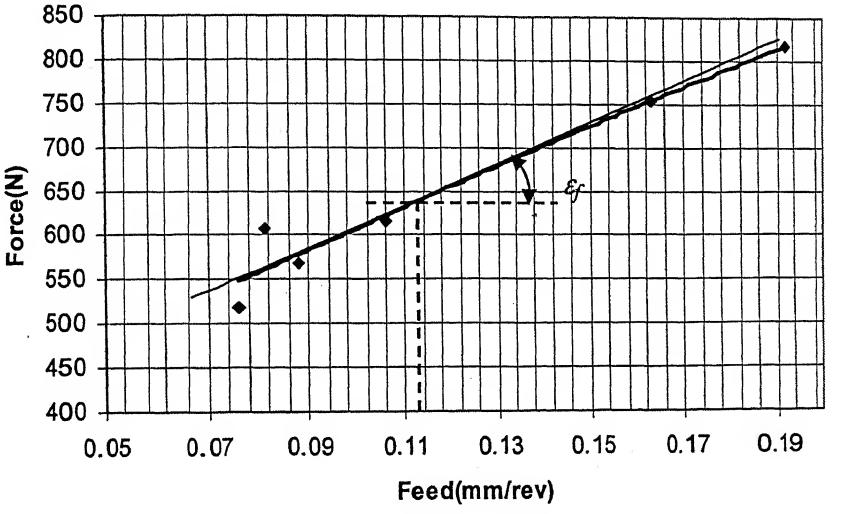

Figure 5.21: Determining the co-efficient k_f

5.6.1.3 Experimental determination of k_l

Unlike the coefficients k_v and k_f, the coefficient k_l cannot be determined by static experimentation as it is a dynamic coefficient. Thus its experimental determination is very complicated. It is defined as $k_l = \left(\frac{\partial F}{\partial f}\right)_{dV=dr=0}$, thus both cutting speed and penetration rates are to be kept constant at different feeds. It is very difficult to keep the penetration rate (r_o) constant at changing feed (f_o), as it is given by $r_o = f_o N$. But this can be experimentally achieved approximately in the vicinity of $f_o = 0$. Thus the experimental graph was extrapolated to obtain the force in the vicinity of $f_o = 0$, as shown in Fig. 5.22.

Thus from the graph k_1 was calculated as given by, $k_1 = \tan\theta_1$, where θ_1 is the slope of the feed force versus feed curve as shown in Fig. 5.22.

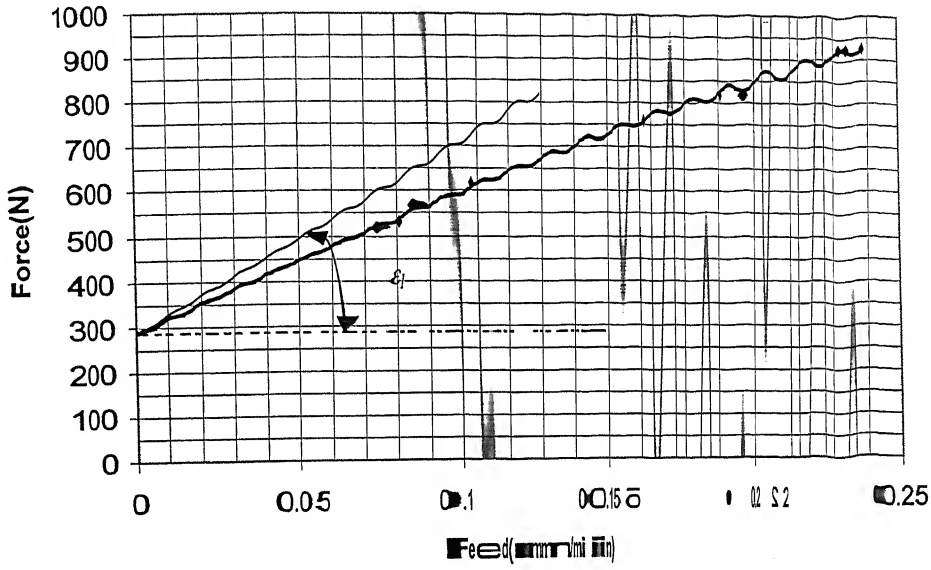

Figure 5.22: Determining the co-efficient k_1

Thus after finding the coefficients k_v, k_f and k_1 experimentally from Figs. 5.20, 5.21 and Fig. 5.22 we get

$$k_v = -0.084\left(\frac{N}{mm/s}\right) \tag{5.23.a}$$

$$k_f = 2343.75\left(\frac{N}{mm/rev}\right) \tag{5.23.b}$$

$$k_1 = 4100\left(\frac{N}{mm/rev}\right) \tag{5.23.c}$$

and taking $N = 800rpm = 13.33rps$; $T = 1/N = 0.075s$; $\Delta t = 0.008s$, Eq. (5.14) can be written as $G_{cp}(s) = 4100 - 2460e^{-0.075s} - 1731.75e^{-s}$ (5.23)

By Padé's approximation, we know,

$$e^{-Ts} \approx \frac{2-Ts}{2+Ts}$$

Applying in Eq. (5.23), we get

$$G_{cp}(s) = \frac{3280 + 228.5s - 9.88s^2}{2 + 0.075s} \tag{5.24}$$

5.6.1.2 System Identification of the Machine Tool Structure

In this step the system parameters of the equivalent spring mass damper assumed to have single degree of freedom was experimentally determined. A known impulse force was supplied to the tool-post and workpiece system with the help of a Bruel and Kjaer Impact Hammer (Model 8202) [Appendix D] and the acceleration response was measured through an accelerometer. Both the impulse load and the response were taken in the radial direction as it was assumed to be the primary direction of vibration. The time-response was converted into frequency-response under unit impulse with Fourier Transform. From the time response of the output vibration, sensed by the accelerometer, the parameters ω_n and ζ were determined as shown in Fig. 5.23.

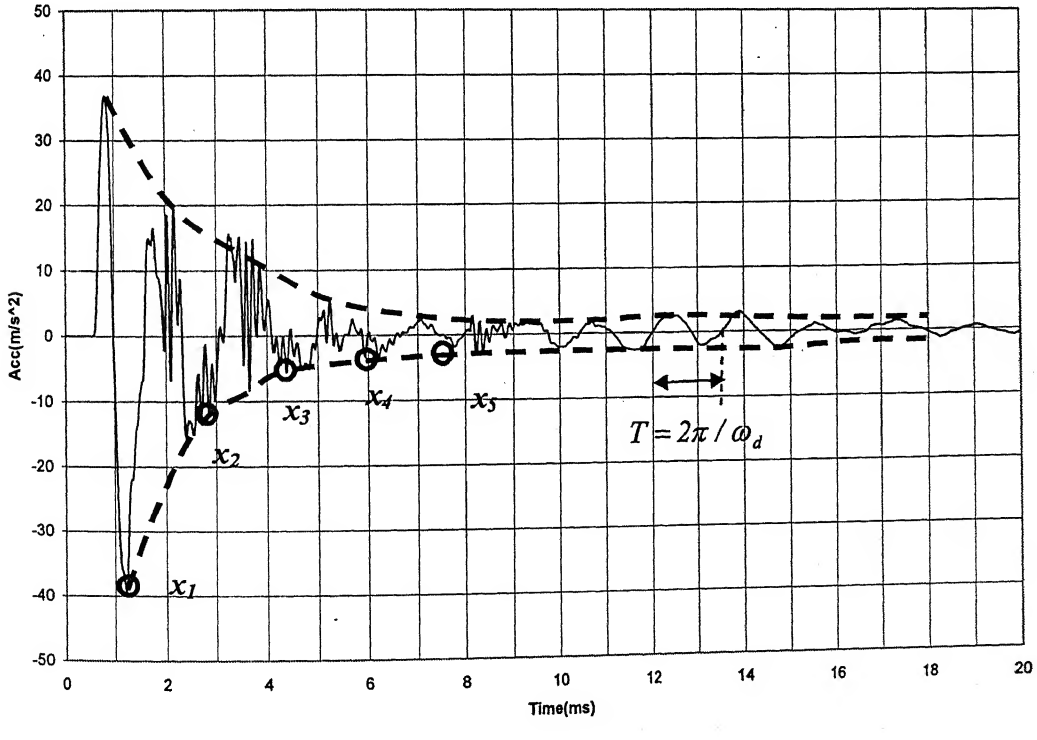

Figure 5.23: Time response of the acceleration of vibration

The logarithmic decrement (δ) is given by [42],

$$\delta = \frac{1}{j} ln \frac{x_1}{x_{j+1}} \tag{5.24}$$

$$\zeta \cong \frac{\delta}{2\pi} \tag{5.25}$$

and $$T = 2\pi / \omega_d \tag{5.26}$$

From the Fig. 5.23, we get

T=1.6ms

$\therefore \omega_d$=3927 rad/s or 625Hz

Now again from Fig. 5.23 we get for j=4

$$\delta = \frac{1}{5} ln \frac{39}{2.5} = 0.549$$

$$\therefore \zeta \cong 0.087$$

$$\text{As } \omega_d = (1-\zeta^2)^{1/2} \omega_n$$

$\therefore \omega_n$=3942 rad/s or 627.4 Hz

From section 5.5.6 and Eq. (5.19) we get,

$$m_m = 3.348(\frac{N}{mm/s^2})$$

$$k_m = 1.32x10^6(\frac{N}{mm})$$

$$c_m = 369(\frac{N}{mm/s})$$

The Eq. (5.17) thus is now given by

$$G_m(s) = -\frac{1}{3.348s^2 + 369s + 1.32x10^6} \tag{5.27}$$

5.6.1.3 System Identification of the Piezoelectric Actuator

The gain of the actuator [Appendix B] used in this particular control system is given by,

$$K_a = 0.116 \mu m/V$$

The Eq. (5.20) becomes $G_a(s) = .000116$ (5.28)

5.6.2 Frequency Response Analysis of the Machine tool system

We know that a linear lumped parameter is stable if and only if all the roots of its characteristic equation have negative real parts. From Fig. 5.17 and Eq. 5.24 and 5.27,

$$G_{cp}(s) = \frac{3280 + 228.5s - 9.88s^2}{2 + 0.075s}$$

$$G_m(s) = -\frac{1}{3.348s^2 + 369s + 1.32x10^6}$$

$$G_{mts} = \frac{G_m}{1 - G_m G_{cp}}$$

Thus the machine tool system represented by

$$G_{mts} = \frac{-208320s^2 - 640390s}{0.2511s^3 + 34.371s^2 + 99738s + 26400000} \quad (5.28)$$

Thus the characteristic equation is given by,

$$0.2511s^3 + 34.371^2 + 99738s + 26400000 = 0 \quad (5.29)$$

The Zeros and poles of the machine tool system transfer function given by Eq. (5.29) are

Poles:

$p_1 = -551.1 + 625.48i$

$p_2 = -551.1 - 625.48i$

$p_3 = -266.7$

Zeros

$z_1 = 0$

$z_2 = -3.0740$

As both the poles and zeros of the machine tool system transfer function are negative or zero, the above transfer function is a *Minimum-Phase Transfer Function* and the system is stable. The Root Locus plot of the transfer function is given in Eq. (5.29) and shown in Fig. 5.24.

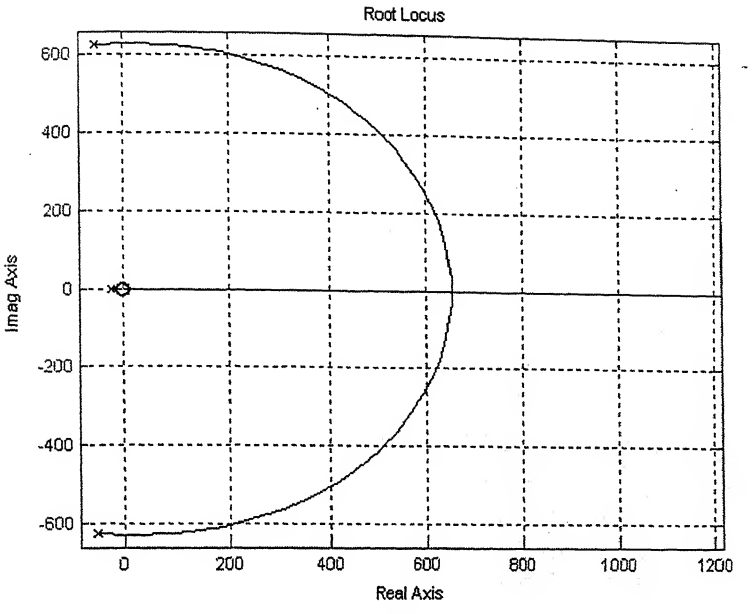

Figure 5.24: Root Locus Plot of G_{mts} (**x**=Poles; **o**=Zeros)

From the root locus plot shown in Fig. 5.24 it can be concluded that the machine tool system transfer function G_{mts}, is stable due to the position of the poles in the left hand plane. The plot shows a predominant second order system, due to the presence of dominating poles close to the imaginary poles.

5.6.3 Machine tool system Time-Response Simulation

The block diagram of the machine tool system is shown in Fig. 5.17. The variation in the radial force arising due to the variability of the independent input parameters feed (*df*) and penetration rate (*dr*) is incorporated. This is achieved with the help of Eq. 5.12 which gives the transfer function between the dF_x with *df* and *dr*. The variations dF_x is the input to the machine tool structure which causes vibration, or undue relative displacement between tool and workpiece. This leads to a variation in the radial cutting force by regenerative chatter. This variation along with the constant radial force due to the initial cutting condition sets the machine tool structure into further vibration.

From the discussion in section 5.5.3 and 5.5.4 we know that

$$df = x(t) - \mu x(t-T) \text{ and } dr = (\frac{K}{N})\frac{dx}{dt}$$

therefore their corresponding transfer functions G_f and G_r are given by

$$G_f(s) = \frac{x(s)}{df(s)} = \frac{1}{1-\mu e^{-Ts}}$$

which can be simplified by Padé's approximation as,

$$G_f(s) = \frac{2+Ts}{2(1-\mu)+T(1+\mu)s} \tag{5.30}$$

Putting the value of the overlapping coefficient $\mu=0.8$ (as for turning operation $\mu<1.0$) and the time per revolution $T=(1/N)=0.075\ sec$ in Eq. (5.30), we get

$$G_f(s) = \frac{+0.075s}{0.8+0.12s} \tag{5.31}$$

and

$$G_r(s) = \frac{x(s)}{dr(s)} = \frac{1}{s} \tag{5.32}$$

5.6.3.1 Introduction of Mode Coupling Coefficient

In turning the chatter amplitudes do not have a constant direction. In this case the cutting edge of the chattering tool describes an approximately elliptical curve of motion. Thus the concept of '*direct receptance*' has to be replaced by '*cross receptance*'. The regenerative feed variation interacts with the cutting process dynamics through a directional factor and affects structure mode dynamics. Usually a 'coupling coefficient' is introduced to connect the variation of the cutting force as a result of feed variation resulted from the structural vibrations.

The coupling coefficient $\wp$, expresses the degree of coupling between the vibration and cutting force variation. The coupling coefficient is proportional to the chop width b for a given set of cutting conditions and tool geometry. Thus, in many experiments limiting value of b would be taken to signify limiting $\wp^*$ denoting stability limits. However as the feed is a factor of $\wp$, these borderline limits of b will be different for different values

of f. A typical example [41] for the stability of length of work pieces can be analyzed as shown in Fig. 5.25 by determining at what value of b, the onset of chatter takes place.

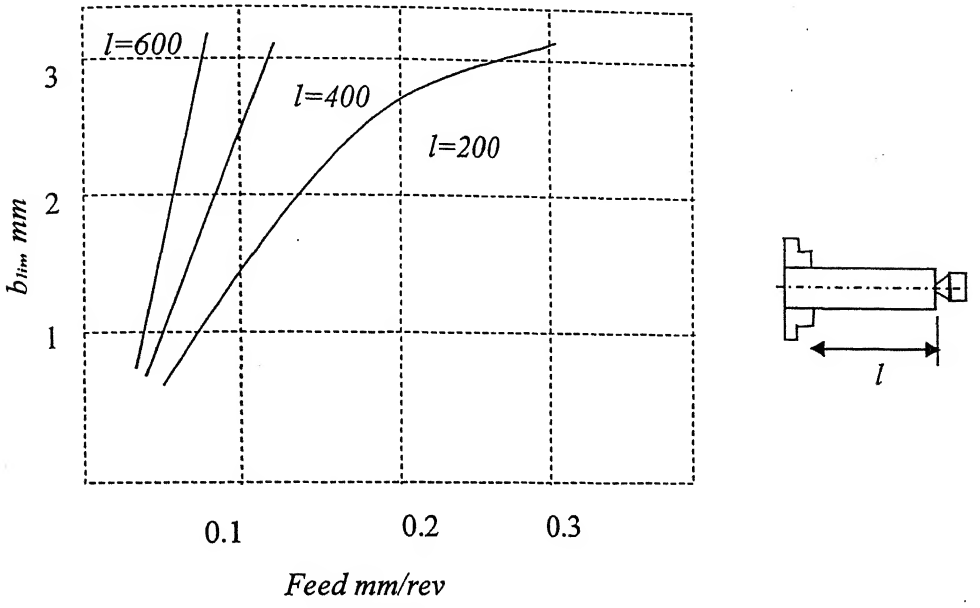

Figure 5.25: Effect of workpiece length on b_{lim} for onset of chatter [41]

The machine tool system time-response simulation for step and random input had been obtained with the help of *Simulink Toolbox, Matlab*. The block diagram is shown in Fig. 5.26.

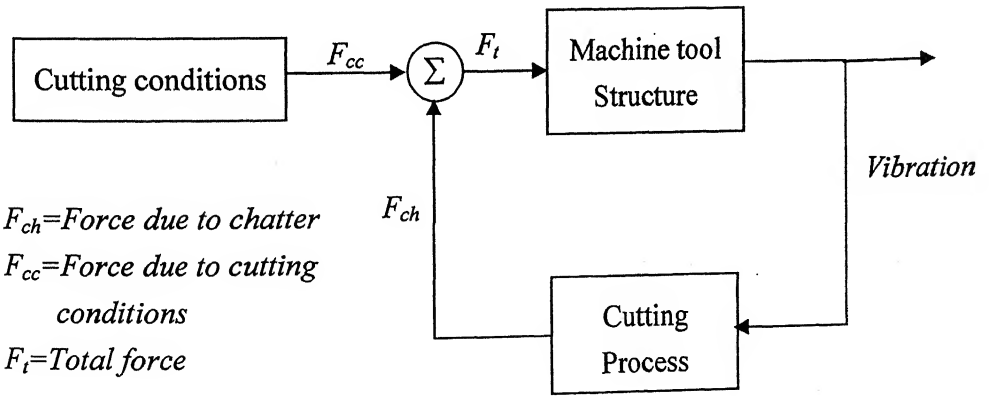

Figure 5.26: Block diagram of implementation strategy of machine tool system

Thus in the control scheme developed in this work, only f was varied which gives rise to the variation in r. The two inputs had been varied by *steps*, as in the case in actual cutting process where the feed increases from zero to a definite set value by the tool engagement. Realistic values of f and r had been taken. Also random inputs about a fixed mean, had been given to simulate the vibration caused by the change in the cutting conditions due to some external disturbances. A typical step and random function has been shown in Fig. 5.27.

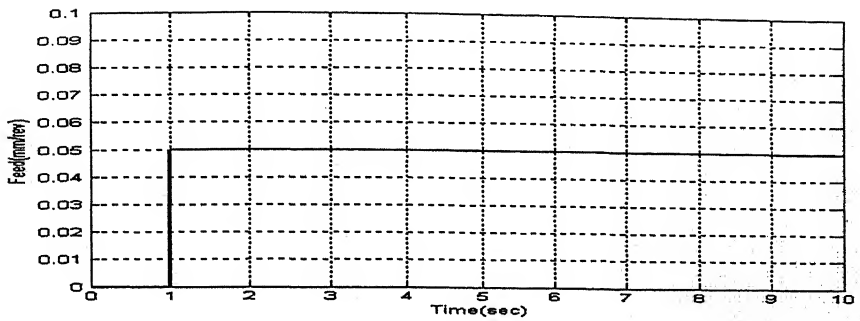

(a) Step Input: feed= 0.05 mm/rev

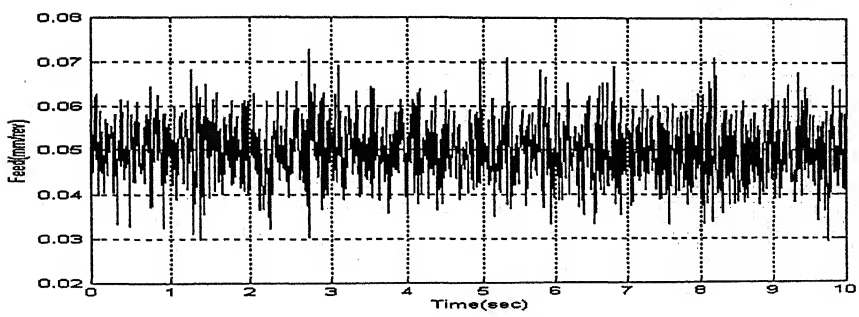

(b) Random Input: feed=0.05 mm/rev with variance of 5%

Figure 5.27: Step and random inputs of feed

The time responses are shown in Fig. 5.28. In this case it has been shown from the time response of the machine tool system in Fig. 5.28 that the value of the limiting $\wp^*$ is approximately 2.9638, for a feed of 0.05 mm/rev (*step*) and 2.9561 for a feed of 0.05 mm/rev (*random*). Thus we have selected the above values of $\wp$ for further simulations. Fig. 5.28 (c) and (f) shows the onset of instability due to chatter.

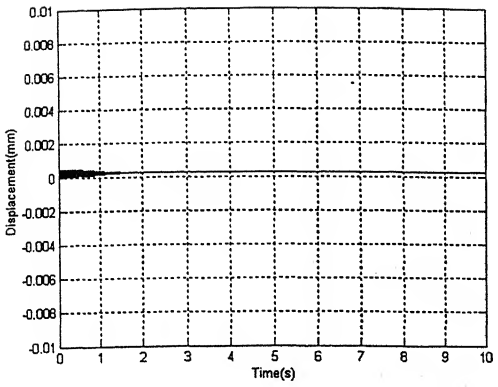

(a) $f=0.05$ (step), $\wp=2.95$

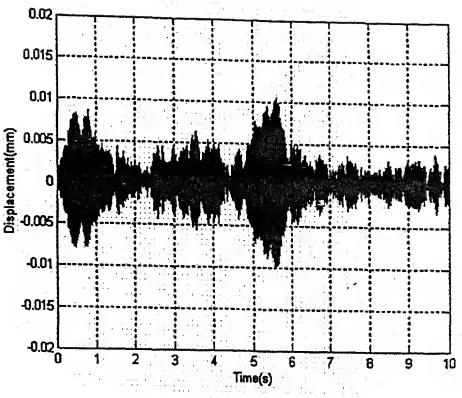

(d) $f=0.05$ (random), $\wp=2.94$

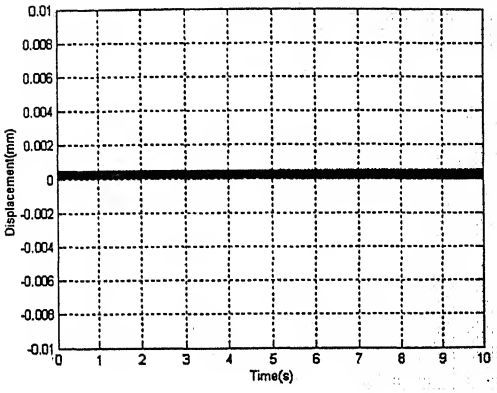

(b) $f=0.05$ (step), $\wp=2.9638$

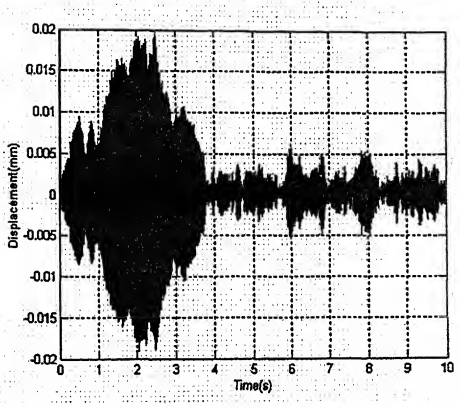

(e) $f=0.05$ (random), $\wp=2.9561$

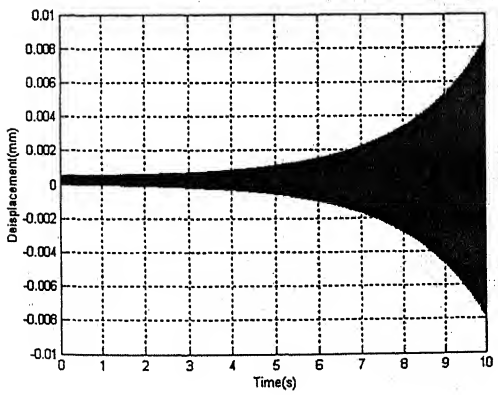

(c) $f=0.05$ (step), $\wp=2.97$

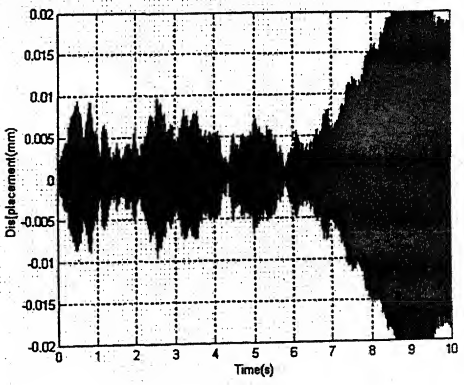

(f) $f=0.05$ (random), $\wp=2.96$

Figure 5.28: The effect of coupling coefficient $\wp$ on the onset of chatter for step (a, b, c) and random (d, e, f)

5.6.4 Design of Closed-Loop Feedback Controller

The time response of the machine tool system for the cutting process and the machine tool cascaded together as shown in Fig. 5.28, gives the idea of the relative displacement between tool and workpiece due to vibration arising from regenerative chatter. This displacement has to be minimized as much as possible to improve the surface roughness of the workpiece being machined. For this purpose a simple closed-loop control scheme is proposed consisting of a PID controller and a piezoelectric controller. The arrangement of the control scheme is shown in Fig. 5.29. The specifications of the actuator and its proposed implementation have been discussed in Appendix B and C respectively.

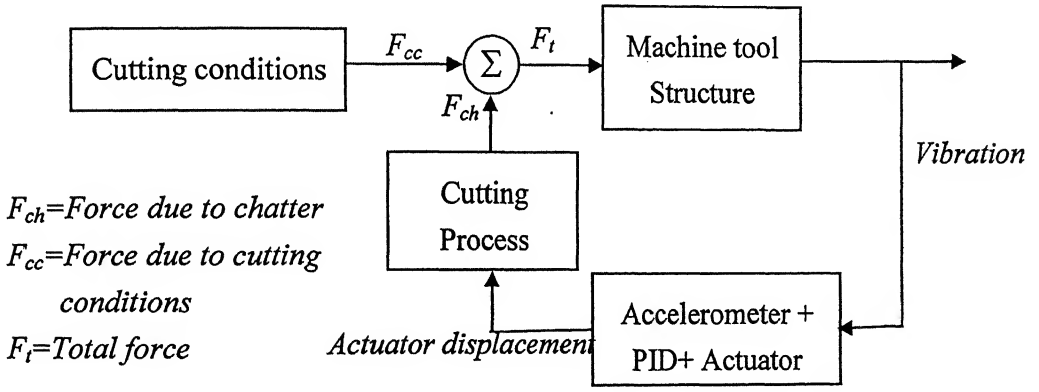

Figure 5.29: Block diagram of implementation of closed-loop feedback control scheme

The piezoelectric actuator is rigidly fixed with the tool post such that it's displacement can be transferred to the tool while the cutting process is taking place. This is achieved with the help of a spring steel plate, which has been designed under a patch loading of 800N. The tool adapter is shown in Fig. C.1 [Appendix C]. The controller for the actuator is proposed to be supplied with a pulse voltage, such that during the constant finite voltage the actuator gives displacement and comes back to the original position when the voltage is removed. This voltage is controlled by the PID controller.

5.6.5 Time Response Simulation of the Closed Loop System

The closed loop negative feedback control system was implemented to reduce the vibration. This will reduce the regenerative chatter, causing the vibration to get minimized and improve the surface finish of the turned part. For this purpose a piezoelectric actuator along with a controller [Appendix B] had been proposed. The vibration was controlled with a PID controller with the transfer function given by Eq. 5.33 and shown in Fig. 5.30.

$$G_{PID} = P + \frac{I}{s} + \frac{Ds}{(\frac{I}{Ns} + 1)} \tag{5.33}$$

where

P= Proportional Term

I= Integral Term

D= Derivative Term

N= Divisor Term

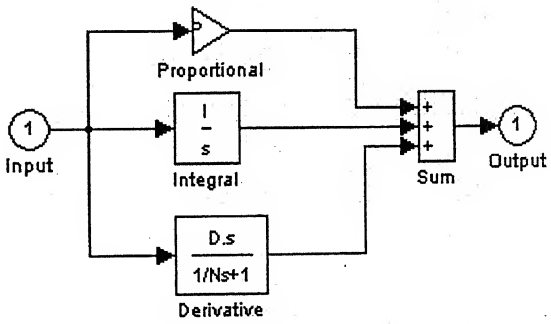

Figure 5.30: Block diagram of the PID Controller

The transfer function for the actuator given by Eq. (5.22) and (5.28) is a gain of 0.000116. The negative feedback loop is added to the machine tool system. The PID controller was tuned manually to obtain the following terms,

$P=10$, $I=0.10$, $D=10$ and $N=10$.

The controller will have the transfer function given in Eq. (5.34) below,

$$G_{PID} = 10 + \frac{0.I}{s} + \frac{10s}{(\frac{1}{10s} + 1)}$$

$$\therefore G_{PID} = \frac{1000s^3 + 1000s^2 + 110s + 1}{100s^2 + s} \tag{5.34}$$

and the transfer function for the feedback loop is given by,

$$\therefore G_{Feedback} = \frac{0.116s^3 + 0.116s^2 + 0.01276 + 0.000116}{100s^2 + s} \tag{5.35}$$

The output vibration of the cutting process and machine tool system with and without control for some specific type and value of feed are shown in Fig. 5.31.

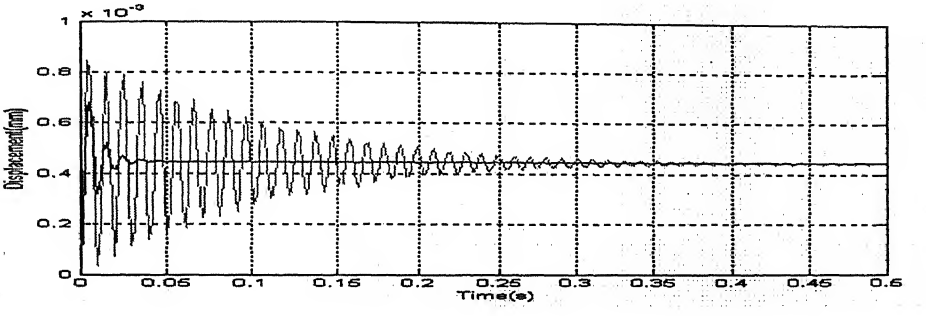

(a) *feed*=0.10 mm/rev (step input), $\wp$=2.5 mm

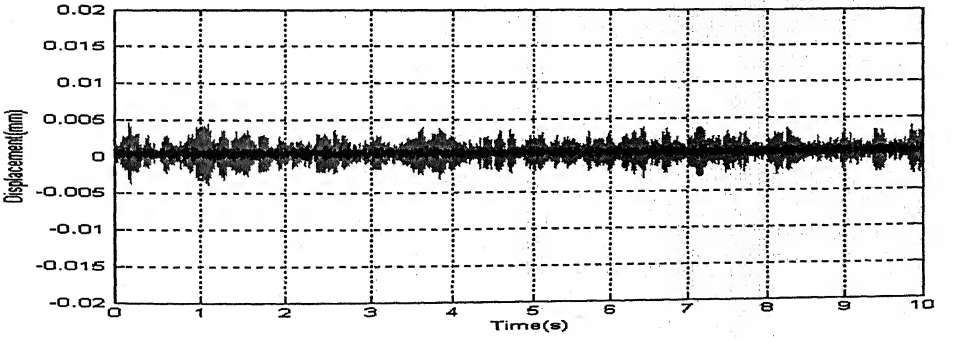

(b) *feed*=0.10 mm/rev, (5% random input) $\wp$=2.5 mm

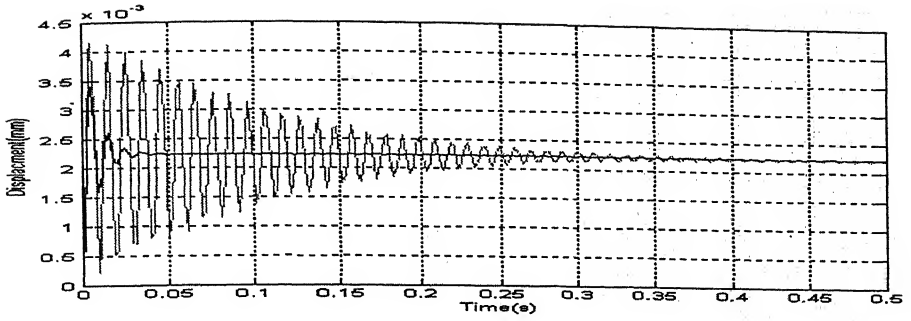

(c) *feed*=0.50 mm/rev, (step input), $\wp$=2.5 mm

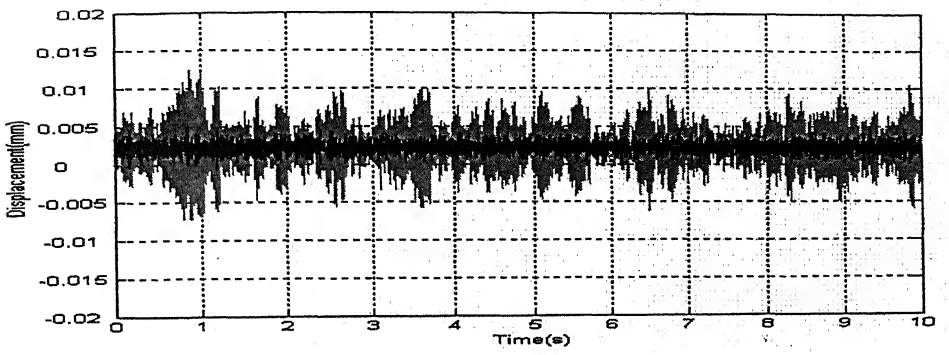

(d) *feed*=0.50 mm/rev, (5% random input), $\wp$=2.5 mm

Figure 5.31: The controlled (darker ▬) and uncontrolled (lighter ▬) vibration displacements for different values and types of feeds.

The feedback and the machine tool system transfer functions given by Eq. (5.35) and (5.28) can be cascaded in to a single transfer function,

$$G_{closed}=\frac{24165s^5+50120s^4-76943s^3-8196s^2-74s}{25.11s^5+3437.4s^4+9973834.4s^3+264099738s^2+2640000s} \quad (5.36)$$

The poles and zeros of G_{closed} is given by,

Poles:

$p_1=-551.1+625.48i$

$p_2=-551.1-625.48i$

$p_3=-266.7$

$p_4=-0.01$

$p_5=0$

Zeros:

$z_1=0$

$z_2=-3.0740$

$z_3=1.1008$

$z_4=-0.0907$

$z_5=-0.0100$

As all the poles are negative or zero G_{closed} is a stable system. The Root Locus plot for the closed loop control system is given in Fig. 5.32.

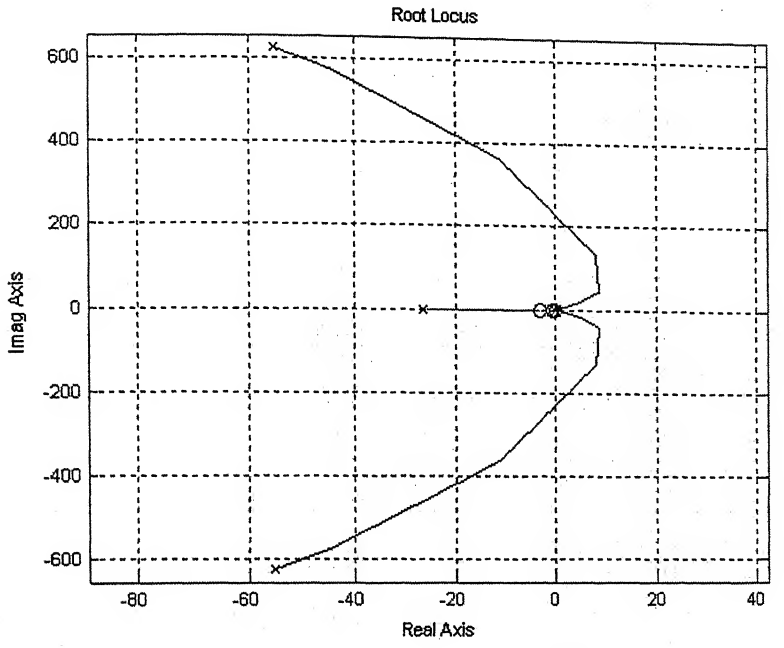

Figure 5.32: Root Locus Plot of G_{closed}

From the above plot it can be said that the closed loop system was stable as all the poles in the left of the imaginary axis i.e. lying on the left hand plane as shown in Fig 5.32.

5.7 Results

The results of the modeling and the control of vibration in machine tool due to regenerative chatter are discussed below.

The machine tool system was found to be stable within the limiting value of $\wp^*$ which was approximately 2.9638, for a feed of 0.05 mm/rev (*step*) and 2.9561 for a feed of 0.05 mm/rev (*random*). It is clear that beyond these values there is onset of instability due to

chatter.

The vibration in machine tool system was more sensitive to the random disturbances in the input, rather than the step input a can be observed from Fig. 5.28.

The Root Locus plot and the position of the poles and zeros for the machine tool system suggests that the transfer function G_{mts} was a stable system within the limiting value of $\wp^*$, as beyond this value there was an onset of instability.

The PID controller designed to control the vibration of the machine tool arising from regenerative chatter was quite effective. As shown in Fig. 5.31.

The gains of the PID controller are realistic and can be implemented along with the particular piezoelectric actuator and controller. This can be achieved with the help of LM-324 (Quad-OPAMP) and commonly available resistors.

The closed loop negative feedback system was stable in nature as suggested by the Root Locus Plot and the position of the poles and zeros, within the limiting value of $\wp^*$.

Chapter VI

Conclusion and Future Directions

6.1 Conclusions

The conclusions made from this work were divided into two parts. First conclusions have been drawn for mathematical modeling of surface roughness. Secondly conclusions were drawn on the control of the above.

6.1.1 Mathematical Modeling

1. The bifurcated optical fiber can be used for *on-line* monitoring the surface roughness in turning operation.
2. The *on-line* and the *off-line* surface roughness values were closely related to each other along with the vibration signals in the radial direction.
3. The surface roughness was found to be decreasing with the increase of speed due to tool wear and formation of continuous chips.
4. The surface roughness was found to be increasing with the increase of feed due to formation of feed marks at lower speeds.

5. The surface roughness was found to be decreasing with the increase of rake angle due to decrease in the cutting force and the more accommodation for the chip to flow.
6. Regression analysis
    I. Speed is the most significant term then feed. When vibration is included, it becomes another significant parameter for modeling of surface roughness.
    II. Under the current selection of other parameters α does not have appreciable effect on surface roughness value.
    III. A four input second order surface response model has maximum accuracy
    IV. Vibration taken as an input parameter as suggested by Chen [13] gives a better result than models which do not consider so.
7. Neural Network Models
    I. The type of learning function has got appreciable effect on the prediction capability of the model
    II. A four input model having vibration as the fourth input as suggested by Chen [13] gives a more accurate model
    III. Type of learning function suitable for a particular model depends on the architecture of the ANN.
    IV. Adaptive Gradient Descent training function is the most accurate ANN model, with a better prediction capability that the models suggested by Rsibood [18].
8. The regression models have a better prediction capability than neural models.

6.1.2 Control of Surface Roughness

The results of the modeling and the control of vibration in machine tool due to regenerative chatter are discussed below.

1. The open loop system is stable within the limiting value of $\wp^*$ which is approximately 2.9638, for a feed of 0.05 mm/rev (step) and 2.9561 for a feed of 0.05 mm/rev (random). It is clear that beyond these values there is onset of instability due to chatter.

2. The Root Locus plot and the position of the poles and zeros for the open loop suggest that the transfer function G_{open} is a stable system within the limiting value of $\wp^*$.
3. The PID controller designed to control the vibration of the machine tool was quite effective.
4. The gains of the PID controller are realistic and can be implemented along with the particular piezoelectric actuator and controller. It can be implemented for the particular machine tool system with the help of *LM 324* (*Quad-OPAMP*).
5. The closed loop negative feedback system is stable in nature as suggested by the Root Locus Plot and the position of the poles and zeros, within the limiting value of $\wp^*$.

6.2 Future Directions

This following research work can be extended in different directions. Some of them can be listed as follows.

1. Vibration can be used as an independent input parameter for modeling of surface roughness rather than a dependent parameter. This can be achieved with the help of the piezo-electric actuator along with its controller.
2. Number of factors as well as level can be increased and experiments can be designed with the help of factorial designs.
3. The reason for the neural networks not being able to predict surface roughness as accurate as the regression models can be investigated.
4. Control strategy developed in this work can be implemented with the help of the proposed PID controller, accelerometer and the actuator for on-line control of surface roughness.
5. *ANN* model can be used to simulate the cutting process and also used for system identification problem.
6. A detailed study on the effect of *ANN* architectures and the training functions on predicting machining parameters can be done.

7. Multiple degree of freedom machine tool model can be developed and the values an be compared with this single degree of freedom model.
8. Different types of controllers Adaptive, Robust, H_∞ controllers can be implemented to achieve better control.
9. Better data acquisition techniques can be incorporated as the surface roughness measurements are in terms of microns.

References

[1] Micheletti G.F., Koenig W, Victor H. R, *In-process tool wear sensors for cutting operations*, Annals of CIRP, Vol. **25**, 2, (1976), pp 483-495.

[2] Shriashi M, *In-process measurement of surface roughness in turning by laser beams*, Transaction of ASME, Journal of Engineering for Industry, Vol. **103**, (1981), pp 203-209.

[3] Coker Scott A, Shin Yung C, *In-process control of surface roughness due to tool wear using an ultrasonic system*, International Journal of Machine Tool and Manufacture, Vol. **36**, 3, (1996), pp 441-422.

[4] Lee C S, Kim S W, Yim D Y, *An in-process measurement technique using a laser for non-contact monitoring of surface roughness and form accuracy of ground surface*, Annals of CIRP, Keynote paper, (1987), pp 425-428.

[5] Shirashi M, *A consideration of surface roughness measurement by optical method*, Transaction of ASME, Journal of Engineering for Industry, Vol. **109**, May (1987), pp 100-106.

[6] Choudhury S K, Ramesh S, *On-line tool wear sensing and compensation in turning*, Journal of Material Processing Technology, Vol. **49**, 3-4, (1995), pp 247-254.

[7] Jin W L, Venuvinod P K, Wang X, *An optical fiber based cutting force measuring device*, International Journal of Machine Tool and Manufacture, Vol. **35**, 6, (1995), pp 877-883.

[8] Zhang K, Butler C, Yang Q, Lu Y, *A fiber optic sensor for the measurement of surface roughness and displacement using ANN*, IEEE Transaction on instrumentation and measurement, Vol. **46**, 4, (1997), pp 899-902.

[9] Vajpayee S, *Analytical study of surface roughness in turning*, Wear, Vol. **70**, (1981), pp 165-170.

[10] Cielo P, *Optical techniques for industrial application*, Academic Press Inc., Boston, (1988).

[11] Choudhury I A, Baradie MA El, *Surface roughness prediction in turning of high strength steel by factorial design of experiments*, Journal of Material Processing Technology, Vol. **67**, (1997), pp 55-61.

[12] Escalona P M, Cassier Z, *Influence of critical speed on the surface of finish of turned steel*, Wear, **218**, (1998), pp 103-109.

[13] Chen J C, Savage M D, *Multiple regression-based multilevel in-process surface roughness recognition system in milling operations*, The Journal of Technology Studies, Virginia Technical University, (2001), pp 28-34.

[14] Choudhury S K, Bartarya G, *Role of temperature and surface finish in predicting tool wear using NN and DOE*, Accepted, International Journal of Machine Tool and Manufacture, (2002).

[15] Rangwala S, Dornfeld D, *Sensor integration using neural networks for intelligent tool condition monitoring*, Transaction of ASME, Journal of Engineering for Industry, Vol. **112**, (1981), pp 219-228.

[16] Dimla Jr D E, Lister P M, Leighton N J, *Neural network solution to the tool condition monitoring problem in metal cutting- a critical review of methods*, International Journal of Machine Tool and Manufacture, Vol. **37**, 9, (1997), pp 1219-1241.

[17] Susič E, Grabec I, *Application to neural network to the estimation of surface roughness from AE signals generated by friction forces*, International Journal of Machine Tool and Manufacture, Vol. **35**, 8, (1995), pp 1077-1086.

[18] Risbood K A, Dixit U S, Sahasrabudhe A D, *Prediction of surface roughness and dimensional deviation by measuring cutting forces and vibrations in turning process*, Journal of Material Processing Technology, Vol. **132**, (2003), pp 203-214.

[19] Sata T, Li M, Takata S, Hiraoka H, Li C Q, Xiao X G, Xing X Z, *Analysis of surface roughness in turning operation and its application*, Annals of CIRP, Vol. **34**, 1, (1985), pp 473-476.

[20] Jang D Y, Choi Y G, Kim H G, Hasiao A, *Study of correlation between surface roughness and cutting vibrations to develop an on-line surface roughness*

measuring technique in hard turning, International Journal of Machine Tool and Manufacture, Vol. **36**, 4, (1996), pp 453-463.

[21] Lin S C, Chang M F, *A study on the effects of vibrations on surface finish using a surface topography simulation model for turning*, International Journal of Machine Tool and Manufacture, Vol. **38**, 3, (1998), pp 763-782.

[22] Beauchamp T M, Youssef A Y, Masounave J, *Effect of tool vibrations on surface roughness during lathe dry turning process*, Computers in Industrial Engineering, Vol. **31**, 3-4, (1996), 637-644.

[23] Azouzi R, Guillot M, *On-line prediction of surface roughness and dimensional deviation in turning using NN based sensor fusion*, International Journal of Machine Tool and Manufacture, Vol. **37**, 9, (1997), pp 1201-1217.

[24] Abouelatta O B, Mádl J, *Surface Roughness prediction based on cutting parameters and tool vibrations in turning operations*, Journal of Material Processing Technology, Vol. **118**, (2001), pp 269-277.

[25] Tobias S A, *Machine Tool Vibration*, Blackie, Glasgow, (1965).

[26] Tlusty J, Polacek M, *The stability of machine tools against self-excited vibration in machining*, Proceedings of Engineering Research Conference, ASME, Pittsburgh, (1963).

[27] Mei Z, Yang S, Shi H, Chang S, Ehmawn K F, *Active chatter suppression by online variation of the rake and clearance angles in turning- principles and experimental investigations*, International Journal of Machine Tool and Manufacture, Vol. 32, 7, (1993), pp 981-991.

[28] Choudhury S K, Goudimenko N N, Kudinov V A, *On-line control of Machine tool Vibration in turning*, International Journal of Machine Tool and Manufacture, Vol. **37**, 6, (1996), pp 801-811.

[29] Choudhury S K, Sharath M S, *On-line control of Machine tool Vibration during turning*, Journal of Material Processing Technology, Vol. **47**, (1995), pp 251-259.

[30] Tarng Y S, Kao J Y, Lee E C, *Chatter suppression in turning operation with a tuned vibration absorber*, Journal of Material Processing Technology, Vol. **105**, (2000), pp 55-60.

[31] Lee E C, Nian C Y, Tarng Y S, *Design of dynamic vibration absorber against vibration in turning operation*, Journal of Material Processing Technology, Vol. **108**, (2001), pp 278-285.

[32] Pan G, Xu H, Kwan C M, Liag C, Haynes L, *Modeling an intelligent chatter control strategy for a lathe machine*, Control Engineering Practice, Vol. **4**, 12, (1996), pp 1647-1658.

[33] Tewani S G, Routh K E, Walcott B L, *A study of cutting process stability of a boring bar with active dynamic absorber*, International Journal of Machine Tool and Manufacture, Vol. **35**, 1, (1995), pp 91-108.

[34] Jang J L, Tarng Y S, *A study of active vibration control of a cutting tool*, Journal of Material Processing Technology, Vol. **95**, (1999), pp 78-82.

[35] Potoçnik P, Grabec I, *Nonlinear model predictive control of a cutting process*, Neurocomputing **43**, (2002), pp 107-126.

[36] Snyder S D, Tanaka Nobuo, *Active control of Vibration using a neural network*, IEEE Transactions on Neural Networks, Vol. **6**, 4, (1995), pp 819-828.

[37] Tewani S G, Walcott B L, Rouch K E, *Active optimal vibration control using dynamic absorber*, Proceeding s of 1991 IEEE, International Conference on Robotics and Automation, Sacaramento, California, (1991), pp 1182-1187.

[38] Marra M A, Rouch K E, Tewani S G, *Vibration control for machining using H_∞ techniques*, IEEE , (1995), pp 436-442.

[39] Mc. Clelland, J. and Rumelhart D. E., *Parallel Distributed Processing. Explorations in the Microstructure of Cognition*, Volume 1: Foundations, Bardford Books, MIT Press, (1986).

[40] Hebb D O, *The organization of behavior: A Neuropsycological Theory*, New York: Wiley, (1949).

[41] Bhattacharya A, *Metal Cutting theory and practice,* Calcutta, Central Book Publishers, (1980).

[42] Meirovitch L, *Elements of Vibration Analysis,* Mc Graw-Hill International Editions, (1986).

[43] Haykins S, *Neural Networks: A comprehensive Foundation,* Pearson Education, (1999).

Appendix A

Specifications of Experimental setups

H.1: Tool and Workpiece Specifications

H.1.1 Tool Specifications

Cutting Tool Material	:HSS with 10% Cobalt
Cutting Tool Composition	:18%W, 4% Cr, 2% V, 10% Co
Tool Dimensions	:0.5"x0.5", 6" long
Tool geometry	:0°-10°-6°-6°-12°-15°-10°-0 mm

H.1.2 Workpiece Specifications

Workpiece Material	:EN24
Workpiece Composition	:0.35-0.45% C
	0.45-0.60% Mn
	1.30-1.80% Ni
	0.90-1.40% Co
	0.20-0.30% Cr
	0.10-0.35% Si
	Rest Iron
Workpiece Hardness	:260 BHN

H.2 Specification of Lathe

Type	:LB25
Center Height	:250 mm
Center Distance	:1500 mm
Swing over bed	:500 mm
Swing over cross slide	:330 mm
Spindle Speeds	:32-1600 rpm
Feeds	:0.03-1.4 mm/rev
Motor	:10 HP, 3000 rpm

H.3 Specification of OP-Amp

Make	:PMI
Type	:OP07CP
PS	:Total Voltage 30V
Max Voltage Drift	:1.8μV/pC
Max Voltage Offset	:250μV
Max Current Offset	:8nA
Max Current Bias:	:9nA

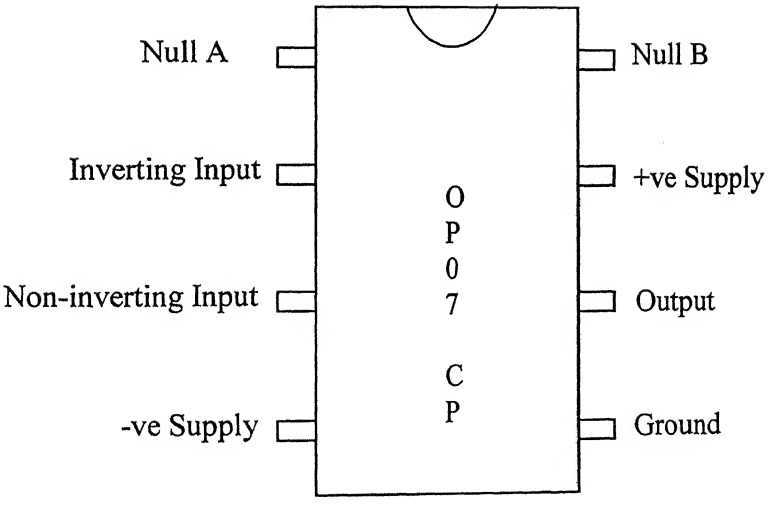

Figure A.1: Pin Diagram of Op-Amp (OP07CP)

Appendix B

Piezoelectric actuator and controller specifications

B.1 The Vibratory Actuator

The AE0505D16 piezoelectric stack sold by Thorlabs is manufactured by NEC Corporation of Japan. These stacks consist of many piezoelectric ceramic layers that are assembled in series mechanically and in parallel electrically. To operate the actuator the red lead of the device is connected to the positive (+) terminal of the voltage source. Reverse biasing will cause damage to the stack.

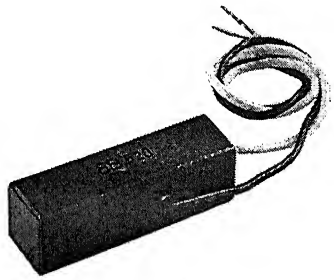

Fig. B.1: The Vibratory Actuator

B.1.1 Specifications

Displacement at Maximum Drive Voltage:	17.4µm + 2.0
Maximum Drive Voltage (short term):	150 volts-see aging curve
Displacement at Recommended Drive Voltage:	11.6µm + 2.0
Recommended Drive Voltage:	100 volts
Operating Temperature Range:	-25 to +85°C
Capacitance:	1.40 + 0.28µF
Tensile Force:	850N
Resonant Frequency:	69 KHz (no mechanical load)
Young's Modulus:	4.4 x 10E10 N/m2
Recommended Preload:	<425 N

B.2 The Vibratory Actuator Controller

The MDT694 is a single channel high voltage amplifier designed to take advantage of the very high resolution achievable with our line of Piezo-electric stacks. The MDT694 combines a precision high voltage output capability with a high output current capability.

B.2.1 Specifications

- Output Voltage: 0-150V
- Output Current: 60 mA/Channel
- Output Noise: 1.5 mV RMS
- Output Stability: 0.01% Over 16 Hrs.
- Power Requirements: 115/230V AC 50-60 Hz

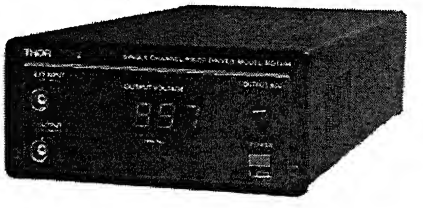

Fig. B.3: The Piezoelectric Controller

Appendix C

Tool Adapter and its Analysis

C.1 The Tool Adapter

A tool adapter had been designed to accommodate the a square sectioned cutting tool such that, the actuator can is co-axially mounted with the tool and both are rigidly fixed relative to each other. A Spring- Steel plate has been used for the propagating the vibration from the actuator to the cutting tool. A pre-loading mechanism is also provided, so that the actuator can be pre-loaded under a desired load. Calculations have been done to design the Spring Steel plate. A plate thickness of 8 mm was found out to be sufficient for a load of 800N. Section C.2 has further details about the adapter design.

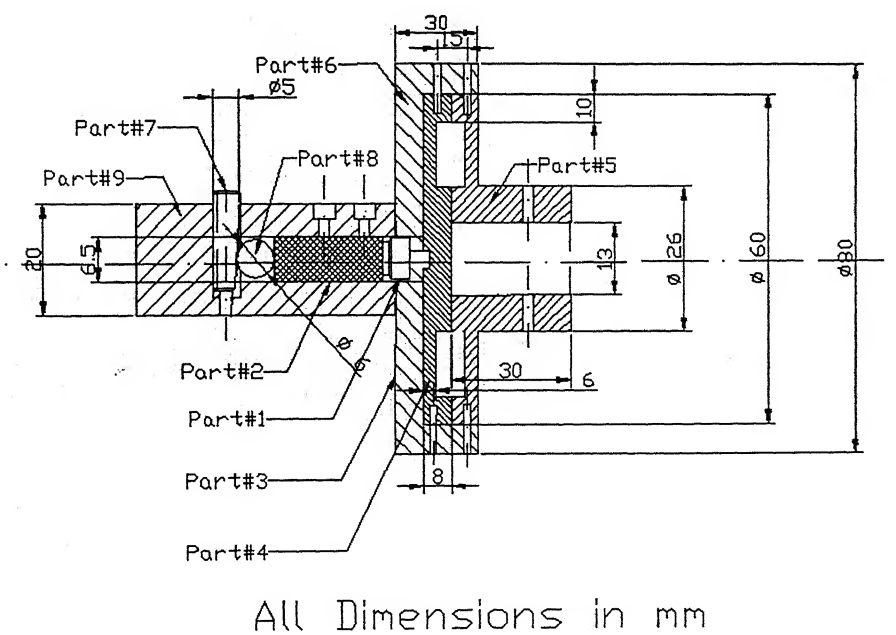

Fig. C.1: The Tool Adapter

The part numbers in Fig. C.1 is given in Table C.1.

Table C.1: Part Specification of the Tool Adapter

Part #	*Part Name*	*Material*	*Use of the part*
1	Stopper	Mild Steel	Transmits the vibration from the Part# 2 to 4
2	Actuator	Piezoelectric	Provides Vibration
3	Outer Casing	EN 24	Rigidly holds Part# 4 & 5
4	Plate Spring	Spring Steel	Transmits the vibration from the Part# 2 to 5
5	Tool Holder	EN 24	Holds the tool and transmits the vibration to it
6	Allen Bolts	Hardened MS	Clamping
7	Tapered Pin	Mild Steel	Helps in pre-loading the actuator
8	Steel Ball	Mild Steel	Helps in pre-loading the actuator
9	Actuator holder	Mild Steel	Holds the actuator rigidly

C.2 Design of the Spring Steel Plate

Navier's method for patch loading is followed for the design of the spring steel plate, which is EN9 and had been heat treated. The algorithm developed for the design is given below:

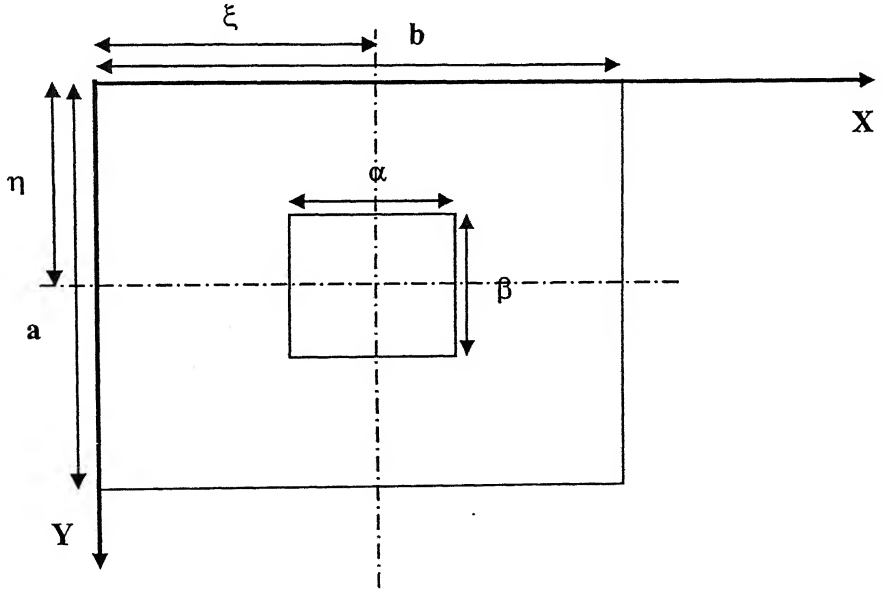

Figure C.2: Design of Rectangular Plate for Patch loading

Step 1: $D = \frac{Eh^3}{12(1-v^2)}$

Step 2: $q_{m,n} = \frac{4P}{\pi^4 abD} sin(\frac{m\pi\xi}{a}) sin(\frac{n\pi\eta}{b})$

Step 3: $c_{m,n} = \frac{q_{m,n}}{Dab(\frac{m^2\pi^2}{a^2} + \frac{n^2\pi^2}{b^2})^2}$

Step 4: $w(x,y) = c_{m,n} \sum_{m=1}^{\infty} \sum_{n=1}^{\infty} q_{m,n} sin(\frac{m\pi x}{a}) sin(\frac{n\pi y}{b})$

The result of the simulation is shown in Fig. C.3.

h= =Thickness of plate

v= =Possion's Ratio

m,n= =Order

D= =Flexural Rigidity of plate per unit width

$q_{m,n}$= =Fourier component of load

$c_{m,n}$= =Fourier component of displacement

$w(x,y)$ =Displacement at every point(x,y)

P =Applied Load

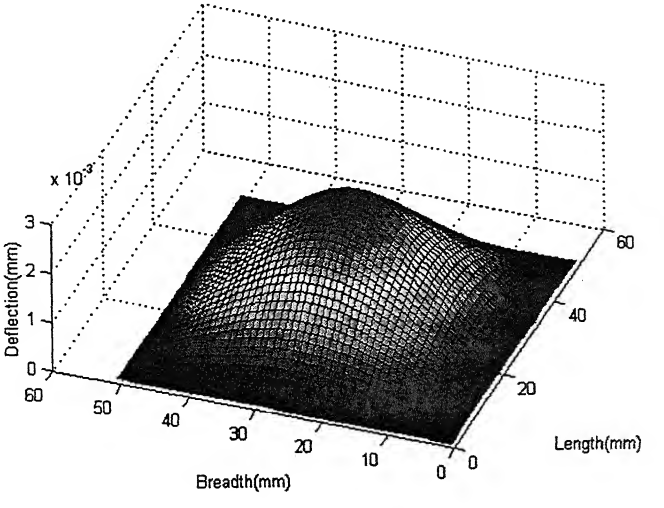

Figure C.3: Result of the Design Analysis (*P=800N, h=8 mm*)

Appendix D

Impulse hammer specifications

Bruel and Kjaer Impact Hammer — Type 8202

D.1 Introduction

The Impact Hammer Type 8202 is an instrumented hammer for testing structural behavior when used in conjunction with a dual- or multi-channel spectrum analyzer. An impact from such a hammer imparts to the test structure a smooth excitation spectrum over a broad frequency range. The force is measured by the built-in Force Transducer Type 8200 while the structural response is measured by separate means, for example an accelerometer fitted to the test object. Fig. D.1 shows the impact hammer along with its force transducer and different tips (steel, plastic and rubber) and the additional mass.

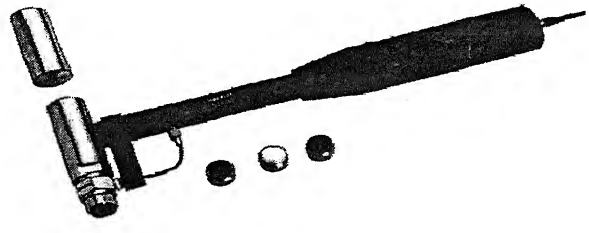

Figure D.1: Impact Hammer Type 8202 with the plastic tip attached. The extra plastic tip, the steel tip, the rubber tip and the additional mass are also pictured

The frequency bandwidth of the first lobe of an impact's spectrum is inversely proportional to the width of the impulse as shown in Fig. D.2.

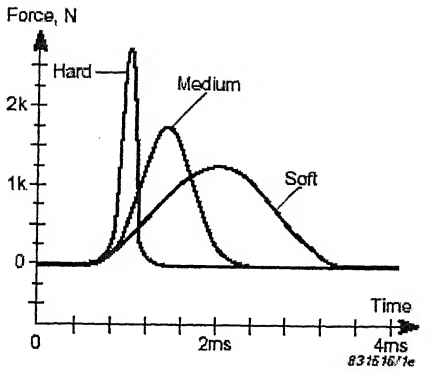

Figure D.1: Impulse shape for various hardnesses of the hammer tip. As the tip becomes softer, the pulse becomes broader and lower in peak value (for a given impact area)

The comparison between various heads of the impact hammer is given in Table D.1 below.

Table D.1: Frequency range (-10 dB point), pulse duration and force range for various hammer configurations when impacting a large steel plate

Tip	Frequency Range	Pulse Duration	Force Range
Steel	0 to 7 kHz	0.20 ms	500 N to 5000 N (112.41 lbf to 1124.10 lbf)
Steel + add. mass	0 to 4.5 kHz	0.23 ms	
Plastic	0 to 2 kHz	0.57 ms	300 N to 1000 N (67.45 lbf to 224.82 lbf)
Plastic + add. mass	0 to 1.3 kHz	0.76 ms	
Rubber	0 to 500 Hz	2.7 ms	100 N to 700 N (22.48 lbf to 157.37 lbf)
Rubber + add. mass	0 to 340 Hz	3.1 ms	

D.3 Impact Testing

A very fast method of performing transient tests is to use a hand-held hammer to impact the structure. The force transducer built into the hammer measures the input force and an accelerometer mounted on the structure measures the response.

The advantages of impact testing are:

- No elaborate fixture for the test structure.
- Small amount of equipment required.
- It is the fastest test method for low noise environments.
- It is ideal for use in restricted spaces where an exciter would not fit.
- Data consistency is maximized by minimal and constant mass loading of the test structure.

The disadvantages of impact testing are:

- It has a very high crest factor which may drive the test structure beyond its region of linear response. The method is therefore not suitable for inherently non-linear systems.
- Since there is little energy input to the system, the method has poor signal to noise characteristics. However, this problem can be greatly reduced by averaging and/or using time weighting functions.
- Special care must be taken to eliminate overloads and multiple impacts.

D.2 Uses

- Impact testing for measuring frequency response functions, to be used for:
- Dynamic structural testing such as modal analysis

D.3 Features

- Individually calibrated force transducer that can be removed and used for other purposes
- Three different tips and an additional mass for tailoring the excitation spectrum
- Cable routed through hammer handle for protection
- Balanced design to maximize impact precision and minimize hammer bounce

The complete specification of the impact hammer as well as the force transducer is given in Table D.2 below.

Table D.2: Complete Specification

Force Transducer Type 8200

CHARGE SENSITIVITY*† (nominal):
4 pC/N (0.90 pC/lbf)
FORCE RANGE:
1000 N tensile to 5000 N compressive (224.8 lbf to 1124.1 lbf)
LINEARITY*:
<±1% of the maximum force or <±5% of the measured force, whichever is smaller
TRANSVERSE SENSITIVITY: 5%

Hammer

RANGE OF FORCE AND DURATION WHEN IMPACTING AGAINST MASSIVE STEEL USING:
Plastic Tip: 300 N to 1000 N (67.5 lbf to 224.8 lbf), 1 ms to 0.5 ms
Rubber Tip: 100 N to 700 N (22.5 lbf to 157.4 lbf), 5 ms to 1.5 ms
Steel Tip: 500 N to 5000 N (112.4 lbf to 1124.1 lbf), 0.23 ms to 0.18 ms
ATTENUATION FACTOR (nominal)*: 4
(Attenuation of signal from force transducer by circuitry in handle)
CHARGE SENSITIVITY FOR FORCE TRANSDUCER INCL. HAMMER*‡ (nominal):
1 pC/N (0.22 pC/lbf)†

Environmental

DEFORMATION OF THE TRANSDUCER (8200) AT MAXIMUM FORCE:
0.01 mm (0.0004 in)
TEMPERATURE TRANSIENT SENSITIVITY (8200): 0.5 N/°C (0.06 lbf/°F)
OPERATING TEMPERATURE (Hammer):
–10 to +55°C (+14 to +131°F)
STORAGE TEMPERATURE (Hammer):
–25 to +70°C (–13 to +158°F)

* Individual values are given on the calibration chart supplied
† Measurement uncertainty: ±1.9%
‡ Measurement uncertainty: ±2.0%

Dimensions and Weight

LENGTH OF:
Hammer: 255 mm (10.0 in)
Handle: 130 mm (5.1 in)
Hammer Head: 52.5 mm (2.1 in)
DIAMETER OF:
Hammer Head: 20 mm (0.8 in)
Additional Mass: 20 mm (0.8 in)
Handle: 30 mm (1.2 in)
WEIGHT OF:
Hammer Handle & Head: 280 g (9.9 oz)

Additional Mass: 122 g (4.3 oz)
Plastic Tip: 3.9 g (0.14 oz)
Rubber Tip: 4.1 g (0.14 oz)
Steel Tip: 10.3 g (0.36 oz)
Force Transducer: 21 g (0.74 oz)

Note: All values are typical at 25°C (77°F), unless measurement uncertainty is specified. All uncertainty values are specified at 2σ (i.e. expanded uncertainty using a coverage factor of 2)

COMPLIANCE WITH STANDARDS:

CE	CE-mark indicates compliance with: EMC Directive.
Safety	EN 61010–1 and IEC 1010–1: Safety requirements for electrical equipment for measurement, control and laboratory use.
EMC Emission	EN 50081–1: Generic emission standard. Part 1: Residential, commercial and light industry. EN 50081–2: Generic emission standard. Part 2: Industrial environment. CISPR 22: Radio disturbance characteristics of information technology equipment. Class B Limits. FCC Rules, Part 15: Class B limits.
EMC Immunity	EN 50082–1: Generic immunity standard. Part 1: Residential, commercial and light industry. EN 50082–2: Generic immunity standard. Part 2: Industrial environment. Note: The above is guaranteed using accessories listed in this Product Data sheet only.
Temperature	IEC 68–2–1 & IEC 68–2–2: Environmental Testing. Cold and Dry Heat. Operating Temperature: –10 to +55°C (+14 to +131°F) Storage Temperature: –25 to +70°C (–13 to +158°F)
Humidity	IEC 68–2–3: Damp Heat: 90% RH (non-condensing at 40°C (104°F))
Mechanical	Non-operating: IEC 68–2–6: Vibration: 0.3 mm, 20 m/s², 10–500 Hz IEC 68–2–27: Shock: 1000 m/s² IEC 68–2–29: Bump: 3000 bumps at 250 m/s² (in three directions)
Enclosure	IEC 529: Protection Provided by Enclosures: IP 67

Appendix E

FFT Analyzer

The CF-3200 portable FFT analyzer (Ono Sokki make) provides on-site precision measurement and analysis of sound and vibration.

Its compact and lightweight attached-case form makes it easy to transport to and around the site. Such features as the battery/AC-powered operation and built-in sensor amplifiers mean that there are virtually no limitations on the location for analysis. There is also a wide choice of application software available for the analyzer, which supports a variety of measurement tasks. These include tracking analysis to evaluate the dynamic characteristics of rotary machines and engines, measurement of natural frequencies using frequency-response functions, precision diagnosis and field balancing of factory equipment, and real-time octave analysis that has proved very effective in sound analysis.

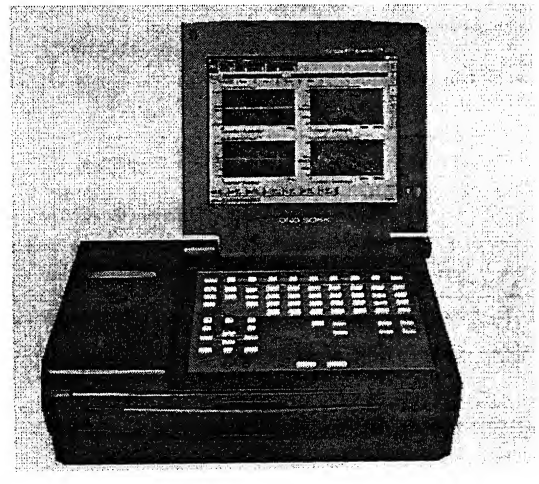

Figure E.1: Ono Sokki CF-3200 FFT Analyzer

Features

- Compact and lightweight at only 6kg / 6.5 kg for better portability
- Operates on either an AC power supply or a battery
- Built-in sensor amplifier (for acceleration pickups, constant current supply type microphones, and rotation sensors)
- Built-in thermal printer
- A highly luminous, 10.4-in. TFT color LCD panel as the display
- External keyboard and mouse input provided.
- Built-in large-capacity flash memory (non-volatile block, time record memory) and floppy drive

Main Specifications

Model	CF-3200
Processing functions	Time-axis waveform, PDF, power spectrum, phase spectrum, cross spectrum, FRF, coherence function, rpm-tracking analysis
Input channels	2 channels
Voltage range	10mVr to 10Vr
Dynamic range	75dB or more
Frequency range	1Hz to 40kHz
Frequency resolution	25 to 1600 lines
Power supply	100 to 240VAC or a battery
Outer dimensions	408x280x125mm (WxDxH)
Weight	Approx. 6 kg
Main options	Pre-processing function (filter processing, headphone output), field-balancing function, real-time octave analysis, signal output

Appendix F

Set-up for using Impact Hammer

The experimental setup for the impulse response of the tool workpiece system, with the help of an Impact Hammer [Appendix D] is given in Fig. F.1.

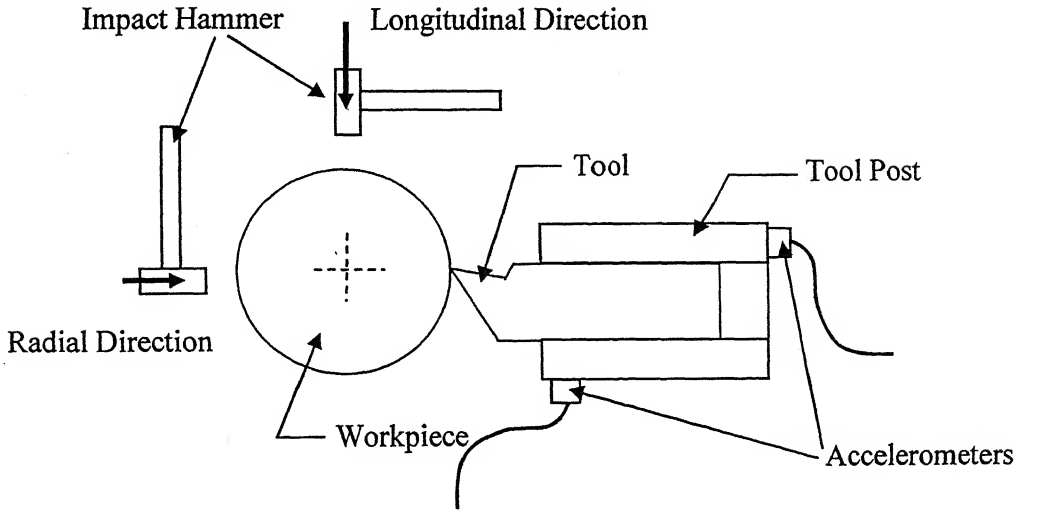

Figure F.1: Set up for using Impact Hammer

Appendix G:

Results of impulse response in different directions

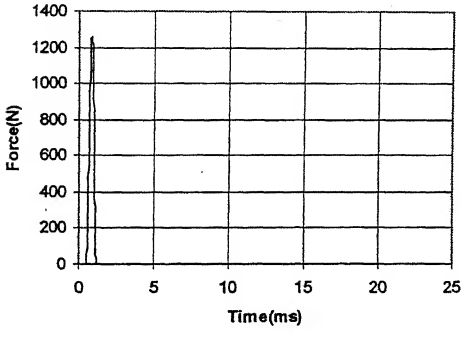

(a) Force Response(Time Domain)

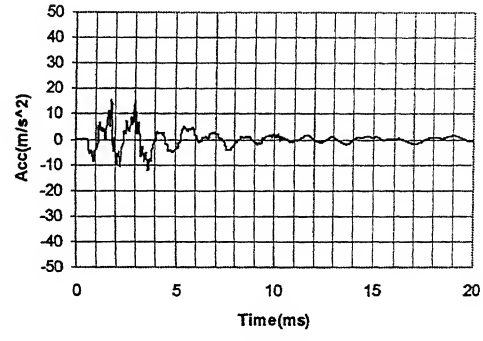

(b) Acc Response(Time Domain)

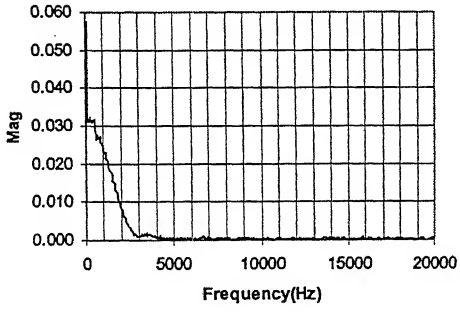

(c) Force Response(Freq Domain)

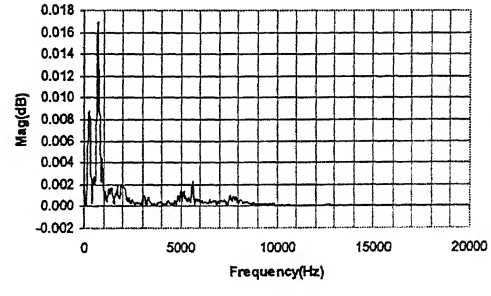

(d) Acc Response(Freq Domain)

Figure G.1: Longitudinal Loading and Radial Accelerometer Position

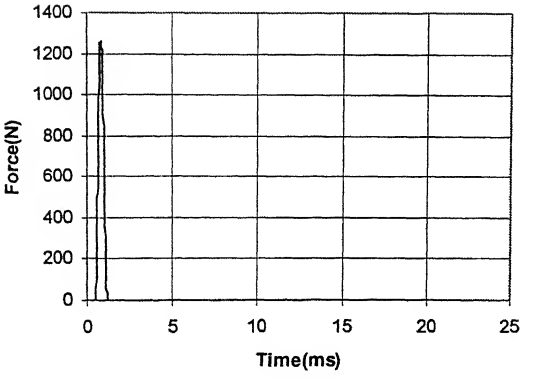

(a) Force Response(Time Domain)

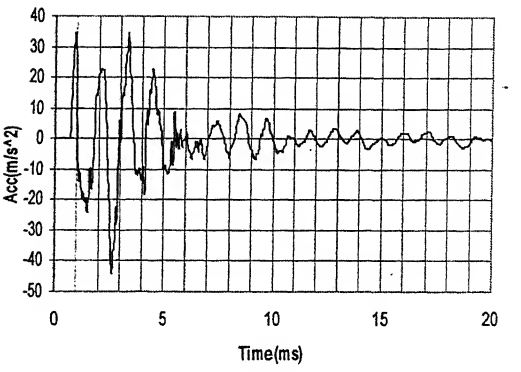

(b) Acc Response(Time Domain)

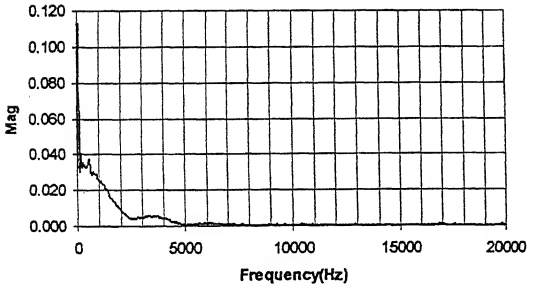

(c) Force Response(Freq Domain)

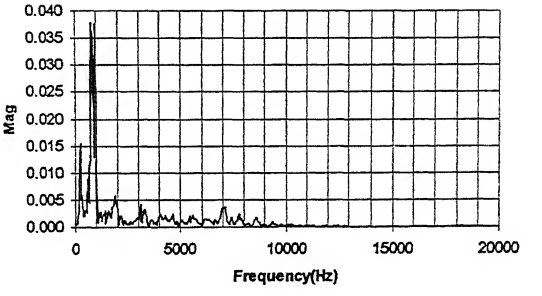

(d) Acc Response(Freq Domain)

Figure G.2: Longitudinal Loading and Longitudinal Accelerometer Position

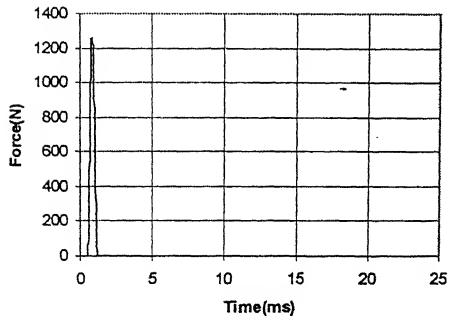

(a) Force Response(Time Domain)

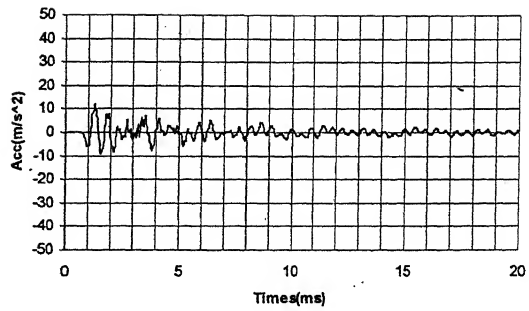

(b) Acc Response(Time Domain)

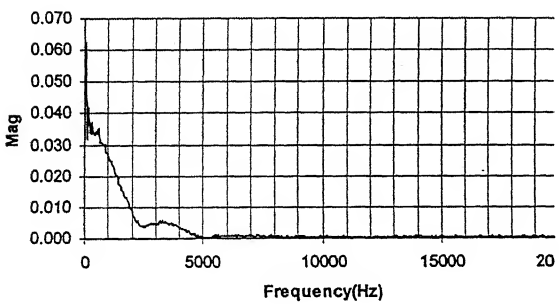

(c) Force Response(Freq Domain)

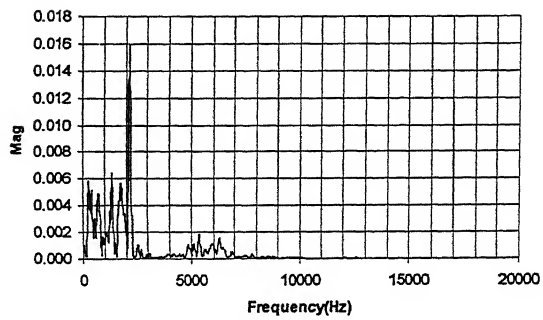

(d) Acc Response(Freq Domain)

Figure G.3: Transverse Loading and Radial Accelerometer Position